

INVESTIGATION ON THE RHEOLOGICAL, THERMAL,
ELECTRICAL PROPERTIES OF ISOTROPIC
CONDUCTIVE ADHESIVES FILLED WITH SILVER
NANOPARTICLES AND AMORPHOUS CARBON
NANOTUBES

CHEW CHEE SEAN

DOCTOR OF PHILOSOPHY IN ENGINEERING

LEE KONG CHIAN FACULTY OF ENGINEERING AND
SCIENCE
UNIVERSITI TUNKU ABDUL RAHMAN
FEBRUARY2018

**INVESTIGATION ON THE RHEOLOGICAL, THERMAL,
ELECTRICAL PROPERTIES OF ISOTROPIC CONDUCTIVE
ADHESIVES FILLED WITH SILVER NANOPARTICLES AND
AMORPHOUS CARBON NANOTUBES**

By

CHEW CHEE SEAN

A thesis submitted to the Department of Mechanical and Materials
Engineering,
Lee Kong Chian Faculty of Engineering and Science,
Universiti Tunku Abdul Rahman,
in partial fulfillment of the requirements for the degree of
Doctor of Philosophy in Engineering
February 2018

ABSTRACT

INVESTIGATION ON THE RHEOLOGICAL, THERMAL, ELECTRICAL PROPERTIES OF ISOTROPIC CONDUCTIVE ADHESIVES FILLED WITH SILVER NANOPARTICLES AND AMORPHOUS CARBON NANOTUBES

Chew Chee Sean

Epoxy polymer-based nanocomposites are widely used as isotropic conductive adhesives (ICAs) in the electronic industry for electronic packaging due to their low processing temperature, environmental friendliness and finer pitch capability. However, there are several research challenges facing this conductive adhesive technology, especially in terms of rheological, thermal and electrical properties. In this study, silver nanoparticles (SNPs) and amorphous carbon nanotubes (a-CNTs) were synthesized via chemical approaches. The nanomaterials were then characterized using X-ray diffraction (XRD), field emission scanning electron microscope (FESEM), energy dispersive X-ray (EDX), ultraviolet–visible spectroscopy (UV-VIS), Fourier transform infrared spectroscopy (FTIR), Raman spectroscopy, and high-resolution transmission electron microscopy (HRTEM). The ICAs samples were prepared according to the varying compositions of nanomaterials, for instance, SNPs and a-CNTs and additional of microcrystalline cellulose (MCC) solution. The objective of this work is to study the effect of the composition on the rheological properties through thermal analysis. An Anton Paar Physica MCR 301 controlled-stress rheometer was used to study the rheology behaviours of ICAs, such as

constant shear rate, amplitude sweep, frequency sweep, hysteresis, three interval thixotropy test (3ITT) and creep recovery. The effects of a-CNTs on ICAs was studied using both dynamic mechanical thermal analysis (DMTA) and thermogravimetric analysis (TGA) methods, and the results used to determine the optimal properties. Forty-five ICAs samples were generated by response surface with a three-level factorial Design of Experimental (DOE) used to study the electrical resistivity of the new ICA formulations to determine the ideal SNPs and a-CNTs properties for ICAs. Our results show that incorporating a-CNTs and MCC solution in ICAs leads to better thixotropic performance while helping lower the gelation temperature. Our results also show that adding 2 wt% of a-CNTs and 5 wt% of MCC solution to ICA system leads to an increase in electrical conductivity of as much as 20 %.

ACKNOWLEDGEMENTS

I would like to express my sincere gratitude to my dearest supervisor Prof Dr Rajukumar A/L Durairaj for his guidance, enormous patience, and encouragement throughout this research. I would like to acknowledge my co-supervisor Dr Liang Meng Suan for his guidance and support during this study. Meanwhile, I would like to especially thank Dr Chen Kah Pin and Dr Tey Jing Yuan for their invaluable suggestions and recommendations.

I also appreciate the University Tunku Abdul Rahman (UTAR) for giving me the permission to carry out experiments in the laboratories and providing the apparatus and materials used throughout this research.

I wish to express my gratitude to my loving parents, husband, my lovely sons, relatives, and best friends for their love and encouragement. Without them, I would not have been able to complete this thesis.

Thank you very much.

APPROVAL SHEET

This dissertation/thesis entitled **“INVESTIGATION ON THE RHEOLOGICAL, THERMAL, ELECTRICAL PROPERTIES OF ISOTROPIC CONDUCTIVE ADHESIVES FILLED WITH SILVER NANOPARTICLES AND AMORPHOUS CARBON NANOTUBES”** was prepared by CHEW CHEE SEAN and submitted as partial fulfillment of the requirements for the degree of Doctor of Philosophy in Engineering at Universiti Tunku Abdul Rahman.

Approved by:

(Prof. Dr. RAJKUMAR A/L DURAIRAJ)

Date:.....

Professor/Supervisor

Department of Mechanical and Materials Engineering

Lee Kong Chian Faculty of Engineering and Science

Universiti Tunku Abdul Rahman

(Dr. LIANG MENG SUAN)

Date:.....

Professor/Co-supervisor

Department of Mechanical and Materials Engineering

Lee Kong Chian Faculty of Engineering and Science

Universiti Tunku Abdul Rahman

SUBMISSION SHEET

LEE KONG CHIAN FACULTY OF ENGINEERING AND SCIENCE

UNIVERSITI TUNKU ABDUL RAHMAN

Date: 08/02/2018

SUBMISSION OF FINAL YEAR PROJECT /DISSERTATION/THESIS

It is hereby certified that CHEW CHEE SEAN(ID No: 13UED06556) has completed this ~~final year project/~~ ~~dissertation/~~ thesis* entitled **“INVESTIGATION ON THE RHEOLOGICAL, THERMAL, ELECTRICAL PROPERTIES OF ISOTROPIC CONDUCTIVE ADHESIVES FILLED WITH SILVER NANOPARTICLES AND AMORPHOUS CARBON NANOTUBES”** under the supervision of Prof. Dr. RAJKUMAR A/L DURAIRAJ (Supervisor) from the Department of Mechanical and Materials Engineering, Lee Kong Chian Faculty of Engineering and Science, and Dr. LIANG MENG SUAN (Co-Supervisor)* from the Department of Mechanical and Materials Engineering, Lee Kong Chian Faculty of Engineering and Science.

I understand that University will upload softcopy of my ~~final year project/~~ ~~dissertation/~~ thesis* in pdf format into UTAR Institutional Repository, which may be made accessible to UTAR community and public.

Yours truly,

(*CHEW CHEE SEAN*)

DECLARATION

I hereby declare that the dissertation is based on my original work except for quotations and citations which have been duly acknowledged. I also declare that it has not been previously or concurrently submitted for any other degree at UTAR or other institutions.

Name: Chew Chee Sean

Date: 08/02/2018

LIST OF PUBLICATIONS

1. R.Durairaj, C. S. Chew*, Investigation of Dynamic and Mechanical Thermal Behavior of Isotropic Conductive Adhesives, EPTC, Grand Copthorne Water Front Hotel 392 Havelock Road Singapore, 11-13 December 2013.
2. C.S. Chew*, R. Durairaj, J Tan, J. Hwang, M. S. Liang , The Effect of Nano Fillers in Electrical and Mechanical Properties of Isotropic Conductive Adhesive, AUN/SEED-NET Regional Conference on Materials Engineering, Sunway Putra Hotel, Kuala Lumpur, 11-12 November 2014
3. C. S. Chew*, Satiga Pamornpol Oon Hean Keat and Rajkumar Durairaj. Mechanical and Electrical Properties of Carbon Nanotubes Based Isotropic Conductive Adhesives, The Electronic Packaging Interconnect Technology Symposium, (EPITS 2015) Penang, 21 November 2015.
4. C. S. Chew*, P. Satiga, H. K. Oon, R. Durairaj, "Mechanical and Electrical Properties of Carbon Nanotubes Based Isotropic Conductive Adhesives", Materials Science Forum, Vol. 857, pp. 93-97, 2016.
5. C. S. Chew, R. Durairaj and S. L Chuah, "Gelation Behaviour of Synthesized Silver Nanoparticles in Isotropic Conductive Adhesives, Journal of Testing and Evaluation, submitted. 2016.

TABLE OF CONTENTS

	Page
ABSTRACT	ii
ACKNOWLEDGEMENTS	iv
APPROVAL SHEET	v
SUBMISSION SHEET	vi
DECLARATION	vii
LIST OF PUBLICATIONS	viii
TABLE OF CONTENTS	ix
LIST OF TABLES	xii
LIST OF FIGURES	xiii
LIST OF ABBREVIATIONS/NOTATION/GLOSSARY OF TERMS	xvi
LIST OF APPENDICES	xvii
CHAPTER	
1.0 INTRODUCTION	1
1.1 Background	1
1.2 Objectives	5
1.3 Overview of the Dissertation	6
2.0 LITERATURE REVIEW	9
2.1 Introduction	9
2.2 Isotropic Conductive Adhesives (ICAs)	9
2.2.1 Polymer Matrix	11
2.2.2 Non-conductive Fillers (Microcrystalline Cellulose, MCC)	12
2.2.3 Conductive Fillers	14
2.2.4 Silver Powders	14
2.2.5 Nanofillers	15
2.2.6 Electrical Conductivity of ICAs	20
2.3 Rheology Behaviours of Paste in Stencil Printing	22
2.3.1 Static Properties: Viscosity and Thixotropic Studies	23
2.3.2 Dynamic Properties: Oscillation and Creep	26
2.4 Thermal Behaviour of the ICAs	28
3.0 METHODOLOGY	30
3.1 Introduction	30
3.2 Materials	31
3.3 Synthesis Silver Nanoparticles (SNPs)	33
3.4 Synthesis and Purification of amorphous carbon nanotubes (a-CNTs)	33

3.5	Characterization Methods of Synthesized SNPs and a-CNTs	34
3.5.1	X-ray Diffraction (XRD)	35
3.5.2	Ultraviolet–Visible Spectroscopy (UV-VIS)	35
3.5.3	Fourier Transform Infrared Spectroscopy (FTIR)	36
3.5.4	Raman Spectroscopy	37
3.5.5	Field Emission Scanning Electron Microscope (FESEM) and Energy Dispersive X-ray (EDX)	38
3.5.6	High-Resolution Transmission Electron Microscope (HRTEM)	38
3.6	Preparation of Microcrystalline Cellulose (MCC) Solution	39
3.7	Preparation of ICA Samples	39
3.8	Rheometry	44
3.9	Thermal Behaviour ICAs by DMTA and TGA	47
3.9.1	Dynamic Mechanical Thermal Analysis (DMTA)	47
3.9.2	Thermogravimetric Analysis (TGA)	48
3.10	Measurement of Electrical Conductivity by Four-Points Probes	49
4.0	STUDY OF THE NANOSTRUCTURE OF SNPS AND A-CNTS	52
4.1	Introduction	52
4.2	Results and Discussion	52
4.2.1	Characterization of synthesized Silver Nanoparticles (SNPs)	52
4.2.2	Characterization of synthesized amorphous carbon nanotubes (a-CNTs)	56
5.0	STUDY OF THE RHEOLOGICAL BEHAVIOUR	62
5.1	Introduction	62
5.2	Results and Discussion	62
5.2.1	Viscosity Test	62
5.2.2	Oscillatory Stress Sweep Stress (OSS) Test	66
5.2.3	Frequency Sweep Test	72
5.2.4	Hysteresis and Three Interval Thixotropy Test (3ITT)	75
5.2.5	Creep Recovery	82
6.0	STUDY OF THE THERMAL STABILITY AND GELATION POINTS	87
6.1	Introduction	87
6.2	Results and Discussion	87

6.2.1	Thermal Stability by TGA	87
6.2.2	Gelation Study by DMTA	92
7.0	ELECTRICAL CONDUCTIVITY	98
7.1	Introduction	98
7.2	Results and Discussion	98
8.0	CONCLUSIONS AND RECOMMENDATIONS	113
8.1	Introduction	113
8.2	Characterization of Chemical Synthesized Silver Nanoparticles (SNPs) and Amorphous Carbon Nanotubes (a-CNTs)	115
8.3	Investigation of the visco-elastic and thixotropic properties of the new formulation isotropic conductive adhesives (ICAs)	116
8.4	Study of the gelation points and weight loss of the new formulation ICAs	117
8.5	Measurement of the electrical conductivity of the ICAs	118
8.6	Recommendations	118
	REFERENCES	121
	APPENDICES	136

LIST OF TABLES

Tables	Page
Table 3-1: All chemicals used in the preparation of ICAs	32
Table 3-2: The formulation of different samples with different composition of polymer matrix and fillers	41
Table 3-3: Experimental parameters of constant shear rate test	44
Table 3-4: Experimental parameters of oscillatory stress sweep (OSS) test	45
Table 3-5: Experimental parameters of frequency sweep test	45
Table 3-6: Experimental parameters of hysteresis loop test	45
Table 3-7: Experimental parameters of Thixotropy test	46
Table 3-8: Experimental parameters of creep recovery test	46
Table 3-9: Experimental parameters for the DMTA test	48
Table 5-1: Linear visco-elastic region's range of ICAs samples	70
Table 5-2: The relative magnitude of loss modulus, G'' and storage modulus, G' within LVER	71
Table 5-3: Viscosity recovery in percentage after shear rate was removed	81
Table 5-4: Creep Recovery Index for All ICA Samples	86
Table 6-1: Gelation points (T_{gel}) of crossover value of the storage modulus (G') and loss modulus (G'')	96

LIST OF FIGURES

Figures	Page
Figure 2-1: Viscosity experienced four stages (<i>I-IV</i>) as a function of time. Stages <i>I</i> -Rest, <i>II</i> -Squeegee, <i>III</i> -Mesh, <i>IV</i> - Recovery (Kaiser, 2009)	25
Figure 2-2: Creep recovery profile (Nguty et al., 1998)	28
Figure 3-1: Flow chart of the study	43
Figure 3-2: Schematic diagram of the test circuit for measuring bar specimen resistivity with the four-point probe method	50
Figure 4-1: X-ray diffraction patterns of synthesized SNPs	53
Figure 4-2: UV-Vis absorption Spectra of synthesized SNPs	54
Figure 4-3: FESEM images of synthesized SNPs	55
Figure 4-4: X-ray spectra obtained by EDX analysis on the synthesized SNPs sample	55
Figure 4-5: X-ray diffraction patterns of untreated and treated a-CNTs	57
Figure 4-6: Raman spectra of the treated and untreated a-CNTs	58
Figure 4-7: FT-IR spectra of the treated and untreated a-CNTs	59
Figure 4-8: FESEM image of (a) untreated and (b) treated a-CNTs	60
Figure 4-9: FESEM images and EDX mappings of untreated and treated a-CNTs	60
Figure 4-10: HRTEM image of treated a-CNTs and SAED of the nanotube	61
Figure 5-1: Constant shear rate measurement of S1, S2, S3, S4 and S5	64
Figure 5-2: Constant shear rate measurement of S6, S7, S8, S9 and S10	65

Figure 5-3: Storage modulus (G') and loss modulus (G'') against strain of S1, S2, S3, S4 and S5	68
Figure 5-4: Storage modulus (G') and loss modulus (G'') against strain of S6, S7, S8, S9 and S10	69
Figure 5-5: Frequency sweep test results of S1, S2, S3, S4 and S5	73
Figure 5-6: Frequency sweep test results of S6, S7, S8, S9 and S10	74
Figure 5-7: Hysteresis test results of S1, S2, S3, S4 and S5	77
Figure 5-8: Hysteresis test results of S6, S7, S8, S9 and S10	78
Figure 5-9: Steady shear rate test of S1, S2, S3, S4 and S5	79
Figure 5-10: Steady shear rate test of S6, S7, S8, S9 and S10	80
Figure 5-11: Creep recovery test of S1, S2, S3, S4 and S5	84
Figure 5-12: Creep recovery test of S6, S7, S8, S9 and S10	85
Figure 6-1: Thermogravimetric analysis curve of S1, S2, S3, S4 and S5	90
Figure 6-2: Thermogravimetric analysis curve of S6, S7, S8, S9 and S10	91
Figure 6-3: Storage modulus (G') and loss modulus (G'') against temperature of S1, S2, S3, S4 and S5	94
Figure 6-4: Storage modulus (G') and loss modulus (G'') against temperature of S6, S7, S8, S9 and S10	95
Figure 7-2: Electrical resistivity of ICAs at 0 wt% a-CNTs as function to MCC solution and DGEBA epoxy resin	101
Figure 7-3: Electrical resistivity of curve fitting vs MCC solution at 0 wt% a-CNTs.	102
Figure 7-4: Electrical resistivity of ICAs as a function of MCC solution and DGEBA epoxy resin at 1 wt% a-CNTs	104
Figure 7-5: Curve fitting of electrical resistivity vs MCC solution at 1 wt% a-CNTs	105
Figure 7-6: Electrical resistivity of ICAs as a function of MCC solution and DGEBA epoxy resin at 2 wt% a-CNTs	107

Figure 7-7: Curve fitting of electrical resistivity vs MCC solution at 2 wt% a-CNTs.	108
Figure 7-8: Electrical resistivity of ICAs as a function of MCC solution and DGEBA epoxy resin at 3 wt% a-CNTs.	110
Figure 7-9: Curve fitting of electrical resistivity vs MCC solution at 3 wt% a-CNTs.	111

LIST OF ABBREVIATIONS/NOTATION/GLOSSARY OF TERMS

G'	Storage modulus, Pa
G''	Loss modulus, Pa
DGEBA	Diglycidyl ether of bisphenol A
DMTA	Dynamic mechanical thermal analysis
EDA	Ethylenediamine
EDX	Energy-dispersive X-ray spectroscopy
FESEM	Field emission scanning electron microscopy
ICAs	Isotropic conductive adhesives
LVER	Linear visco-elastic region
SNPs	Silver nanoparticles
a-CNTs	Amorphous carbon nanotubes
HRTEM	High resolution transmission electron microscopy
MCC	Microcrystalline cellulose
3ITT	Three interval thixotropy test
TGA	Thermogravimetric Analysis
OSS	Oscillatory stress sweep
UV-VIS	Ultraviolet–Visible Spectroscopy
XRD	X-ray Diffraction
FTIR	Fourier Transform Infrared Spectroscopy
T_{gel}	Gelation points

LIST OF APPENDICES

Appendixes	Page
APPENDIX A: Forty five ICAs samples composition generated by surface response. The remaining material is silver powder.	134
APPENDIX B: Preparation of the amount of ethylenediamine (EDA).	137

CHAPTER 1

INTRODUCTION

1.1 Background

Lead-tin solders have been widely used in electronics assemblies for several decades. These fit the electrical and mechanical requirements for the interconnections of electronics components on printed circuit boards (PCBs). However, the usage of lead-tin solders has begun to decrease with increasing of environmental awareness and policies related to the Restriction of Hazardous Substances (RoHS) directive. Isotropic conductive adhesives (ICAs) are a promising candidate to replace lead solders. ICAs offer simpler processing and belong to green materials. Its advantages over traditional soldering process include lower curing temperatures than normal soldering, more flexibility and being lead free in nature (Liu et al., 1997, An and Qin, 2014, Zhang et al., 2015).

Basically, ICAs consists of a polymer matrix and conductive fillers. The polymer matrix is made up of polymer resin or epoxy resin, curing agents and additives. The epoxy resin works as a binder that offers mechanical interconnection between electronic components and PCBs. Diglycidyl ether of bisphenol A (DGEBA), also known as bisphenol A diglycidyl ether, is one of the most common epoxy resins. It is widely used as polymer matrix due to its outstanding processability, chemical resistance, and thermal resistance

properties (Amaral et al., 2012). Ehylenediamine (EDA), $C_{18}H_{21}NO$ is a well-known curing agent for low-temperature curing of the epoxy resin.

The conductive fillers in ICAs provide electrical conductivity in all direction. One of the most popular conductive fillers is silver powder due to its high conductivity and high chemical stability (Zwolinski et al., 1996, Sangsuk, 2010, Durairaj and Man, 2011). Unfortunately, compared with lead solders (Resistivity: $1.5 - 3.0 \times 10^{-5} \Omega \text{ cm}$), ICAs have higher electrical resistivity (Resistivity: $1.4 \times 10^{-4} \Omega \text{ cm}$) (Bolotoff, P. V., 2010, Zhang, May 2011). One of the major problems of ICAs properties is low conductivity compared to tin lead solder. In order to achieve good conductivity, the ICAs have to load at higher silver ratios of around 80 wt% (Chueh et al., 2015, Youngseok et al., 2008). However, the high loadings of silver conductive fillers remain very expensive and may cause the mechanical integrity of adhesive joints to deteriorate. In fact, ICAs can provide higher conductivity, higher strength, lighter weight, and more durability if formulated properly (Yim et al., 2014).

Recently, some advanced nanotechnology materials have been introduced as fillers into ICA systems (Yu et al., 2013, Marcq et al., 2011). The advancement of nanotechnology such as silver nanoparticles (SNPs) has been used as conductive filler (Chen et al., 2013, Chee and Lee, 2012, Durairaj et al., 2016, Xianxue et al., 2012). Over the past few decades, nanoparticles of noble metals such as silver have exhibited significantly distinct physical, chemical, and electrical properties from their bulk

counterparts (Tao et al., 2015, Zhang et al., 2016, Vijayaraghavan and Nalini, 2010, Quang Huy et al., 2013).

In addition to SNPs, nanotubes have been used in ICAs to improve its properties. Carbon nanotubes (CNTs) are also widely used in the various researches to discover its potentials in ICAs (Allaoui et al., 2002, Durairaj et al., 2016, Garg et al., 2011, Montazeri et al., 2010, Yim and Kim, 2016, Yim et al., 2014). CNTs have high mechanical strength and toughness, good electrical conductivity and excellent thermal conductivity (Zhao et al., 2014). CNTs are either crystalline CNTs or amorphous CNTs (a-CNTs).

A-CNTs have different tube wall structures than crystalline CNTs. The tube walls are composed of many discontinuous graphene sheets and carbon clusters, which exhibit features of short-range order and long-range disorder, and have many defects, dangling bonds and huge specific surfaces (Zhao et al., 2014, Zhao et al., 2011, Singh et al., 2012, Ci et al, 2001). In some of the latest findings, a-CNTs possess excellent conductivity even though there are many defects on the tube walls. Due to the large aspect ratio, a-CNTs easily form conductive networks in composite materials to transfer the electrons (Zhao et al., 2014, Zhao et al., 2011, Singh et al., 2012, Cheung et al., 2016).

To minimize the cost of ICAs by reducing the use of silver fillers, SNPs and a-CNTs are used as additional fillers. Nanomaterials incorporated into the ICAs system could increase the number of contact between the polymer matrix and silver fillers, resulting in higher conductivity. For better

dispersion of nanoparticles into the polymer matrix, microcrystalline cellulose (MCC) is added to the ICAs. Microcrystalline cellulose (MCC) could be acted as bridges to toughen the epoxy composites while it belongs to a green material. According to Liao et al. (2012), cellulose fibre content ranging from 5 to 30 wt% indicates good interfacial adherence between the epoxy resin and the cellulose fibres through hydrogen-bonding interaction and increasing the mechanical strength.

Besides incorporating the nanomaterials to boost its conductivity, the rheological behaviour of the ICAs is also investigated in this study. In stencil printing process, ICAs must have the conditions to be squeegeed through the force to stencil apertures, while recovering its shape when the force is removed (Durairaj et al., 2008). The viscosity of the paste must decrease and flow steadily during the printing process (Durairaj et al., 2011). The rheological behaviour of the paste is crucial for good processability or printability.

In the rapid assembly processing of flip chip device, the ICAs with lower gelation temperature are more desired as they could solidify at faster rate and adhere well to the substrates, resulting in saving the cost. Thermal stability of the ICAs is studied in order to understand the weight loss of the new formulation samples.

In this study, the silver nanoparticles (SNPs) and amorphous carbon nanotubes (a-CNTs) are prepared using a bottom-up approach. And the

nanoparticles are added to various ICAs systems to study the rheological behaviour, thermal stability and gelation behaviour. Finally, based on the results mentioned above, new formulation of ICAs are generated by response surface, three-level factorial, Design of Experimental (DOE) and its electrical resistivity is measured by four-point probes.

1.2 Objectives

The aim of this research is to develop new isotropic conductive adhesives (ICAs) formulations by adding the in-house prepared silver nanoparticles (SNPs) and amorphous carbon nanotubes (a-CNTs) with satisfactory characteristics based on their visco-elastic and thixotropy, gelation points and thermal stability.

The objectives of this research are:

1. To characterize chemical synthesized silver nanoparticles (SNPs) and amorphous carbon nanotubes (a-CNTs) using ultraviolet–visible spectroscopy (UV-Vis), Fourier transform infrared spectroscopy (FTIR), X-ray diffraction (XRD), Raman Spectroscopy, field emission scanning electron microscope (FESEM), energy dispersive X-ray (EDX) and high-resolution transmission electron microscopy (HRTEM) to determine the size, morphology and structure of SNPs, treated a-CNTs and untreated a-CNTs.

2. To investigate the visco-elastic and thixotropic properties of the new formulation isotropic conductive adhesives (ICAs).
3. To study the gelation points and weight loss of the new formulation ICAs by dynamic mechanical thermal analysis (DMTA) and thermogravimetric analysis (TGA), respectively.
4. To measure the electrical conductivity of the ICAs by four-point probes.

1.3 Overview of the Dissertation

This thesis is organized into the following chapters:

Chapter 2 introduces the overview of isotropic conductive adhesives (ICAs) from its polymer matrix to the conductive fillers. The usage of nanomaterials in ICAs system is reviewed. Rheological properties such as visco-elastic and thixotropic behaviours are discussed. Finally, the electrical conductivity of the ICAs is reviewed.

Chapter 3 describes the preparation of the SNPs and a-CNTs by chemical routes. The formulation of the ICAs is further optimized based on the results of rheological behaviours, gelation points and thermal stability. The characterization methods are also briefly discussed to determine the nanostructure of the synthesized nanomaterials. The parameters of the tests are described for rheological test and thermal analysis.

Chapter 4 discusses the characterization of synthesized SNPs and a-CNTs. The results obtained from Field Emission Scanning Electron Microscopy (FESEM) and Energy-Dispersive X-ray spectroscopy (EDX); X-ray Diffraction; UV-Visible; High-Resolution Transmission Electron Microscope (HRTEM); Raman spectroscopy and Fourier Transform Infrared Spectrometer (FTIR) are presented. The results obtained from characterization methods are discussed to confirm the nanostructure of the synthesized nanomaterials.

Chapter 5 studies the results obtained from rheological behaviour of ICAs in constant shear rate vs time; amplitude sweep; frequency sweep; hysteresis; three-interval thixotropy test (3ITT) and creep recovery. Reasons why ICAs with microcrystalline cellulose (MCC) and a-CNTs have better thixotropy behaviour are discussed.

Chapter 6 investigates the results obtained from thermal stability and gelation temperature and of the ICAs samples. These are to study the influence of SNPs, a-CNTs and MCC solution to the gelation points and weight changes of ICAs samples when the heat was imposed.

Chapter 7 investigates the effect of the different composition of a-CNTs and MCC solution in electrical conductivity. The bulk resistivities of the ICAs samples were calculated and discussed.

Chapter 8 summarizes the important findings of this research and proposes of future work.

CHAPTER 2

LITERATURE REVIEW

2.1 Introduction

This chapter gives a brief introduction of isotropic conductive adhesives (ICAs) and materials that made up its systems, such as a polymer, fillers, and nanofillers. In this study, silver nanoparticles (SNPs) and amorphous carbon nanotubes (a-CNTs) are prepared by chemical approach and incorporated into new formulation ICAs. To investigate this rheological behaviour, thermal stability and gelation points of the new ICAs formulations, the second section of this chapter discusses the rheological properties of the ICAs paste for stencil printing, for instance, viscosity, viscoelasticity, hysteresis and thixotropic behaviour and creep recovery. This chapter also includes the review of thermal analysis and gelation points of the ICAs. Finally, to overcome the major challenge of the ICAs which is lower conductivity, the effects of nanoparticles on electrical conductivity of ICAs are also investigated.

2.2 Isotropic Conductive Adhesives (ICAs)

In semiconductor electronic industry, lead solders have been slowly replaced by isotropic conductive adhesives (ICAs) for interconnections in electronic packaging. The microelectronic assemblies include flip chip technology, pin through hole, surface mount technology and as well as ball grid array package

(Nana et al., 2016, Li and Wong, 2006, Li et al., 2010, Chueh et al., 2015, Hvims, 1995, Keusseyan et al., 1994). There are advantages of using ICAs as compared to solders. Firstly, ICAs are more environmentally friendly than lead solders. Secondly, the processing temperature requirements of ICAs are relatively low while promoting finer pitch capability and flexibility. Lastly, ICAs require no flux removal and can stick on almost any surface (Périchaud et al., 2000, Wong and Daoqiang, 2000, Liu et al., 1998, Jagt et al., 1995). Those benefits are the driving forces for the development of ICAs.

Even though there are many benefits of using ICAs technology, it is still unable to completely replace the solder usage in electronics packaging. The drawbacks of using ICAs (Resistivity: $1.4 \times 10^{-4} \Omega \text{ cm}$) are its relatively lower electrical conductivity as compared to lead solders (Resistivity: $1.5 - 3.0 \times 10^{-5} \Omega \text{ cm}$) (Zhang et al., 2010, Li and Wong, 2006), lacking of rheological records for materials processing, poor impact resistance (Wong and Daoqiang, 2000) and lack of long-term electrical and mechanical stability (Jagt et al., 1995, Jagt, 1998).

However, to overcome the major challenge which is lower conductivity, a numbers of researches have been studied to improve the electrical properties without sacrificing its mechanical strength (Pettersen et al., 2016, Chew et al., 2014, Lim Fui et al., 2011, Lu et al., 1999, Liu et al., 1998, Jagt et al., 1995). The mechanical strength of ICAs is mainly contributed by the polymer matrix of the ICAs.

2.2.1 Polymer Matrix

ICAs consist of a polymer matrix and conductive fillers. The polymer matrix provides mechanical strength, whilst, conductive fillers give the electrical properties. During the curing process, epoxy resins shrink and enables the metals fillers to contact with each other and enhances its conductivity (Chueh et al., 2015, Youngseok et al., 2008). During the curing reactions, volumetric shrinkage occurs as the bonding changes from van der Waals to covalent and shortens the distance between the molecules. The shrinkage causes the intimate contact between conductive fillers, contributing to improve its electrical conductivity. The polymer matrix can be either thermosets or thermoplastics materials (Keusseyan et al., 1994). The most common adhesives that used in the industries are the thermoset epoxies. The epoxies are typically filled with silver particles to form ICAs.

Thermoset epoxies have been widely used for decades due to superior properties, such as high chemical and corrosion resistance, outstanding adhesion to various substrates high tensile and modulus strength, the ability to be processed under a variety of conditions, high glass transition temperature, low creep, good moisture resistance and high thermal stability (Manson, 2012, Samanta and Maity, 2012, Saleh et al., 2009, Liu, 1999).

Diglycidyl ether of bisphenol A (DGEBA) is a commonly used epoxy resin for most applications in many industries. DGEBA is often selected as composite matrix due to its simplicity in processing under various conditions.

In addition, it has good fluidity before curing process (Amaral et al., 2012). DGEBA is crosslinked using hardener (curing agent) to form the networking in the polymer matrix. Thus, DGEBA serves as the cross linker that connects the fillers in the ICAs.

The most common curing agents for epoxy resins are polyalkylene amines, polyamines, aminoamides and phenolic compounds (Fink, 2005, Forrest, 2007). Polyalkylene amines can provide a low temperature for curing. One of the examples of polyalkylene amines is ethylene diamine (EDA). The hardener acts as a multifunctional cross-linking agent and chemically bound the final three-dimensional structure of the DGEBA during the cross-linking process (Goodman, 1999). In addition to epoxy resin, the biodegradable polymers are introduced in this study.

2.2.2 Non-conductive Fillers (Microcrystalline Cellulose, MCC)

A non-conductive filler, microcrystalline cellulose (MCC), is utilized to enhance the thermal and mechanical behaviours. Cellulose fibre, glass fibre and organo-montmorillonite nanoclay (OMMT) (Zulfli et al., 2012), nano-calcium carbonate (He et al., 2011), metal fibres and powders and alumina nanoparticle embedded glass and carbon fibre (Mohanty and Srivastava, 2012) have been used extensively in adhesives composites. However, the use of biodegradable materials into ICAs has seen limited success.

Microcrystalline cellulose (MCC) could act as a bridge to toughen the epoxy composites and disperse the conductive fillers homogeneously in the ICAs system while it belongs to a green material. A number of researchers have reported the benefits of using cellulose to enhance the nanocomposites' properties. According to Liao et al. (2012), with the cellulose fibre content that ranging from 5 to 30 wt%, indicated good interfacial adherence between the epoxy resin and the cellulose fibres through hydrogen-bonding interaction and increasing mechanical strength.

Commonly, MCC takes a powder form which is not diluted in common organic solvents or water because of its strong inter-molecular and intra-molecular hydrogen bonding. Thus, before adding it to the polymer matrix, it must be dissolved into a solution to enable complete and homogeneous mixing whenever possible. There are several methods to dissolve the cellulose, for instance, by using LiCl / DMAc (Ishii et al., 2008, Chrapava et al., 2003), NaOH / urea (Zhou et al., 2004, Cai et al., 2007, Jia et al., 2010, Ma et al., 2012), N-methylmorpholine-N-oxide monohydrate (Kulpinski, 2005), NaOH/H₂O (Roy et al., 2003), LiOH / urea (Cai et al., 2006), NaOH / thiourea aqueous solution (Weng et al., 2004) and ionic liquids (Wu et al., 2004, Zhu et al., 2006). Based on the methods, the NaOH / urea solvent was selected for the dilution of MCC as it is a rapid method which is both eco-friendly and cost effective (Wang, 2008).

2.2.3 Conductive Fillers

In addition to polymer matrixes, which provide mechanical strength to the ICAs, conductive fillers are also very important. The concentrations of the conductive filler in ICAs is between 20 vol.% to 35 vol.% (Tao et al., 2009, Lam,2011 and Zhang, May 2011). ICAs are conductive in all directions due to the higher percentage of fillers contents. There are several types of conductive fillers used for ICAs systems, such as silver, gold, copper, nickel, metal coated particles or conductive nanoparticles.

2.2.4 Silver Powders

Silver is usually added to ICAs because of high chemical stability and electrical conductivity. Meanwhile, its cost is relatively lower as compared to gold (Liu, 1999). Furthermore, silver is a promising conductive filler owing to its electrical conductivity. Unlike another metal oxide, silver oxide is also highly electrically conductive (Chen et al., 2013). Silver can also be prepared in varying sizes (Chrissafis and Bikiaris, 2011, Liu, 1999).

Silver has been investigated and developed in various structures and sizes in order to enhance the performances of the silver-based conductive adhesives. For examples, a highly porous silver powder was prepared by Kotthaus et al. (1997) as filler material for ICAs. A mixture of silver flakes and low-melting-point alloy fillers (LMPA) was utilized by Lu and Wong (2000) as the conductive filler. These studies have proven that these newly

developed silver systems have improved the electrical conductivity with those filled with silver flakes.

In common ICA systems, mixtures of silver flakes, silver powder, and silver nanoparticles are often incorporated in order to achieve closer pack and better conductivity. However, the flake-like silvers are generally produced by mechanical milling of silver powders. The flakes were produced from milling, chemical treatment, and lastly washing and drying (Li et al., 2010).

In this study, silver powder has been selected, as it does not have to go through the others processes in order to get the silver flakes. This is suggested to reduce the processing cost for the newly formulated ICAs incorporated with the in-house prepared silver nanoparticles (SNPs) and amorphous carbon nanotubes (a-CNTs).

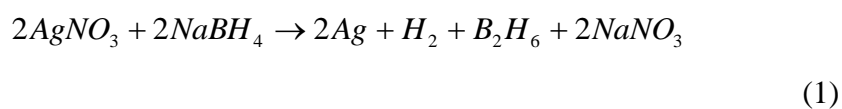
2.2.5 Nanofillers

Silver nanoparticles (SNPs) have been synthesized and anchored into ICA systems in order to boost electrical conductivity (Chen et al., 2013, Chee and Lee, 2012, Durairaj et al., 2016, Xianxue et al., 2012). Based on the researched results, the cured ICAs containing the silver added with 1 wt. % nanoparticles enhanced electrical conductivity due to their filling the gaps between non-contacting silver.

SNPs show great potential for many applications in medicine, cosmetics, optics, catalysis, renewable energies, environmental remediation, biomedical and electronic devices due to their unique properties (Quang Huy et al., 2013, Anh-Tuan et al., 2012, Vertelov et al., 2008, Shivananda et al., 2016, Govindappa et al., 2016). In addition, SNPs offer the low sintering temperatures important for flexible electronic applications.

There are a few methods to prepare SNPs, such as chemical and photo reduction (Hsu and Wu, 2011, Ohde et al., 2001), chemical reduction in aqueous solutions (Liz-Marzán and Lado-Touriño, 1996) and ultrasonic irradiation (Lei and Fan, 2006). However, these methods and procedures are not suitable for large-scale manufacturing because they can only render the stable dispersions of Ag at a relatively low concentration (Sondi et al., 2003). In this study, SNPs were synthesized by the chemical approach, where AgNO_3 (metal salt) was mixed with sodium borohydride, NaBH_4 (a reducing agent) (Kheybari et al., 2010, Abou El-Nour et al., 2010, Gudikandula and Charya Maringanti, 2016, Guzmán et al., 2008). The chemical reduction of metal salts is the simplest and the most commonly used bulk solution synthesis method for SNPs. The targeting size of the SNPs is less than 100 nm. The chemical reactions are stated in equation

(1)



In addition to silver nanoparticles, nanotubes have been used in ICAs to improve its properties. Carbon nanotubes (CNTs) are also widely incorporated into ICAs to expand its potential (Allaoui et al., 2002, Durairaj et al., 2016, Garg et al., 2011, Montazeri et al., 2010, Yim and Kim, 2016, Yim et al., 2014). The benefit of nanofillers is that they can be mixed homogeneously within the polymer matrix thus enhance the properties of the mixtures. Extensive research has been carried out to study the potential suitability of this nanocomposite in the ICAs system. Nanocomposite ICAs may have the potential to overcome the limitations of conventional micro-composites such as electrical properties (Chrissafis and Bikiaris, 2011).

Generally, CNTs are the most representative of one-dimensional (1D) nanoscale materials. CNTs can be divided into two types of tubes based on their crystalline structures: crystalline CNTs and amorphous CNTs (a-CNTs). Carbon nanotubes have extremely high mechanical strength and toughness, good electrical conductivity, and excellent thermal conductivity (Zhao et al., 2014). A-CNTs have distinct tube wall structures compared with crystalline CNTs. The tube walls are composed of many discontinuous graphene sheets and carbon clusters, which exhibit features of short-range order and long-range disorder, and have many defects, dangling bonds, and huge specific surfaces (Zhao et al., 2014, Zhao et al., 2011, Singh et al., 2012, Ci et al, 2001).

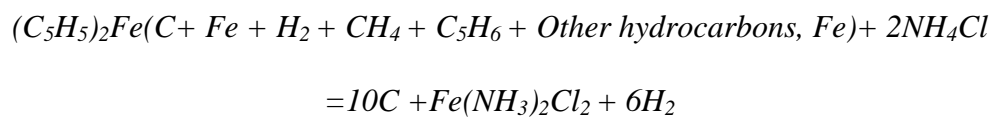
The formation of point defects of the a-CNTs is due to the broken bonding between the atoms during the reactions and graphitization of its crystal structure (Ci et al, 2001). Chu and Li (2006) have suggested that the

amorphous and nanocrystalline carbon films can exist in threefold (sp^2 bonding) and fourfold (sp^3) bonding coordination. The sp^3 dominates to establish a diamond-like framework. In sp^2 , a carbon atom forms three sp^2 orbitals and forming three σ bonds, meanwhile, the remaining p orbital forms a π bond. The π orbital geometrically lies normal to the σ bond plane and is the weaker bond which is closer to the Fermi level, E_f . The three σ bonds and π bond usually constitute a ring plane in sp^2 clusters. However, there is some evidence of sp as well in Cho et al.'s (1992) studies. Generally, graphite consists of sp^2 hybridized bonds, whereas diamond has just sp^3 hybridized bonds. Graphite can easily conduct electricity due to the delocalization of the π bond electrons above and below the planes of the carbon atoms, while diamond-like carbon is totally an insulator. Thus, the characterization of amorphous carbon materials is in terms of the bonding ratio of sp^2/sp^3 which distinguish properties between graphite and diamond. Research is currently ongoing into ways to characterize and expand the range of properties offered by amorphous nanocarbons. In some of the latest findings, a-CNTs possess excellent conductivity even though there are many defects on the tube walls. Due to the large aspect ratio, a-CNTs easily form conductive networks in the composite materials to transfer the electrons (Zhao et al., 2014, Zhao et al., 2011, Singh et al., 2012, Cheung et al., 2016).

The a-CNTs can be easily produced by chemical approaches (Awasthi et al., 2011, Banerjee et al., 2010, Sarkar et al., 2015, Xiong et al., 2004). The benefits of using a-CNTs prepared by chemical synthesis are that it does not require high temperatures, is much more cost effective, and offers

much higher yields. The a-CNTs were prepared by chemical reaction of a mixture of ammonium chloride 1g of ammonium chloride, NH_4Cl , and 0.5g of ferrocene, $\text{Fe}(\text{C}_5\text{H}_5)_2$ and then rinsed through with hydrochloric acid and followed by deionized water (Banerjee et al., 2010). The chemical reactions are described by equation

(2).



(2)

A chemical reaction occurs where the ferrocene (precursor) was reduced into atomic iron and cyclopentadienyl group (C_5H_5) by the metallic sodium as reported in Xiong et al. (2004). Later, the atomic iron agglomerated into the iron cluster that acted as the catalyst to convert hydrocarbon into carbon nanotubes through pyrolysis and catalyzes the decomposition of cyclopentadienyl group into amorphous CNTs. The C_5H_5 group was converted into amorphous CNTs as its structure was non-graphite (Xiong et al., 2004).

In order to obtain purified a-CNTs, the purification steps are relatively crucial. There are many impurities present on the surface of nanotubes, such as disordered carbon, graphite, and fullerenes. Thus, the process purification is essential to remove the metal catalyst, as the electrical and structural properties of carbon nanotubes are affected by those impurities present within the wall structure of carbon nanotubes (Ko et al., 2004).

2.2.6 Electrical Conductivity of ICAs

As discussed earlier, conductive fillers play an important role in determining the electrical conductivity in the ICAs. Generally, ICAs have lower electrical conductivity as compared to conventional solders. In order to improve conductivity, high loading fillers have been incorporated into ICAs systems. The silver paste is added to around 80 wt% of silver powders or silver flakes, which is more than $1 \times 10^{-4} \Omega \cdot \text{cm}$, in bulk resistivity.

In particular, in ICAs, high-cost silver flakes have been used extensively as a booster to increase conductivity. This increases the price of the ICAs. Moreover, a higher loading of the silver as conductive fillers restricts the wide applications of ICAs (Zhang, May 2011). In this research, new formulations of ICAs are investigated to reduce the usage of silver powder in ICAs, yet improve its conductivity by implementing in-house prepared SNPs and a-CNTs.

Several approaches have been studied to improve the electrical conductivity which included the adding of SNPs, multi-walled carbon nanotubes (MWCNTs), single wall carbon nanotubes (SWCNTs) and silver nanowires (Lin and Lin, 2004, Youngseok et al., 2008, Tao et al., 2009, Chen et al., 2010, Wu et al., 2006).

By adding the silver nanoparticles (SNPs) into ICAs at the temperature of 180 °C for one hour, the electrical resistivity was found at $4.8 \times 10^{-5} \Omega \cdot \text{cm}$ based on Zhang et al. (2010) studies. Meanwhile, Wu et al. (2006) studied the electrical resistivity of ICAs by incorporating with silver nanowires and SNPs. It was found that when 56 wt % of nanowires was added into ICAs, resistivity reached $1.2 \times 10^{-4} \Omega \cdot \text{cm}$, which is lower as compared to those with 100 nm silver nanoparticles. It was suggested the tunnelling effects within the nanoparticles enhanced the contact between the conductive fillers and thus increase the conductivity of ICAs. Other reports also indicated that with the addition of silver nanowires and SNPs, a significant change in resistivity was observed (Tao et al, 2009).

The addition of CNTs has shown that electrical conductivity improves dramatically in the ICAs system due to the one-dimensional fillers come in good 3-D contact with epoxy resins. With the addition of 0.24 wt% of MWCNTs, the bulk resistivity of ICAs is around $1.43 \times 10^{-3} \Omega \cdot \text{cm}$. Youngseok et al. (2008) reported that the resistivity of ICAs filled with single-wall CNTs was $5.1 \sim 6.36 \times 10^{-5} \Omega \cdot \text{cm}$, which was significantly (83 %) lower than the commercial silver filled ICAs. Moreover, the acid treated single-wall CNTs should lead to significant results in reducing ICAs resistivity.

Besides SNPs, silver nanowires and carbon nanotubes, the epoxy resin of polymer matrix plays an important role in increasing ICAs conductivity. As suggested by Lu and Wong (2000), the epoxy resin shrinks during curing reactions, which contributed to lower resistivity. In the

formulations with higher cross-linkage, the resistivity of ICAs is around $3 \sim 0.58 \times 10^{-5} \Omega \cdot \text{cm}$.

In this study, before measuring the electrical conductivity of the newly formulated ICAs, it is tested by rheometer to investigate the visco-elastic and thixotropy. Furthermore, it is vital that the new formulation of the prepared pastes is optimized through the addition of nanomaterials and MCC in terms of its rheological properties in order to suit the screen printing applications.

2.3 Rheology Behaviour of Paste in Stencil Printing

Rheology describes the science of the deformation and flow of a matter under fluid or semi-solid conditions. Rheometers are used to determine the rheological properties of a material that function either as a controlled stress or a controlled rate instrument. The measurements of the rheology tests describe the printing behaviour of pastes or solders. During stencil printing, a high pressure forces the paste into the stencil aperture and squeegee blade travels at between 10- 200 mm/s. Apertures are filled and the paste particles are squeezed into the apertures and then stop moving. In the final step, the stencil and a substrate are separated away as the board moves away, the stencil apertures are then empty (Tsai, 2008, Dusek et al., 2002). During this process, the printing media is exposed to different stress levels and time-dependent situation. In order to improve the printability and joint reliability of paste,

rheology of pastes have been studied extensively (Dusek et al., 2002, Durairaj et al., 2009, Durairaj et al., 2013, Durairaj, 2011, Leong, 2016, Shapee, 2012).

Rheological tests play an important role to access the behaviours of pastes corresponding to various stress during stencil printing. There are different types of tests which have been carried out to assess the rheological properties of the pastes, either depending on static properties (viscosity and thixotropy) or dynamic properties (creep and oscillation) (Phair and Kaiser, 2009, Dušek et al., May 2002).

2.3.1 Static Properties: Viscosity and Thixotropic Studies

In static properties, viscosity, flow curve and thixotropic studies were investigated in order to study the paste printability. Viscosity is the main parameter used to measure the flow properties of the paste during printing (Gilleo, 1989). It is a measurement of the resistance of a fluid to an applied stress. The pseudoplasticity or shear thinning of the non-Newtonian fluid exhibit a decreasing viscosity with an increasing shear rate (Barnes, 1997, Hoornstra et al., 1997, Reddy et al., 2015). In addition, the shear thinning behaviour of paste materials is typically addressed that the particles adopting a more flow-oriented arrangement and well-separated particles moving slowly through a viscous fluid (Mewis and Wagner, 2009, Foss and Brady, 2000, Puisto et al., 2015). Shear thinning behaviour is classically described as the

time-dependent reduction of viscosity under a constant shear rate, such as thixotropy.

Moreover, in screen printing, the paste should be thixotropic in nature. When the thixotropic fluid is subjected to the higher shear rate (for instance, mixture of squeegee pressure, velocity or screen tension), the paste turns significantly thinner, resulting in more steady flow (Shapee, 2012). Durairaj et al. (2011) reported that this thixotropic property may be important for understanding the rolling motion of the paste during the printing process as the squeegee pushes the paste back and forth. It is worth noting that excellent thixotropy is quite essential for good processability or printability which showing low viscosity at a higher shear rate.

Thixotropy can be measured using modern rheometers by the 3-interval-time-test (3ITT). Figure 2-1 shows the pattern of viscosity when the paste is in the printing stage. At stage I, the paste is at rest. The first interval (stage II) represents the state at which the paste begins to squeegee. The second interval (stage III) represents the application stage, and the final interval measures the viscosity recovery after the application. For good thixotropy, the original viscosity must be rebound quickly and excellently. The thixotropic indicates that when a paste material is at rest, yet it shows fluid behaviour when subjected to stress. The thixotropy test aims to measure the structural breakdown and recovery of the ICAs, which is reported in terms of recovery index (%).

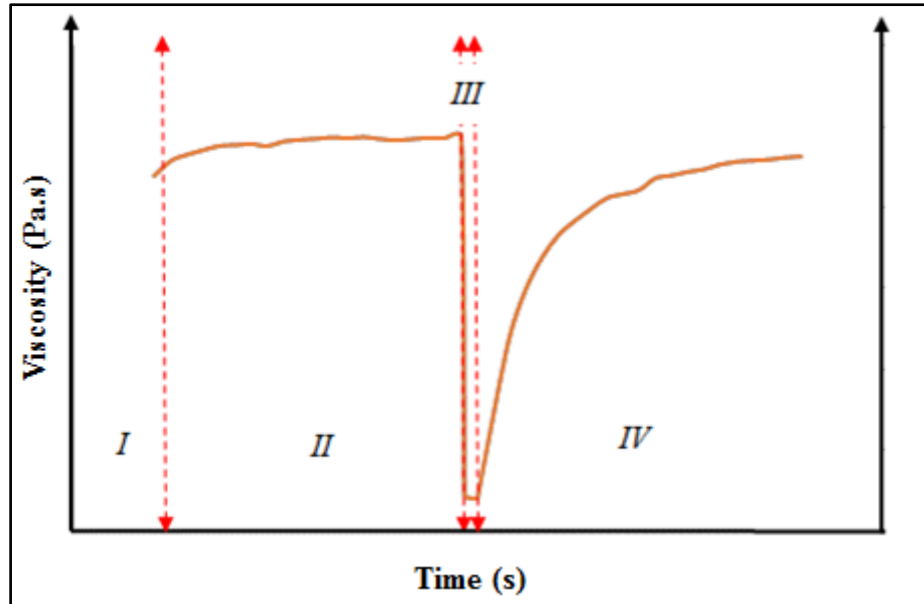


Figure 2-1: Viscosity experienced four stages (I-IV) as a function of time.

Stages I-Rest, II-Squeeze, III-Mesh, IV- Recovery (Kaiser, 2009)

In addition, the recovery (%) between the shear interval and recovery interval in the steady shear rate is measured using equation (3)(Kaiser, 2009, Lam 2011, Patel and Dewettinck, 2015).The structure recovery properties have been evaluated by studying 3ITT. Viscosity changes were followed as a function of time under alternative intervals of low and high shear rates. Ideally, a sample is considered to have a good thixotropic recovery if the peak viscosity value in the third interval is at least 70% of the viscosity value obtained at the end of the first interval (Patel and Dewettinck, 2015, Hong et al., 2013).

$$Recovery (\%) = 100 - \left(\frac{Viscosity (rest) - Viscosity (recovery)}{Viscosity (rest)} \times 100\% \right) \quad (3)$$

Typically, thixotropic properties are measured via hysteresis loop test. The region in between the upward curve and downward curve in hysteresis curve is evidence of thixotropic behaviour of the paste (Durairaj, 2011, Lam, 2011). The smaller hysteresis loop area demonstrates that the structure within the inter-particles and composite materials in ICAs would recover at a much faster speed as compared to bigger hysteresis loop area (Durairaj, 2011).

2.3.2 Dynamic Properties: Oscillation and Creep

In dynamic properties, oscillation and creep tests were investigated in order to access the tackiness and slump propensity of the paste. Oscillatory rheology performs a sinusoidal shear deformation in the sample to measure the resultant stress response which characterized by storage modulus, G' (elastic) and loss modulus, G'' (viscous). If $G' > G''$, the paste is predominantly to possess elastic behaviour throughout the test. Materials that exhibit elastic and viscous properties simultaneously are known as visco-elastic materials. (Durairaj et al., 2008, Durairaj and Man, 2011, Mallik et al., 2008)

In the oscillation test, the paste behaviour in the viscoelastic range can be determined. The tackiness of the paste can be described as the ratio of G''/G' . When the ratio of G''/G' is high, the paste is less cohesive or tackiness and suitable for screen printing process (Durairaj et al., 2009, Durairaj and Man, 2011, Phair and Kaiser, 2009). However, the linear visco-elastic region (LVER) can also be determined in the oscillation test. The linear visco-elastic

region is measured up to a constant (plateau) modulus value before the storage modulus declines on the graph. In the larger length of LVER, pastes are more stable and well-dispersed in suspension (Bao et al., 1998, Lam, 2011, Koe, 2012). Beyond the LVER is the point at which the material's structure begins to break down.

Frequency sweep test is the other type of oscillatory test which is to study the effect of timescale on the elastic and viscous behaviour of the paste. In the test results, when the loss modulus G'' is higher than storage modulus G' , it is considered as a weak structure and there is a strong possibility that sedimentation could occur (Hong et al., 2013, Lam, 2011, Mir and Kumar, 2008). This information proves that the paste can be kept for a longer period without settling down.

Creep test is another technique in the dynamic analysis of rheology to determine the levelling scenarios and slump propensity in the degree of relaxation after an applied stress has been removed. During the test, the sample is subjected to a constant stress and the deformation in strain is recorded as shown in Figure 2-2. The creep recovery index can be measured by equation

(4), with ratio J_3 to J_2 (dimensionless) defining the tendency to paste slump. If creep recovery index is = 1, then there is no recovery, whereby the paste a higher tendency to slump. However, when the creep recovery index is < 1, there is some amount of recovery and thus a lower tendency to slump (Nguty et al., 1999, Nguty et al., 1998).

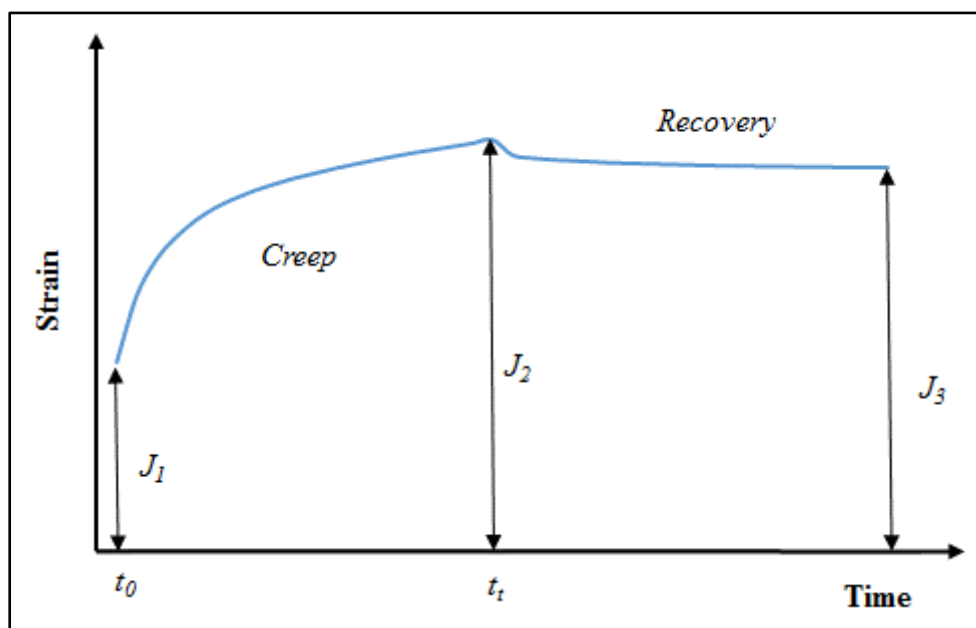


Figure 2-2: Creep recovery profile(Nguty et al., 1998)

$$CreepRecoveryIndex = \left(\frac{J_3}{J_2}\right)$$

(4)

2.4 Thermal Behaviour of the ICAs

In addition to rheological properties, gelation points and thermal stability of the ICAs were studied by dynamic mechanical thermal analysis (DMTA) and thermogravimetric analysis (TGA). In DMTA, the visco-elastic behaviour of the paste was measured with the changes of time. The gelation points were identified as the crossover values of storage modulus (G') and loss modulus (G''). Gelation happens when the cross-linked structure starts to form. The

degree of chemical conversion at which the cross-linked structure first forms is called the gel point (Núñez et al., 2001). It is an irreversible transformation from liquid-like to solid-like behaviour (Pearce et al., 1981). Malkin and Kulichikhin (1981) described gelation as a process of fluidity loss due to the formation of chemical bonds network (Malkin et al., 1984).

After the gelation point, the material cannot flow like a true liquid. At this point, the mechanical loss tangent becomes independent of frequency and it indicates the starting point of gelation. In short, the macroscopic determination of the gelation point may be based on mechanical and rheological changes that occur when the material begins to change from liquid to rubber. For the mechanical aspect, gelation happens at the equilibrium of G' and G'' modulus while the rheological aspect accounts for the changes in viscosity (Pittroff, 2007). A lower gelation temperature is usually desired, as this will allow cross-linking and formation of a long network across the specimens to occur faster at a lower temperature. It is suggested that as cross-linking happens faster, the paste will cure at a faster rate.

CHAPTER 3

METHODOLOGY

3.1 Introduction

This chapter describes the chemical approaches used to prepare silver nanoparticles (SNPs) and amorphous carbon nanotubes (a-CNTs). To further confirm the nano structure of the synthesized SNPs and a-CNTs, a series of characterization tools were used. The second part presents the methods used to investigate the rheological behaviour, weight loss and gelation point of the new isotropic conductive adhesives (ICAs) formulations. Finally, the methods used to measure the electrical resistivity of the ICAs are described.

Ultraviolet–visible spectroscopy (UV-Vis), Fourier transform infrared spectroscopy (FTIR), X-ray diffraction (XRD), Raman Spectroscopy, field emission scanning electron microscope (FESEM), energy dispersive X-ray (EDX) and high-resolution transmission electron microscopy (HRTEM) were used to characterize the synthesized SNPs and a-CNTs.

An Anton Paar Physica MCR 301 controlled-stress rheometer was used to study the rheology behaviours of ICAs. The gelation points and weight loss of the new ICAs formulations were investigated by dynamic mechanical

thermal analysis (DMTA) and thermogravimetric analysis (TGA), respectively. Four-point probes were used to measure the electrical conductivities of ICAs.

3.2 Materials

The basic materials of the ICAs are polymer matrix or epoxy resin, conductive fillers and curing agents. In this study, diglycidyl ether of bisphenol-A (DGEBA), $C_{21}H_{24}O_4$ was used as the epoxy resin, silver (Ag) powder was used as the conductive filler, ethylenediamine (EDA), $C_{18}H_{21}NO$ was used as the curing agent. In this study, silver nanoparticles (SNPs) and amorphous carbon nanotubes (a-CNTs) were synthesized by chemical approaches. Silver nitrate ($AgNO_3$) and sodium borohydride ($NaBH_4$), ferrocene, $Fe(C_5H_5)_2$, and ammonium chloride, NH_4Cl , hydrochloric acid, HCl were used. The microcrystalline cellulose (MCC) solution was prepared in the laboratory. MCC, sodium hydroxide ($NaOH$) and urea ($CO(NH_2)_2$) were used. Most chemicals were purchased from Sigma-Aldrich Company. Meanwhile, EDA was purchased from Merck Company. The chemical reagents were used without any further purification. Table 3-1 shows a list of chemicals used in the preparation of isotropic conductive adhesives (ICAs).

Table 3-1: All chemicals used in the preparation of ICAs

Chemical Functions		Chemicals	Manufacturers
Polymer matrix	Epoxy resin	Diglycidyl Ether of Bisphenol-A (DGEBA)	Sigma-Aldrich Co.
	Biodegradable polymer	Microcrystalline cellulose (MCC) powder Urea Sodium hydroxide, NaOH	Sigma-Aldrich Co.
Conductive fillers		Silver (Ag) powder (44 μ m)	Sigma-Aldrich Co.
		SNPs (In house prepared) Silver nitrate (AgNO ₃) and sodium borohydride (NaBH ₄)	Sigma-Aldrich Co.
		a-CNTs (In house prepared) Ferrocene, Fe(C ₅ H ₅) ₂ , and ammonium chloride, NH ₄ Cl, hydrochloric acid, HCl	Sigma-Aldrich Co.
Curing agents		Ethylenediamine (EDA)	Merck and Co.

3.3 Synthesis Silver Nanoparticles (SNPs)

Silver nanoparticles were synthesized by reducing silver nitrate (AgNO_3) with sodium borohydride (NaBH_4) at a ratio of 1:2 molar concentrations, respectively. Excessive sodium borohydride was needed in order to reduce the ionic silver and stabilize the SNPs that formed. A 30-mL volume of 1.0 mM silver nitrate was added dropwise to 90 mL volume of 2.0 mM sodium borohydride at room temperature. A greyish precipitation was formed and filtered. It was then dried at room temperature for 24 hours.

X-ray diffraction studies of the SNPs have been carried out using a Shimadzu, XRD 6000 with X-rays of wavelength (λ) = 1.54056 Å in the 2θ range of 20° to 70° . The size and morphology of SNPs were obtained by Field Emission Scanning electron microscope (FESEM), JEOL JSM-6701F. Energy Dispersive X-ray (EDX) was used to analyse the SNPs compositions. Whilst, the UV-Visible studies were investigated by CARY 100 Conc UV-VIS spectrophotometer in the wavelength range of 200 nm to 800 nm to investigate its Plasmon resonance.

3.4 Synthesis and Purification of amorphous carbon nanotubes (a-CNTs)

Amorphous carbon nanotubes (a-CNTs) were produced by the mixture of ferrocene ($\text{Fe}(\text{C}_5\text{H}_5)_2$) and ammonium chloride (NH_4Cl) at a ratio of 1:2. They were then heated inside an oven at 200°C for 40 minutes and allowed to cool

to room temperature. Dark colour mixtures were obtained and labelled as untreated a-CNTs.

In order to purify the as prepared a-CNTs, the untreated samples were soaked with 5M HCl for 24 hours to remove the impurities. A precipitate was filtered and washed three times with distilled water with the aid of centrifuge at 3000 rpm for 15 minutes. The precipitate was then dried in an oven for 30 °C for a day. The sample was labelled as treated a-CNTs.

3.5 Characterization Methods of Synthesized SNPs and a-CNTs

X-ray diffraction studies of the a-CNTs have been carried out using Shimadzu, XRD 6000 with X-rays of wavelength (λ) = 1.54056 Å in the 2θ range of 20° to 70°. The tube size and morphology of a-CNTs were obtained by Field Emission Scanning Electron Microscope (FESEM), JEOL JSM-6701F and High-Resolution Transmission Electron Microscope (HRTEM), JEOL 2100 F TEM. While, Selected Area Electron Diffraction (SAED) for crystallographic analysis. Energy Dispersive X-ray (EDX) was used to analyses the a-CNTs compositions. A 514 nm wavelength laser Raman spectroscope from Renishaw was used to characterize the a-CNTs. A Fourier Transform Infrared Spectrometer (FTIR) from Thermo SCIENTIFIC was used to characterize the untreated and treated a-CNTs.

3.5.1 X-ray Diffraction (XRD)

X-ray Diffraction studies of the synthesized SNPs and a-CNTs have been carried out using Shimadzu, XRD 6000 with X-rays of wavelength (λ) = 1.54056 Å in the 2θ range of 20° to 70° . In this study, XRD was used to investigate the crystallinity of synthesized SNPs and a-CNTs. It was used to determine the crystallite size of SNPs. XRD is a powerful tool to identify the ‘fingerprint’ of crystalline materials.

X-rays are produced by bombarding a specific metal such as copper with electron beams emitted from a hot filament (tungsten). Bragg law was discovered in 1913 by physicists Sir W.H. Bragg and his son Sir W.L. Bragg. X-ray wave interference is derived from the reflected X-ray beams at different angles of incidence at a particular wavelength.

Before performing the tests, the specimen was placed on an aluminium flat plate and compacted by a glass slide. The test procedure was set at a step size of 4° per minute at 50 kV and 40 mA.

3.5.2 Ultraviolet–Visible Spectroscopy (UV-VIS)

UV-VIS has been used to identify the absorption and reflectance spectroscopy of a sample within the ultraviolet-visible spectral region. When a material absorbs energy from the ultraviolet or visible light, it excites the electrons to a higher energy band; the more easily excited electrons, the longer the

wavelength of electromagnetic spectrum absorbed. The diffraction grating separates the wavelength of the light source thus the intensity of the light can be measured as a function of wavelength. The detector detects the beam intensity of the light source and the beam intensity after passing through the light source. The difference in intensity, or in another word different wavelengths, are known and the absorbance of the specimen can thus be measured.

The specimen with few milligrams was suspended in 20 ml of distilled water and dispersed by immersion into an ultrasonic cleaner at a frequency of 5 Hz at room temperature for 60 minutes. Eventually, 1 ml of the colloid was taken for testing. The data of testing was interpreted. Whilst, the UV-Visible studies were investigated by CARY 100 Conc UV-VIS spectrophotometer in the wavelength range of 200 nm to 800 nm at 600 nm/min scan rate.

3.5.3 Fourier Transform Infrared Spectroscopy (FTIR)

Fourier Transform Infrared Spectrometer (FTIR), Thermo SCIENTIFIC was used to characterize the untreated and treated a-CNTs (with HCl). The infrared spectra of the specimens were obtained corresponds to the frequencies of vibrations between the bonds of the atoms making up within the materials. Infrared spectroscopy results indicate the qualitative analysis of a-CNTs before and after purification of HCl at different wavenumber. This corresponds to different kind of compounds, bonding, and elements present in

the sample. The absorption peak consists in the spectra refer to the presence of that particular compound in a specimen.

Attenuated total reflectance (ATR) was used as the examination method due to none sample preparation steps before testing. The measurement was set from 400 to 4000 cm^{-1} at 45° angle of incidence. It measures the changes that occur in total internal reflected infrared beam when the beam contacts with the sample. The spectrums of absorption and transmission of the molecule were recorded.

3.5.4 Raman Spectroscopy

A 514-nm wavelength laser Raman spectroscopy from Renishaw was used to characterize the a-CNTs. Raman spectroscopy provides the information of the molecular through the vibration, rotational, or low-frequency modes in the system. Through the unique vibration of each molecular, the unknown samples were identified. The spectroscopy uses the inelastic scattering of monochromatic light which generated from a laser source. The phrase of inelastic scattering is referring to the frequency of photons in monochromatic light varies with contact of the sample. When the photons emitted from the laser source, the sample will absorb and reemit the photon back to the detector. Thus, the frequency of reemitted photons is used to compare with the frequency of original monochromatic light. The powder sample was placed on the glass slide and the test was started.

3.5.5 Field Emission Scanning Electron Microscope (FESEM) and Energy Dispersive X-ray (EDX)

FESEM uses higher energy electrons beam generated by field emission to capture images at higher magnifications, especially for nanomaterials. By using the FESEM, the surface morphologies of SNPs and a-CNTs can be observed. The EDX analysis was attached to the FESEM, and the X-ray technique was used to verify the elemental composition. The peak of spectra and its mappings were generated by this analysis corresponding to the presence of the element in the specimens.

The characterization test was conducted by JEOL JSM-6701F, FESEM at an accelerating voltage of 15 kV and the surface morphologies were studied. The samples were coated with platinum to minimize the charging effect and enhance imaging quality.

3.5.6 High-Resolution Transmission Electron Microscope (HRTEM)

High-Resolution Transmission Electron Microscope (HRTEM), JEOL 2100 F TEM was used in this study. While Selected Area Electron Diffraction (SAED) was equipped to verify its crystallographic analysis. HRTEM provides the structural information at 0.2nm spatial resolution which is better than FESEM. HRTEM image shows the distribution and structure of defects, interfaces and

grain boundaries, none crystalline or crystal arrangement (SAED), and morphological features of the prepared specimen.

Samples were prepared before carrying out the tests. About 10 ml of ethanol was added to few milligrams of sample powder and kept in a closed tube. The mixture was then dispersed by an ultrasonic cleaner at a frequency of 5 Hz for few hours. Next, a drop of resultant colloidal was deposited on a Formvar-covered carbon-coated copper grid of 300 mesh and dried on filter paper and then it was placed in a desiccator at room temperature for three days. SAED was performed in this test in order to determine the crystallographic nature of the specimen.

3.6 Preparation of Microcrystalline Cellulose (MCC) Solution

The MCC solution was prepared by using the similar method by Ma et al. (2012). 7.00 g of sodium hydroxide (NaOH) and 12.00 g of urea ($\text{CO}(\text{NH}_2)_2$) were added into 81 mL of distilled water under vigorous stirring. It was then stirred vigorously on a magnetic stir plate at room temperature for 30 minutes. Next, 3.24 g of MCC was added into the NaOH/urea aqueous solution and stirred for 10 minutes. It was cooled in a freezer at $-12\text{ }^\circ\text{C}$ for 12 h.

3.7 Preparation of ICA Samples

In the early stage of this study, ten formulated ICAs samples were prepared as shown in Table 3-2. The samples were prepared accordingly to a different

composition of nanomaterials, for instance, SNPs and a-CNTs and additional of MCC solution. The remaining material was the silver powder. This approach was used to study the effects of those compositions on rheological properties, thermal properties, and electrical properties. Based on the optimize results from the mentioned analysis. There were 45 ICAs samples compositions as shown in Appendix A were generated by response surface, three-level factorial, Design of Experimental (DOE) using Design Expert 6.0. This was used to study the effects of varying compositions of a-CNTs, MCC, and DGEBA on electrical conductivity.

Table 3-2: The formulation of different samples with different composition of polymer matrix and fillers

Sample	Matrix (wt%)		Filler (wt%)
	DGEBA	MCC	SNPs / a-CNTs
S1	40	0	1 (SNPs)
S2	40	0	2 (SNPs)
S3	40	0	4 (SNPs)
S4	40	0	6 (SNPs)
S5	40	0	8 (SNPs)
S6	40	0	10 (SNPs)
S7	35	5	10 (SNPs)
S8	30	10	10 (SNPs)
S9	40	0	1 (a-CNTs)
S10	40	0	2 (a-CNTs)

Firstly, the Diglycidyl Ether of Bisphenol-A (DGEBA) epoxy resin was added to the weighing dish and followed by silver powder and SNPs, a-CNTs, MCC solution. The mixture was mechanically mixed for 30 minutes and sonicated for five minutes to ensure the materials to be thoroughly and homogeneously mixed into paste form. Finally, samples were mixed with the ratio of curing agent, ethylenediamine (EDA) to DGEBA is 0.088:1 (Appendix B) based on their stoichiometric quantities. The mixtures were placed inside a

mould and initial cured under the fume hood for approximately 24 hours. It was then heated at 100°C in a vacuum oven for 2 hours.

The rheological properties of ICAs were investigated using Physica MCR 301 controlled stress rheometer. The gelation studies were recorded by Dynamics Mechanical Thermal Analysis (DMTA) with convection heating system CTD 450 device, Physica MCR 301 controlled-stress rheometer from Anton Paar. Thermogravimetric analysis (TGA) of ICAs were carried out by using Mettler Toledo TGA/SDTA851 machine. The electrical conductivity of the ICAs was characterized by the bulk resistivity of cured ICAs using Keithley 4200. A flow chart for this study is shown in Figure 3-1.

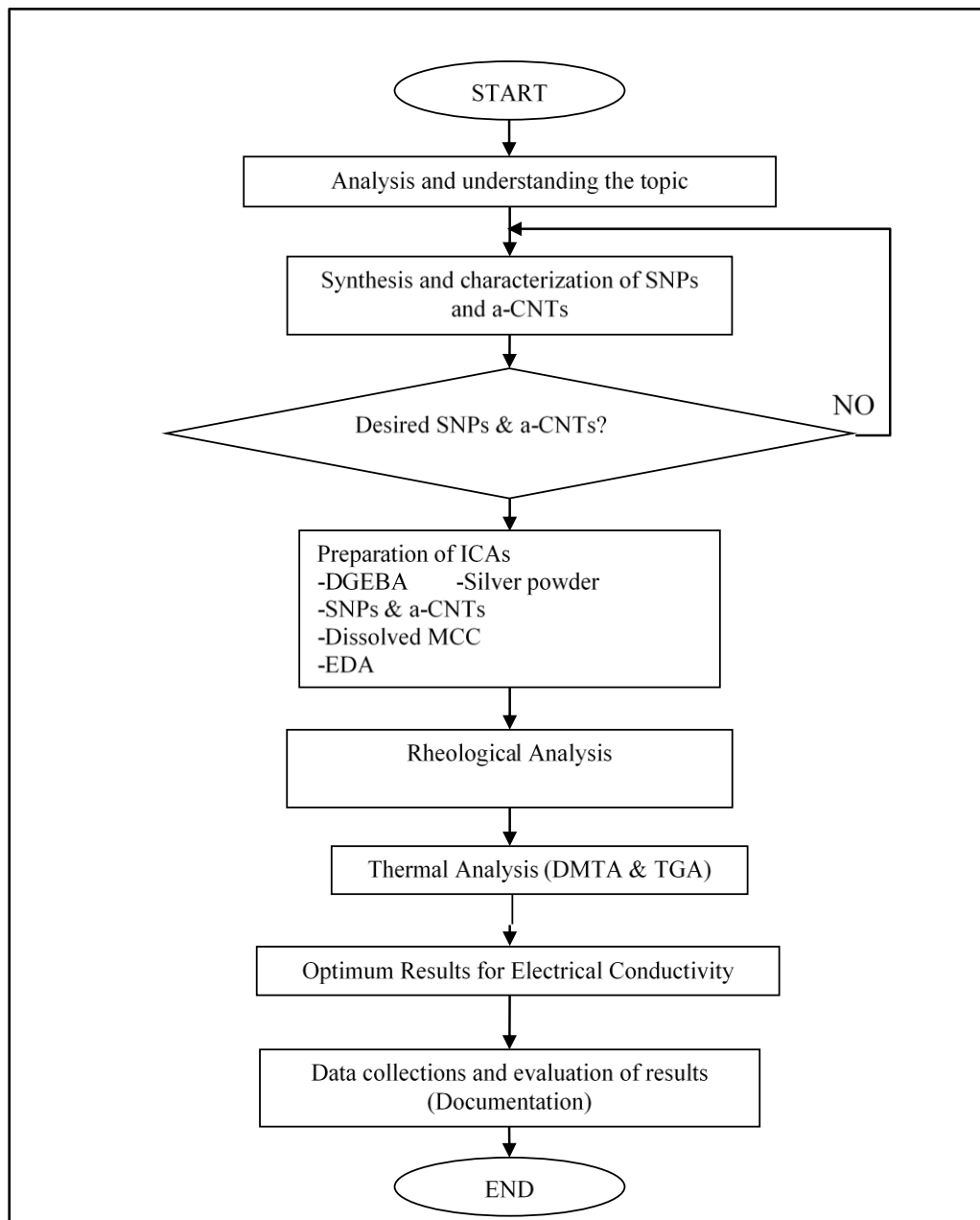


Figure 3-1: Flow chart of the study

3.8 Rheometry

In this work, an Anton Paar Physica MCR 301 controlled-stress rheometer was used to study the rheology behaviours of ICAs. A parallel plate with 25 mm diameter (PP25) was chosen in this test in order to minimize the effect of wall-slip between the plate and samples. The gap between upper and lower plate was set to 0.5 mm. The measurement temperature was set to 25 °C. The temperature of the rheometer parallel plate was controlled by using the Peltier-Plate system. There were a series of tests have been carried in order to confirm the flow character of ICAs, such as constant shear rate vs time; amplitude sweep; frequency sweep; hysteresis; three interval thixotropy test (3ITT); and creep recovery. The parameters used for each test are tabulated in Table 3-3 to Table 3-8.

Table 3-3: Experimental parameters of constant shear rate test

Experimental Values			
Constant Shear Rate (s^{-1})	Number of measuring points	Interval between measuring points (s)	Overall Duration (s)
25	20	6	120

Table 3-4: Experimental parameters of oscillatory stress sweep (OSS) test

Experimental values					
Strain (%)	Angular frequency (s^{-1})	Number of measuring points		Interval between measuring points (s)	Overall duration (s)
0.01 – 100	10	30		5	150

Table 3-5: Experimental parameters of frequency sweep test

Experimental values					
Strain (%)	Angular frequency (s^{-1})	Number of measuring points		Interval between measuring points (s)	Overall duration (s)
0.1	0.1 – 100	30		5	150

Table 3-6: Experimental parameters of hysteresis loop test

Experimental Values					
Low Shear Rate (s^{-1})	High Shear Rate (s^{-1})	Number of measuring points		Interval between measuring points (s)	Overall Duration (s)
1	10	20	20	5	200

Table 3-7: Experimental parameters of Thixotropy test

Experimental Values				
Shear Rate (s ⁻¹)	Number of measuring points		Interval between measuring points (s)	Overall Duration (s)
0.25	4	4	5	20
0.1	20	20	5	100
10	10	10	0.5	5
0.1	20	20	5	100

Table 3-8: Experimental parameters of creep recovery test

Experimental Values				
Constant Shear Stress (Pa)	Number of measuring point		Interval between measuring point (s)	Overall Duration (s)
5	20	20	6	240

Before loading the sample to the Peltier plate, the sample was stirred for a few minutes to ensure homogenously of the paste. The sample was monitored using ‘Start Rheoplus’ software. The geometry plate was lowered until it reached a gap of 0.5 mm from the bottom plate. The excess sample around the edge of the plate was trimmed using a spatula. Meanwhile, the sample was allowed to rest for about 60 seconds before starting the test. This ensured that the sample had reached its equilibrium state. Once the test was completed, the upper geometry plate was lifted up automatically by the computer to its original position. Before measuring another test, the parallel

plates were cleaned using ethanol to ensure that no leftover paste was brought forward to the next sample. New samples were used for each test.

3.9 Thermal Behaviour ICAs by DMTA and TGA

To study the gelation behaviour and weight loss of the newly formulated ICAs, Dynamic Mechanical Thermal Analysis (DMTA) and Thermogravimetric Analysis (TGA) were used.

3.9.1 Dynamic Mechanical Thermal Analysis (DMTA)

DMTA was used to determine the storage modulus, (G') and loss modulus, (G'') as a function of temperature, frequency or time. From the tests, the gelation temperatures of each specimen were obtained from the cross-over point between storage modulus (G') and loss modulus (G'') curves. The Anton Paar Physica MCR 301 controlled stress rheometer with convection heating system CTD 450 was used to perform DMTA test of the formulated ICAs. Four grams of test samples were prepared for the test. Parallel plate geometry was chosen by using the disposable dish and plate. The gap between the disposable dish and plate was set to 0.5 mm. The temperature ramp test was chosen and all samples were initially uncured. A constant frequency of 1 Hz was used for all samples. The temperature ramp rate was set as 5 °C/min, and the temperature range was set from 50 °C to 130 °C. The experimental parameters are summarised in Table 3-9.

Table 3-9: Experimental parameters for the DMTA test

Experimental values	
Strain (%)	0.01 - 10
Frequency (Hz)	1
Temperature ramp rate (°C/min)	5
Temperature range (°C)	50 – 130
Number of measuring points	201
Interval between measuring points (min)	0.2
Overall duration (min)	40.2

3.9.2 Thermogravimetric Analysis (TGA)

Thermogravimetric analysis was used to identify the changes in physical and chemical properties of the specimen as the function of temperature. TGA is usually used for compositional analysis, kinetic studies, material characterization and thermal stability of the specimen. The samples which characterized by TGA, recording the weight loss or gain due to decomposition, oxidation or volatility of the sample under thermal condition. The TGA curve was then analysed to obtain qualitative information on the thermal stability of formulated ICAs by performed range of temperature.

Thermogravimetric analysis (TGA) test was carried out by using Mettler Toledo, TGA/SDTA851 instrument. The scans were performed at a rate of 6 °C/min in the temperature range from 25 to 900 °C. Air flow was kept at a rate of 50 mL/min in all experiments. The sample mass for each experiment was not more than 15 mg.

3.10 Measurement of Electrical Conductivity by Four-Points Probes

In this research, the electrical properties of the ICAs were measured by the bulk resistivity of cured samples. The bulk resistivity of the 45 samples was determined with the aid of four points probe. The specimens were cast on a silicone mould and as shown in Figure 3-2. The length of the mould was 49.66 mm, with a width of 7.46 mm and thickness of 3.24 mm. The probes were placed in a distance of 8.27 mm at the specimen, this is to measure the voltage that passed through the specimen at constant current, 0.105 A. The bulk resistivity was calculated using equation (5) (Fan et al., 2011):

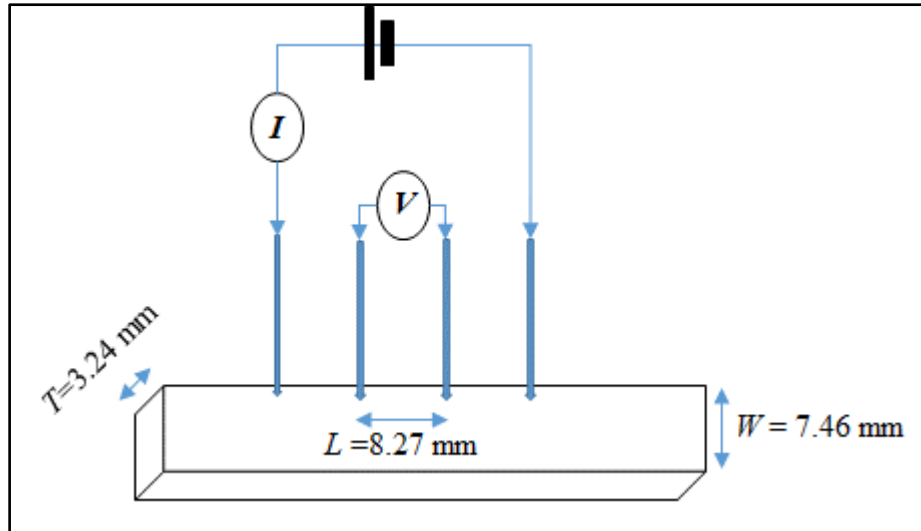


Figure 3-2: Schematic diagram of the test circuit for measuring bar specimen resistivity with the four-point probe method

$$\rho = \frac{VWT}{IL} \quad (5)$$

where,

ρ = bulk resistivity, $\Omega \cdot \text{cm}$

V = voltage, V

I = current, 0.105 A

$W = T = L$ = length, mm

$WT/L = 0.2919 \text{ cm}$

$WT/IL = 2.78 \text{ cm/A}$

The bulk resistivity of the 45 ICAs samples were plotted using Polynomial Curve Fitting by MATLAB™. In order to reduce the errors on the resulted bulk resistivity data, curve fitting was applied. The numerical software of MATLAB™ computed the coefficients in the least squares method to best fit the data (Weisstein E., 2017). In the 3 surface fitting, the

data was fit by a polynomial function as shown in equation (6). In the 2D curve fitting, the data was fit by the second degree of polynomial as shown in equation (7).

$$f(z) = a_0 + a_1x + a_2y + a_3 x^2 + a_4xy + a_5y^2 \tag{6}$$

$$y = b_1x^2 + b_2x + b_3 \tag{7}$$

The polynomial coefficients vector, a and b were calculated by MATLAB. Then, the surfaces and curves of the bulk resistivity were plotted.

CHAPTER 4

STUDY OF THE NANOSTRUCTURE OF SNPS AND A-CNTS

4.1 Introduction

In this chapter, characterization of SNPs and a-CNTs are discussed. In order to study the nanostructure of SNPs and a-CNTs, a few characterization methods were used. The results obtained from Field Emission Scanning Electron Microscopy (FESEM) and Energy-Dispersive X-ray spectroscopy (EDX); X-ray Diffraction; UV-Visible; High-Resolution Transmission Electron Microscope (HRTEM); Raman spectroscopy and Fourier Transform Infrared Spectrometer (FTIR) were presented.

4.2 Results and Discussion

4.2.1 Characterization of synthesized Silver Nanoparticles (SNPs)

Figure 4-1 shows the X-ray diffraction pattern of SNPs synthesized by chemical reduction using sodium borohydride and silver nitrate. All peaks correspond to the pure silver metal with face centred cubic symmetry (JCPDS, no 04-0783) (Li et al., 2015). The reflections were indexed as (111), (200) and (220) with 2θ values of 38.1691, 44.3483 and 64.5150, respectively. The intensity of peaks reflected the high degree of crystallinity of the silver

nanoparticles. The high intense peak for FCC materials is generally (1 1 1) reflection, which is observed in the sample. The XRD shows that silver nanoparticles formed are crystalline in structure.

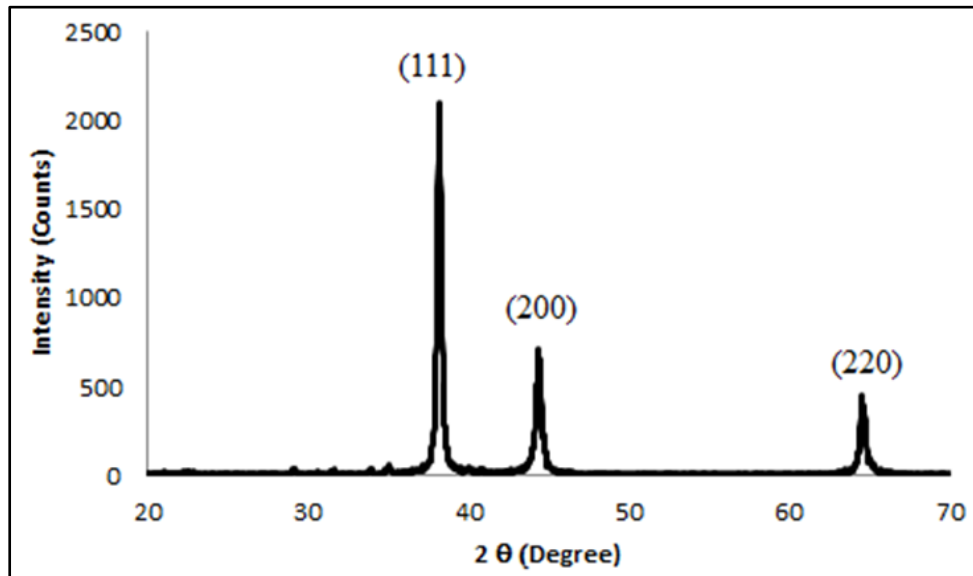


Figure 4-1: X-ray diffraction patterns of synthesized SNPs

The UV-VIS absorption spectra of synthesized the SNPs is shown in Figure 4-2. A strong absorption peak is observed at 402 nm when the frequency of the electromagnetic field is resonant with the coherent movement of electrons. Factors such as dielectric medium, particle size, and chemical surroundings significantly affect the absorption spectra. As reported by some researchers, the appearance of such a band in UV-VIS spectrum is a consequence of the excitation of surface plasmon resonance band (SPR) of spherical SNPs (Wani et al., 2011, Aswathy et al., 2011, Quang Huy et al., 2013). However, based on Brown et al. (2000), the full width at half maximum (FWHM) from the UV-Vis data, is correlated to the diameter size of the colloidal nanoparticles. As stated, the 12 nm diameters of nanoparticles were

observed when the FWHM is more than 85 nm (Brown et al., 2000). In this study, the FWHM of colloidal SNPs is 120 nm. This indicates that silver has been successfully produced in nano range size.

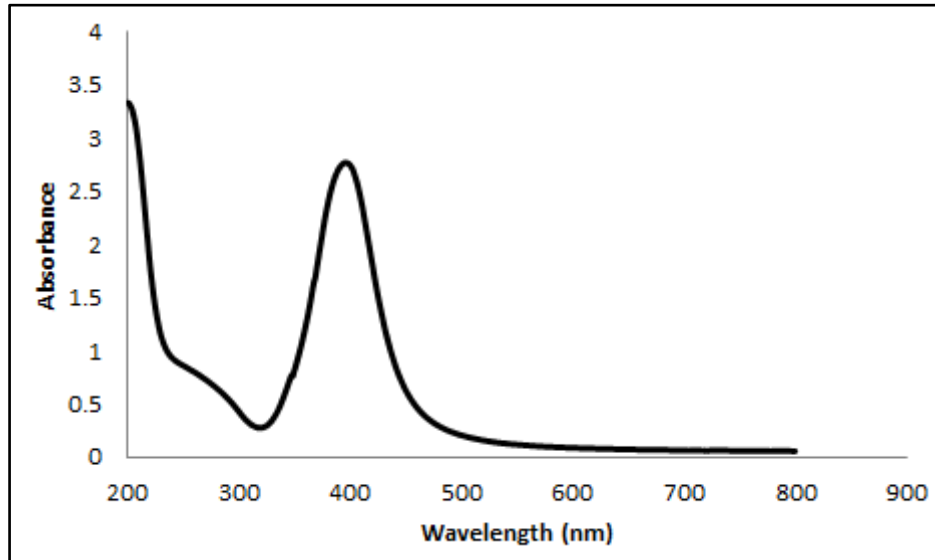


Figure 4-2: UV-Vis absorption Spectra of synthesized SNPs

The size and its structure were further confirmed by FESEM. Figure 4-3 shows the microstructure of synthesized SNPs. The surface morphology of SNPs is spherical and the average size of particles is 15.13 nm. However, the SNPs tend to agglomerate into larger size, some are more than 100 nm.

The spectrum obtained from EDX studies is shown in Figure 4-4. It is found that high content of silver was present in the examined sample. The peaks can be identified at 3.0, 3.2, and 3.4 keV. These peaks correspond to the binding energies of silver at $Ag L_{\alpha}$, $Ag L_{\beta}$, and $Ag L_{\beta 2}$, respectively (Quang Huy et al., 2013, Majeed Khan et al., 2011). There are no other element peaks

were detected. Thus, the EDX profile of the sample has shown that the synthesized SNPs are of pure silver with no oxide.

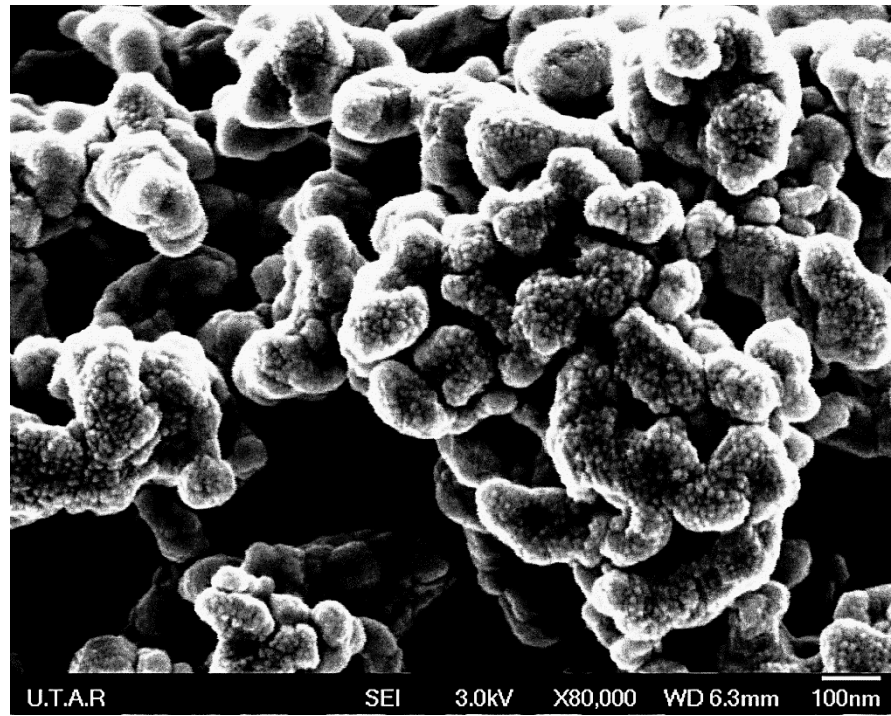


Figure 4-3: FESEM images of synthesized SNPs

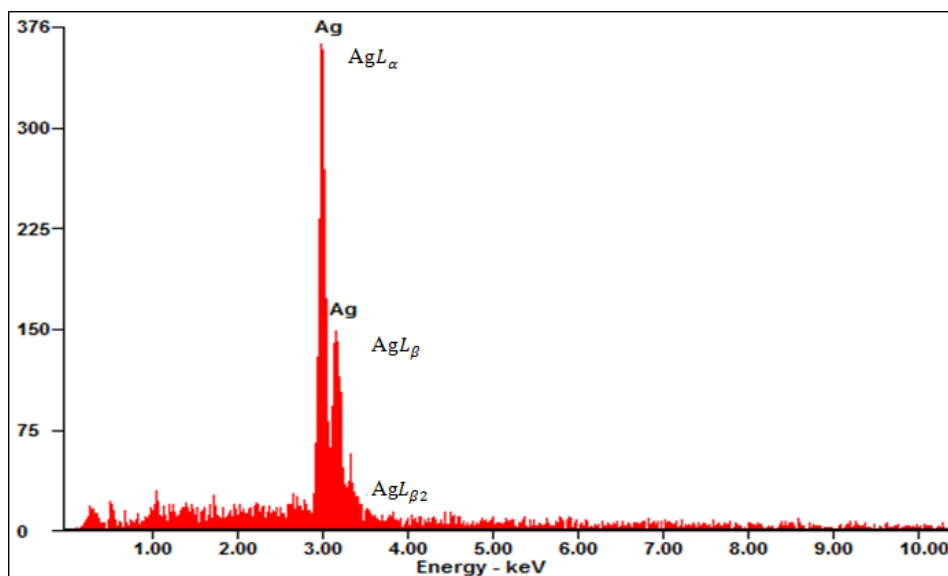


Figure 4-4: X-ray spectra obtained by EDX analysis on the synthesized SNPs sample

4.2.2 Characterization of synthesized amorphous carbon nanotubes (a-CNTs)

Figure 4-5 shows the XRD pattern of untreated a-CNTs and treated a-CNTs. In the diffractogram of the untreated a-CNTs, a small bump can be observed at 26° . This broad peak indicates the amorphous structure of the synthesized CNTs, which is similar to related findings (Xiong et al., 2004, Tan et al., 2012, Sarkar et al., 2015). However, all other peaks found from the untreated a-CNTs are corresponded to ammonium chloride (JCPDS, no 07-0007) and aluminium (JCPDS, no 04-0787), respectively. The aluminium peaks were found to belong to the XRD sample holder. Whilst, the ammonium chloride salt was found as the untreated a-CNTs were surrounded by NH_4Cl before treated with hydrochloric acid. Once treated and washed with 5 M HCl, the ammonium chloride peaks were no longer found as it is shown in Figure 4-5. A very broad peak can be seen in the treated sample. It is clearly shown that the synthesized carbon nanotubes are an amorphous structure.

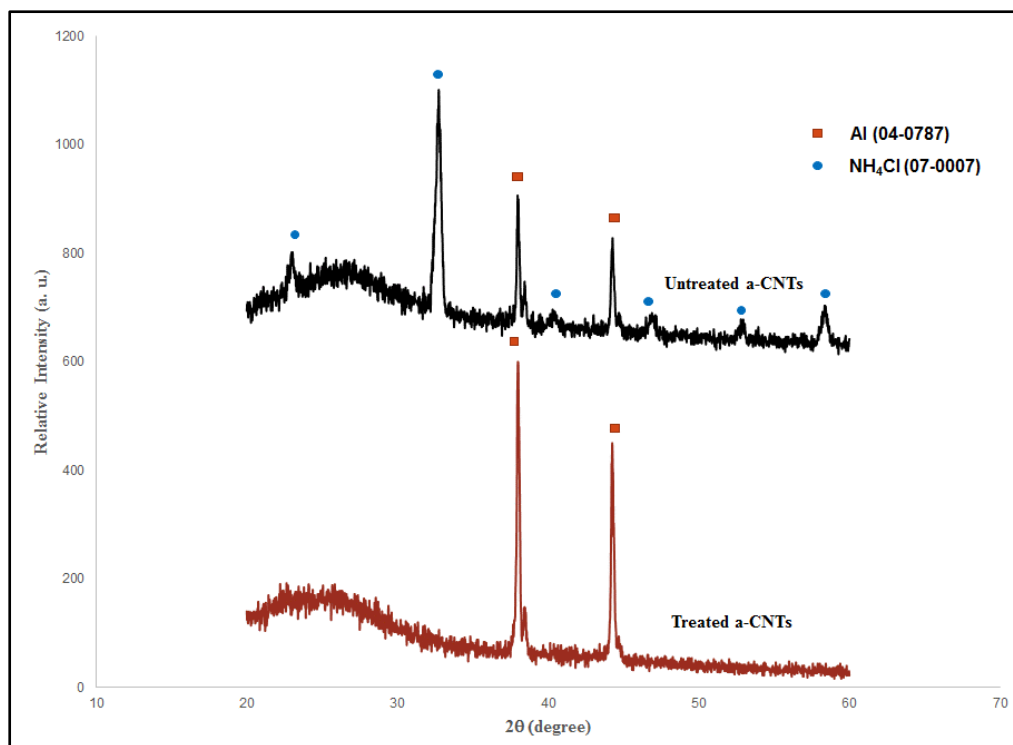


Figure 4-5: X-ray diffraction patterns of untreated and treated a-CNTs

The quality of the a-CNTs is indicated by Raman spectra shown in Figure 4-6. There are two characteristic peaks were observed deriving from the untreated and treated a-CNTs. It is corresponded to D and G bands of nanotubes, at around 1360 cm^{-1} , 1580 cm^{-1} , respectively. The D band shows the presence of defects such as sp^3 carbon system, foreign atoms, and lattice distortions in the carbon structures (K.H. Tan et al. 2013, Yang et al., 2015). However, G band indicates the tangential modes of CNTs and relate to all sp^2 carbon system (Yang et al., 2015). The intensity ratios between the D band and G band (I_D/I_G ratio) were found to be 0.856 and 0.725 for untreated and treated a-CNTs, respectively. It has shown that untreated a-CNTs have higher I_D/I_G ratio due to more defects created after the chemical synthesizing process. A decrease in I_D/I_G ratio was found after washing with HCl, indicating a higher quality of nanotubes.

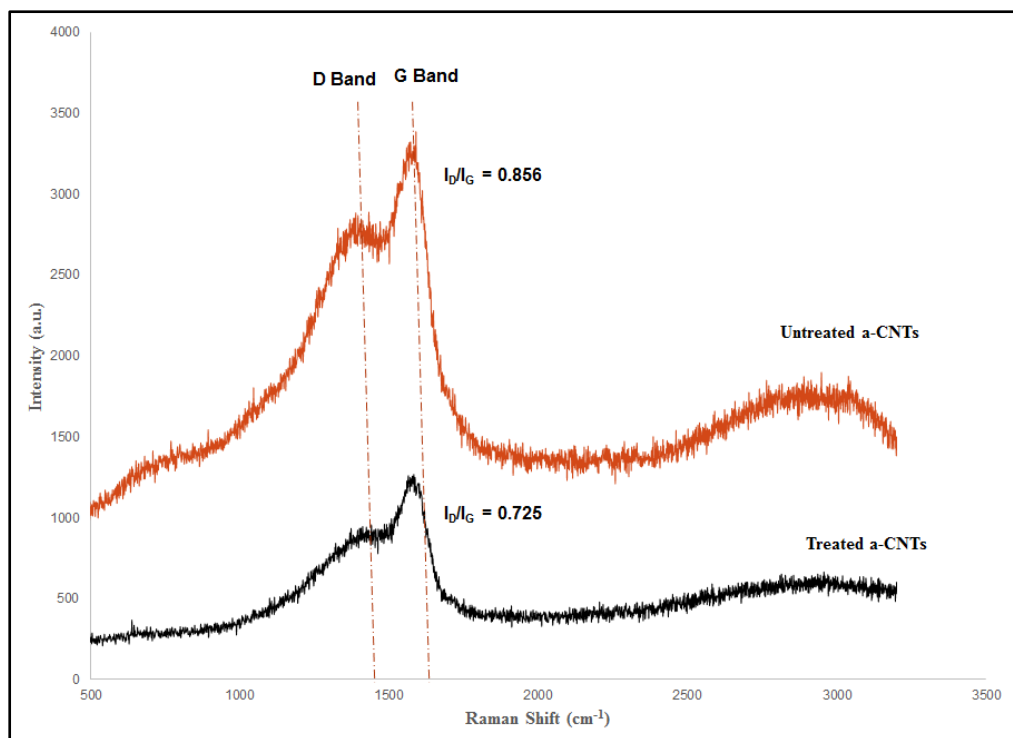


Figure 4-6: Raman spectra of the treated and untreated a-CNTs

Figure 4-7 shows the FTIR analysis of treated and untreated a-CNTs. It can be observed that more peaks are found in untreated a-CNTs, which are 1378, 1652, 1726, 2810, 2988 and 3110 cm^{-1} . The peak at 1378 cm^{-1} shows the O-H group due to the chemical reaction process (Sankal and Kaynak, 2013). The peaks at 1652 cm^{-1} and 1726 cm^{-1} indicate the presence of C-C and C=O, respectively. (Roy et al., 2013, Sankal and Kaynak, 2013, Mombeshora et al., 2015). The peaks from 2800 ~ 3500 cm^{-1} are assigned to O-H bonds associated with hydroxyl groups (Roy et al., 2013). In the treated a-CNTs spectrum, the prominent groups of C=O at 1726 cm^{-1} disappeared. This is due to the double bond being attacked by HCl. However, it can be seen that lesser peaks are identified in treated a-CNTs and O-H group is present at 3400 cm^{-1} . It is suggested that various hydroxyl moieties at the carbon surface were introduced during purification process (Yudianti et al., 2011). It can be

observed that IR shifted towards lower wave number side. This shifting is due to the presence of hydrogen bonding at 3400 cm^{-1} . Thus, it can be suggested that treated a-CNTs are fewer contaminants. These results are agreement with the XRD and Raman results.

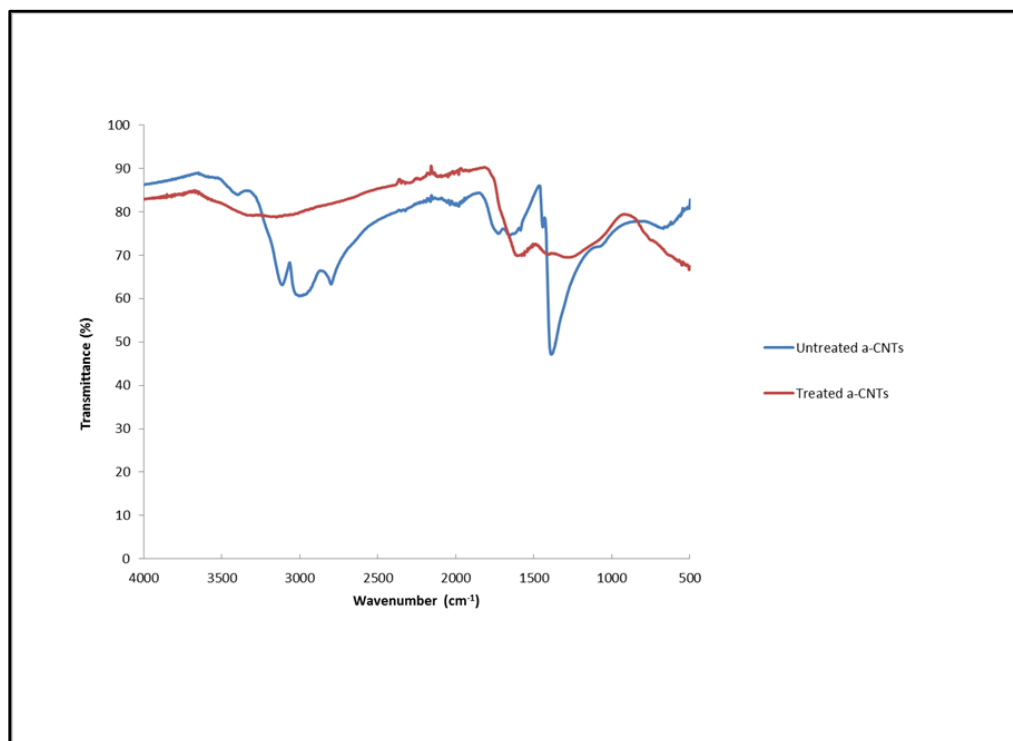


Figure 4-7:FT-IR spectra of the treated and untreated a-CNTs

Figure 4-8 shows the FESEM image of untreated and treated a-CNTs. A bundle of nanotubes with the tube size that less than 100 nm and the average length of 5 μm can be observed. Additionally, the nanotubes are surrounded by small spherical contaminants. Figure 4-9 shows the FESEM images and EDX mappings of untreated and treated a-CNTs. It can be seen that the nanotubes are free of chloride (Cl) and iron (Fe) impurities after treatment with HCl. From the result of EDX mapping analysis, the weight percentages of chloride and iron elements in untreated a-CNTs are 54.8 wt% and 12.7 wt%, respectively. After treatment, the weight percentages reduced to

(Cl) 1.5 wt% and (Fe) 0.2 wt%. This is in agreement in XRD result, as untreated a-CNTs are the presence of chloride compounds.

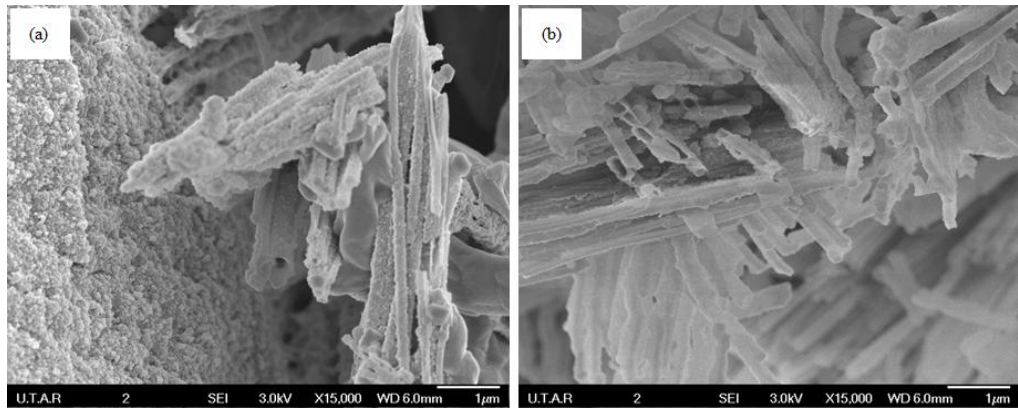


Figure 4-8:FESEM image of (a) untreated and (b) treated a-CNTs

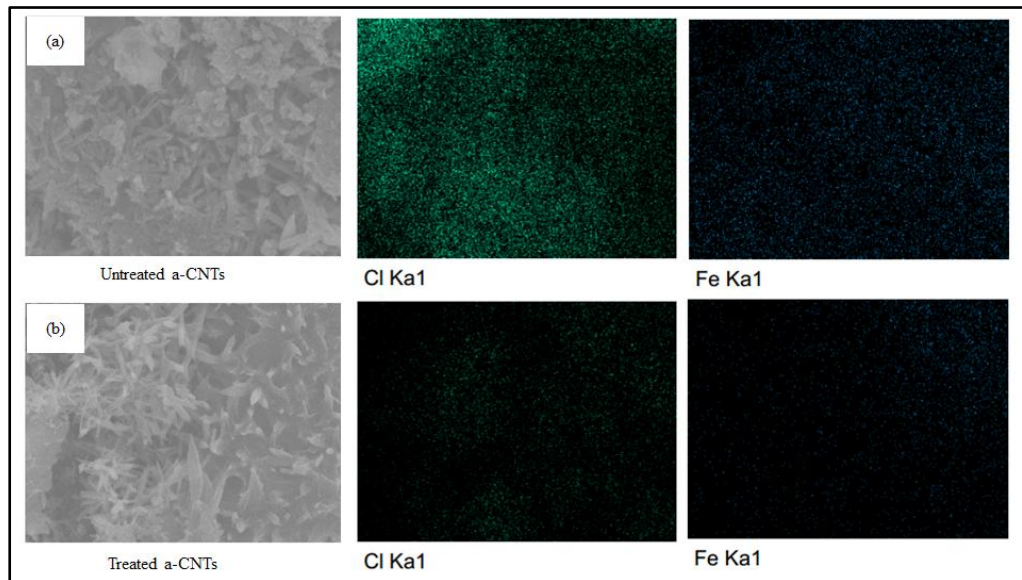


Figure 4-9:FESEM images and EDX mappings of untreated and treated a-CNTs

Figure 4-10 shows an HRTEM image and SAED of treated a-CNTs. The diameter of the nanotubes is around 80 nm, which is in agreement of FESEM result. The SAED depicts the ring and blue pattern of the nanotubes.

It can be suggested that CNTs are not a crystallize structure and but an amorphous CNTs. This result agrees with the XRD result.

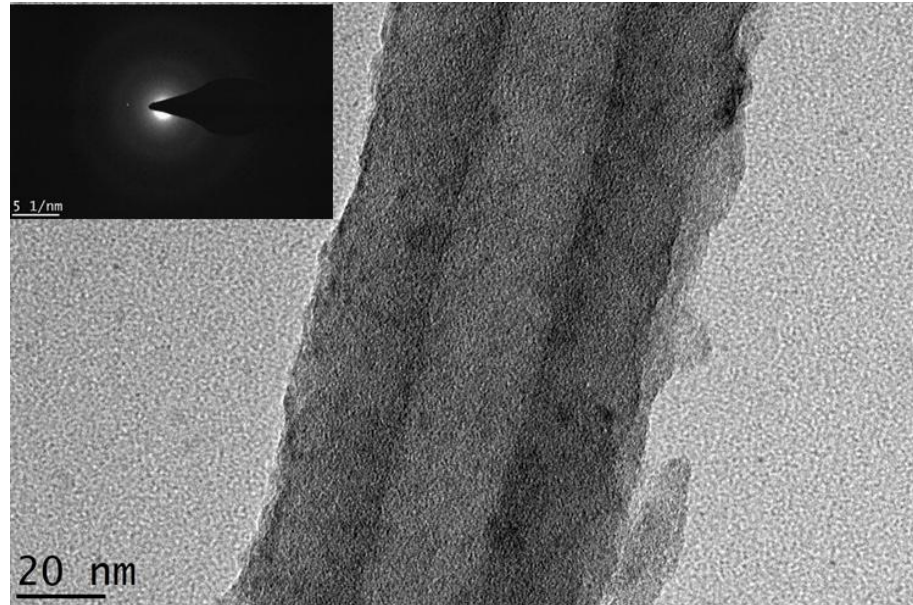


Figure 4-10:HRTEM image of treated a-CNTs and SAED of the nanotube

CHAPTER 5

STUDY OF THE RHEOLOGICAL BEHAVIOUR

5.1 Introduction

In this study, an Anton Paar Physica MCR 301 controlled-stress rheometer was used to study the rheology behaviours of ICAs samples. A series of tests were carried in order to study the flow character of SNPs and a-CNTs filled ICAs, for instance, constant shear rate vs time; amplitude sweep; frequency sweep; hysteresis; three interval thixotropy test (3ITT) and creep recovery. The results obtained from each test are discussed accordingly.

5.2 Results and Discussion

5.2.1 Viscosity Test

Figure 5-1 and Figure 5-2 show the transition of the viscosity of the ICAs sample at the constant shear rate of 25 s^{-1} . The viscosity of all samples remains stable after two minutes. The highest viscosity can be observed in S7 and S8, in average among the rest. It can be suggested that incorporate with MCC, the viscosity increase around 30 % as compared to those without MCC solution. The fluctuation value of S8 at the first 40 seconds may be due to a rheopexy fluid. It is then further confirmed by hysteresis and thixotropy test. While the viscosity of the rest of the samples is ranging between 6.5 to 8.5 Pa.s. The

viscosity of the ICAs increases when adding with MCC due to the movement was blocked in the matrix macromolecular chains. Under the preliminary procedural conditions used to further evaluate the rheological behaviour of new ICAs formulations samples, it can be seen that, when added with the small percentage of nanomaterials to the ICAs, the viscosity is low (Leong, 2016). This will enhance particle-to-particle interactions and increase the resistance to flow.

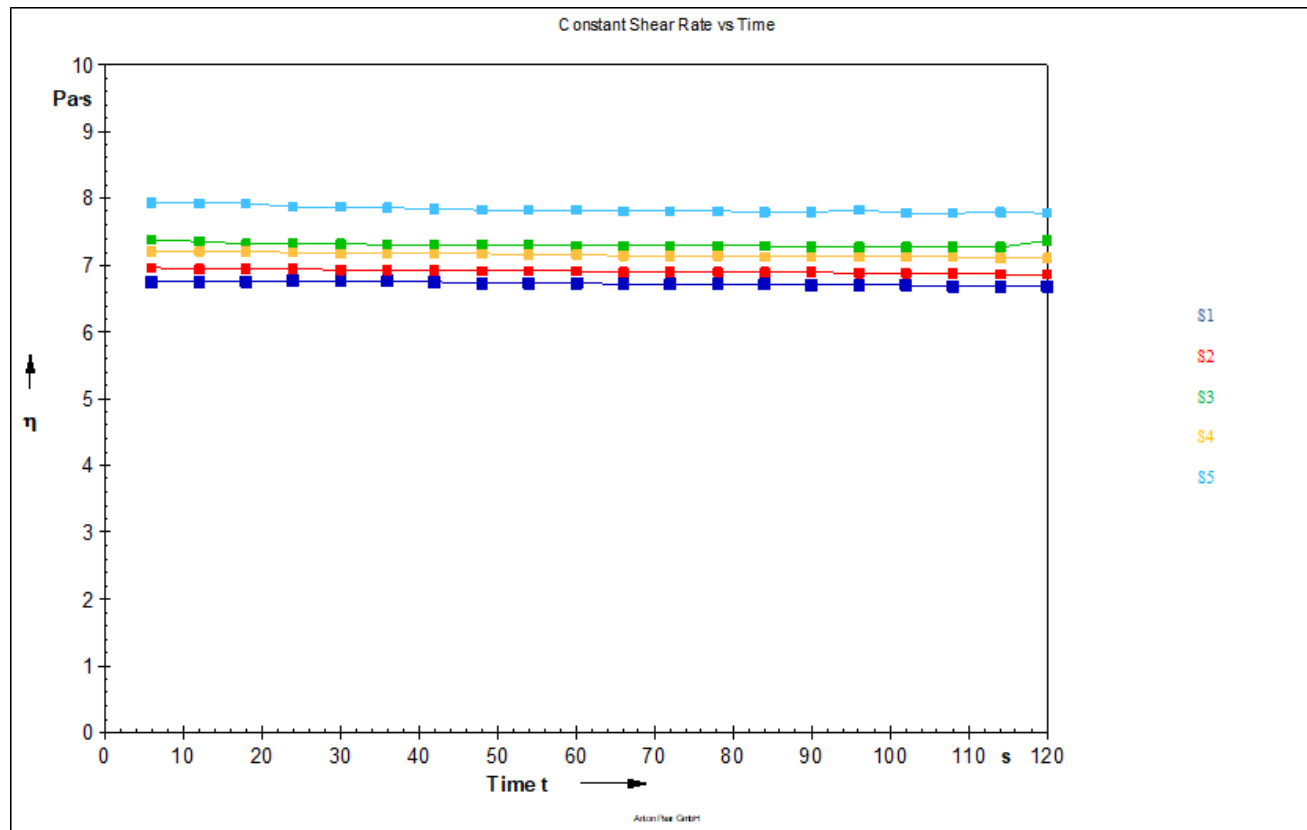


Figure 5-1: Constant shear rate measurement of S1, S2, S3, S4 and S5

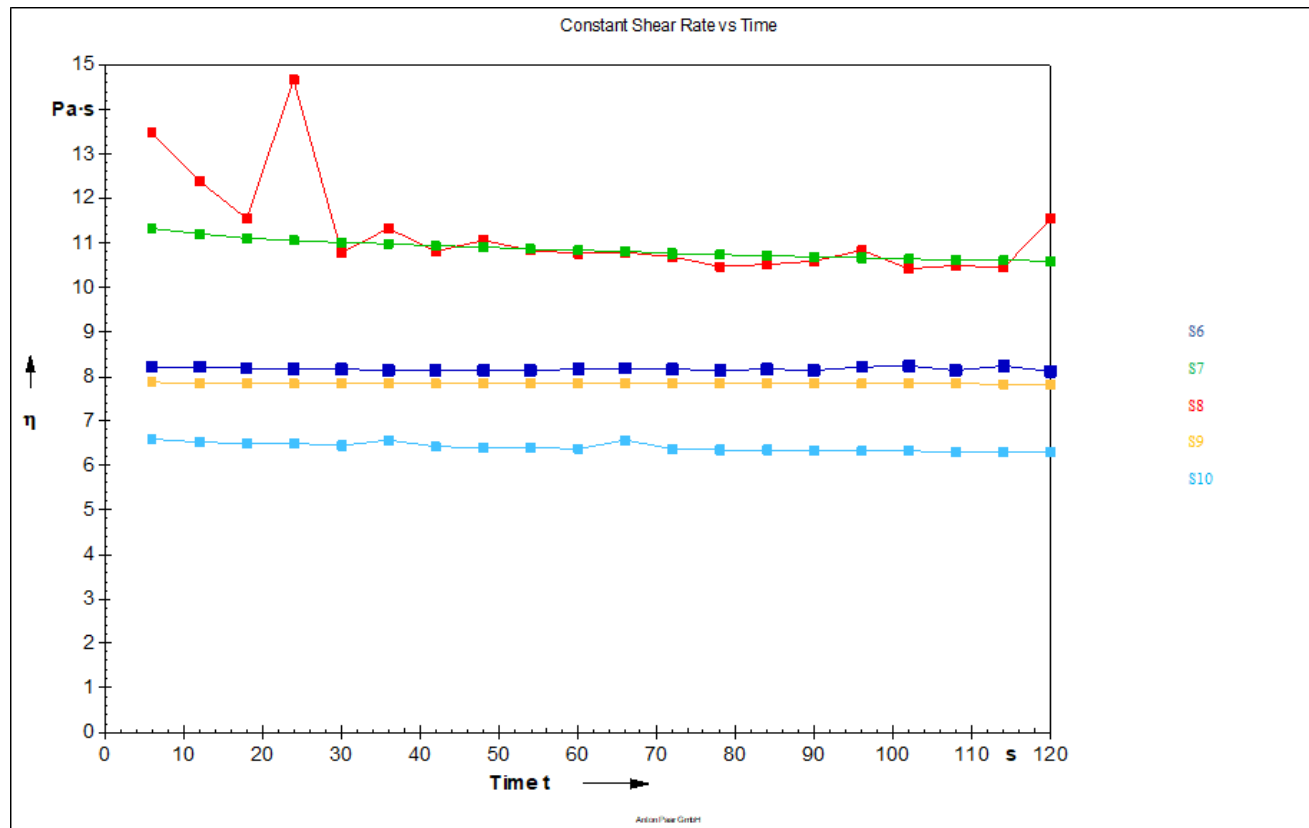


Figure 5-2: Constant shear rate measurement of S6, S7, S8, S9 and S10

5.2.2 Oscillatory Stress Sweep Stress (OSS) Test

Figure 5-3 and Figure 5-4 indicate the storage modulus (G') and loss modulus (G'') against the strain of the ten formulated samples. The graphs display a linear increase of the storage modulus, G' and loss modulus, G'' at low strain, followed by a sharp decrease when the system passes from linear to a nonlinear viscoelastic regime, where S1, S7, S8 and S10 display that $G' > G''$. This reveals that the elastic property is predominant with increasing of filler content such as MCC solution and a-CNTs in this case (Pal, 2005). It can be seen that S1 and S8 have higher storage modulus, G' among the rest. In S1, SNPs levels are just 1 wt%. This small amount of nanoparticles does not have significant effect on the ICAs system. The graphs are similar to the results found in Lam (2011). Moreover, in S8, when higher MCC is incorporated to the ICAs system, higher storage modulus, G' can be observed clearly. This indicates that MCC plays an important role in stabilize the mixture of fillers in polymer matrix. In S10, where 2 wt% of a-CNTs was added and the elastic property is prevailed. As known, the elastic properties should dominate during printing process. It is suggested that 1 wt% SNPs content, a-CNTs and MCC in ICAs system, indicating a better contact within fillers and polymer matrix (Irfan and Kumar, 2008, Lam, 2011).

On the other hand, when higher SNPs content was loaded to ICAs system, which is more than 2 wt%, loss modulus, $G'' >$ storage modulus, G' can be seen clearly in the graphs. The samples predominantly demonstrate

viscous behaviour throughout the test. As reported by Irfan and Kumar (2008), this is considered as weakly structure and sedimentation can be occurred easily. Based on Choi and Lee (2005) results, the SNPs is not well adsorbed on polymers if the mixture temperature is less than 45 °C. In the non-linear region, the G' and G'' gradually decrease and the paste structure starts to break down, causing a more liquid-like behaviour (Durairaj et al., 2006, Durairaj and Man, 2011).

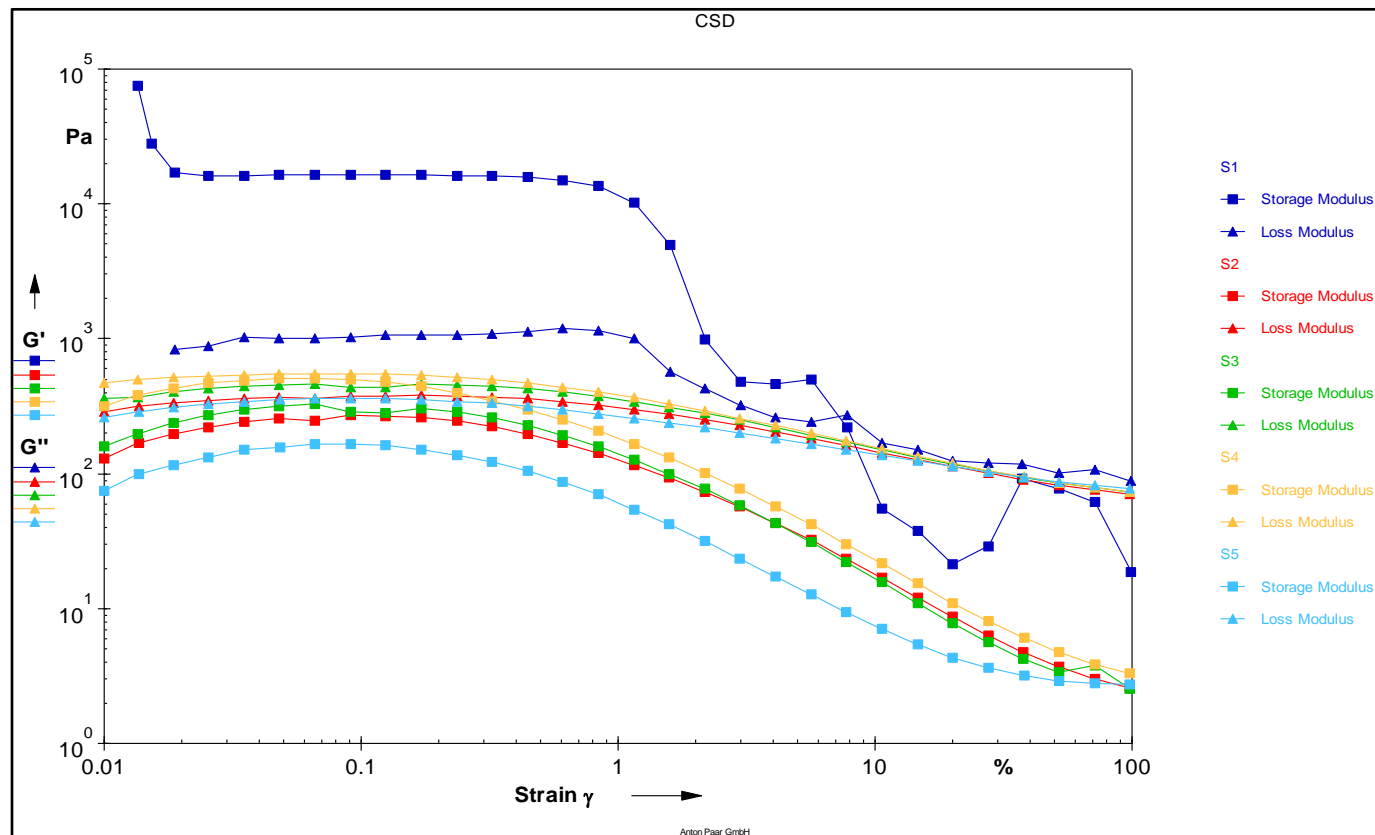


Figure 5-3: Storage modulus (G') and loss modulus (G'') against strain of S1, S2, S3, S4 and S5

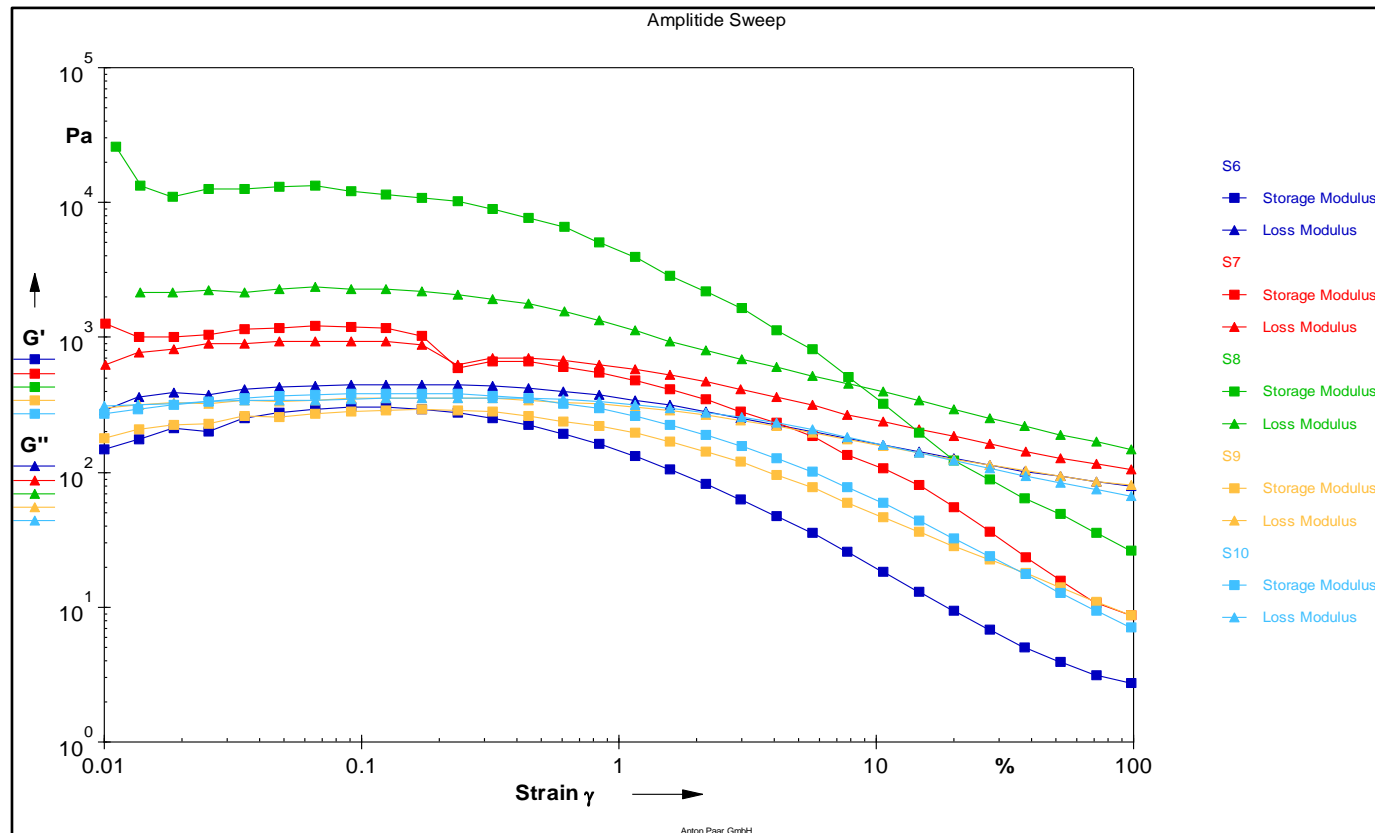


Figure 5-4: Storage modulus (G') and loss modulus (G'') against strain of S6, S7, S8, S9 and S10

Table 5-1: Linear visco-elastic region's range of ICAs samples

Sample	Linear Visco-elastic Region's Range (Strain %)
S1	Up to 0.611
S2	Up to 0.236
S3	Up to 0.324
S4	Up to 0.125
S5	Up to 0.125
S6	Up to 0.324
S7	Up to 0.171
S8	Up to 0.236
S9	Up to 0.611
S10	Up to 0.839

From the test results, the linear visco-elastic region (LVER) was determined and tabulated in Table 5-1. Since the structural properties are best related to elasticity, the length of the LVER of the elastic modulus (G'') is used to measure the stability of a sample's structure. A long LVER shows a well-dispersed and stable system. S10 denote the longest LVER and indicate a well-dispersed and stable system (Bao et al., 1998, Lam, 2011, Koe, 2012). Meanwhile, the G' is slightly larger than G'' within the LVER of S10, it can be suggested that nanotubes are strongly associated, so sedimentation is unlikely to occur. This is in agreement with other research studies (Durairaj et al., 2006, Durairaj and Man, 2011). Thus, it indicates that incorporate with a-

CNTs, the system is more stable. This is because a-CNTs have extreme aspect ratios and mix well with others in ICAs.

Table 5-2: The relative magnitude of loss modulus, G'' and storage modulus, G' within LVER

Sample	Storage Modulus, G' , (Pa)	Loss Modulus, G'' , (Pa)	G''/G'
S1	14900	1190	0.07987
S2	259	380	1.46718
S3	260	446	1.71538
S4	476	546	1.14706
S5	165	378	2.2500
S6	254	433	1.70472
S7	1020	890	0.87255
S8	10200	2060	0.20196
S9	238	326	1.36975
S10	368	353	0.95924

The tackiness of the paste can be determined by the ratio of G''/G' , as shown in Table 5-2. S1 and S8 have the lowest ratio of G''/G' , followed by S7. The lower ratio of G''/G' displays that the paste is very tackiness and could result in poor withdrawal and unsuitable for screen printing (Durairaj et al., 2009, Durairaj and Man, 2011, Phair and Kaiser, 2009). However, the rest of the samples possess a higher ratio of G''/G' , indicating that those pastes are

less stickiness or less tackiness of ICAs. Both a-CNTs and the higher percentage of SNPs may be suitable for screen printing process as they are less cohesive. In spite of that, based on the results of LVER, a-CNTs samples are slightly more dominated due to larger LVER and sedimentation would be less likely to occur.

5.2.3 Frequency Sweep Test

Figure 5-5 and Figure 5-6 show the frequency sweep tests of the ICAs. The 0.1 % strain was used as it is within the linear viscoelastic region (LVR) for all formulated samples from the oscillatory stress results (Moakes et al., 2015). The trend of the graphs indicates that G'' is larger than G' for most of the samples, except for S8 and S10 at low frequency. However, if an ICA system has loss modulus, G'' that higher than storage modulus, G' , it is considered a weak structure with a high possibility of sedimentation (Hong et al., 2013, Lam, 2011, Mir and Kumar, 2008). Meanwhile, S8 and S10 show G' as slightly bigger or similar to G'' at 0.259 rad/s. Hence, from the results, it can be suggested that the aid of MCC solution and a-CNTs may slightly improve the dispersion behaviour of the ICA system.

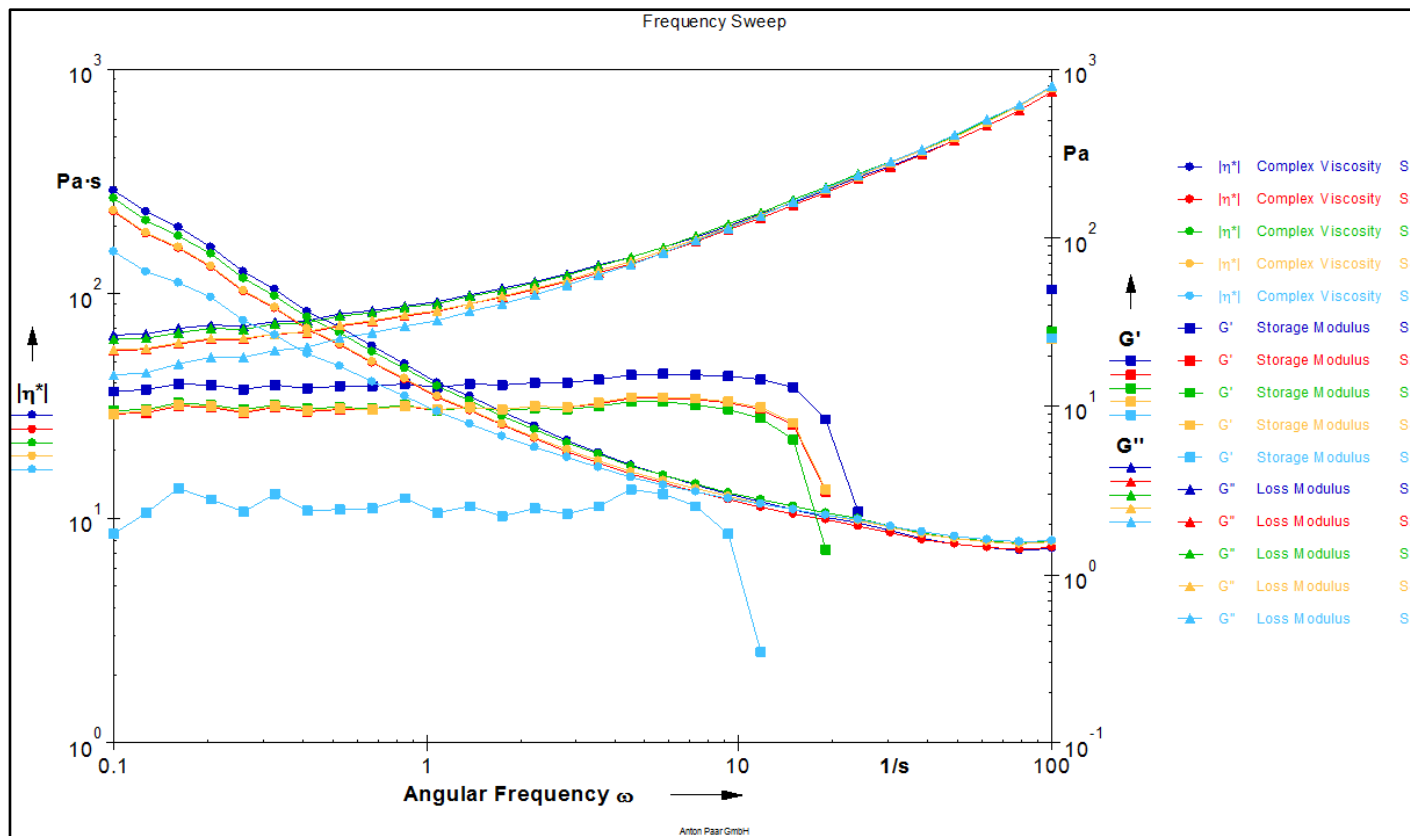


Figure 5-5: Frequency sweep test results of S1, S2, S3, S4 and S5

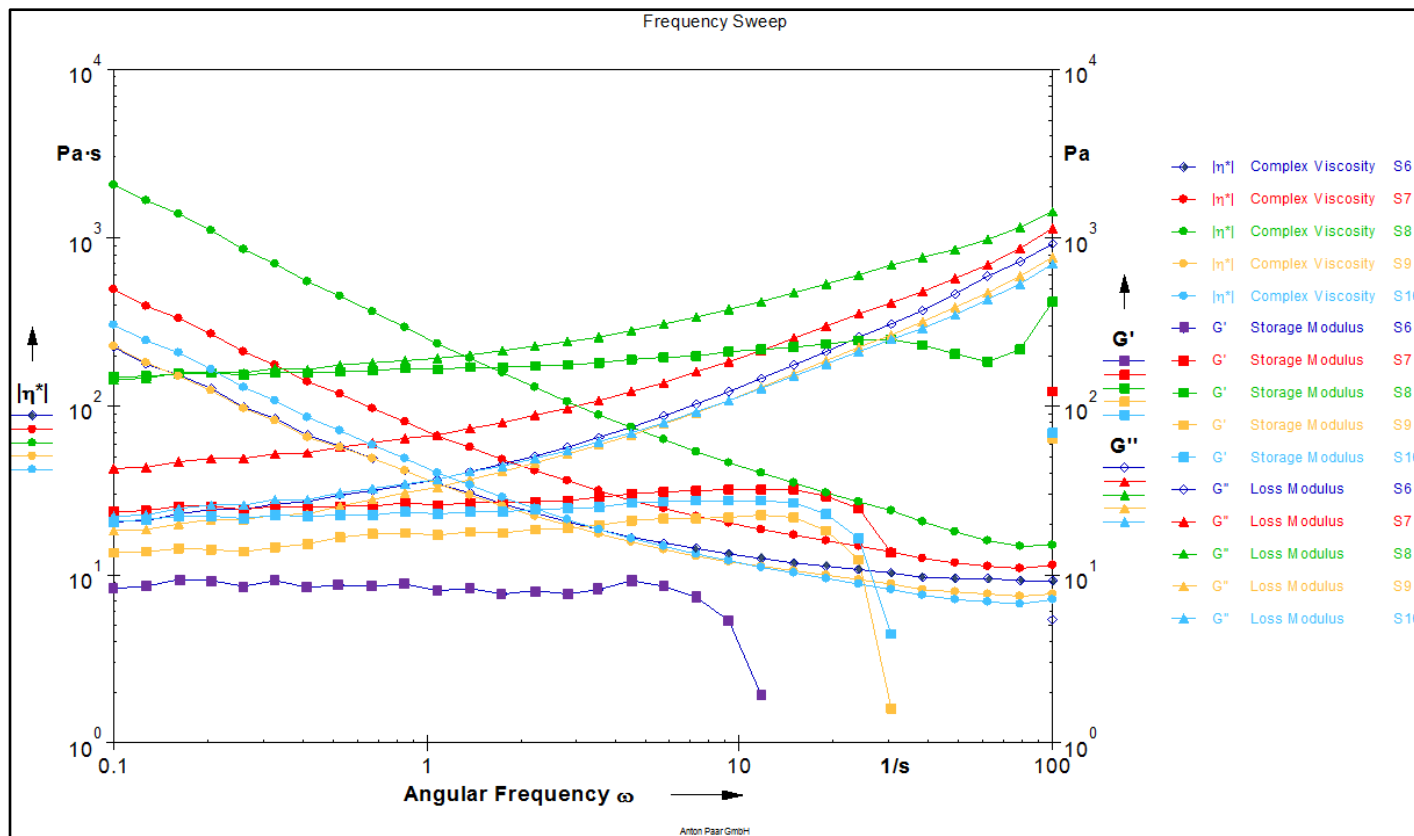


Figure 5-6: Frequency sweep test results of S6, S7, S8, S9 and S10

5.2.4 Hysteresis and Three Interval Thixotropy Test (3ITT)

Figure 5-7 and Figure 5-8 show the hysteresis loop of all samples. In the hysteresis loop test, the shear rate was increased from 1 to 10 s⁻¹ and then decreased from 10 to 1 s⁻¹. The decrease in viscosities of all the samples with increasing of shear rate can be observed in the graphs. This is in agreement by some researchers' works (Bell et al., 1987, Morissette et al., 2001, Hoornstra et al., 1997). This phenomenon is called pseudoplastic behaviour and indicates a decreasing viscosity with an increasing shear rate. This indicates that the samples experienced shear thinning in nature and its structure underwent changes due to destructive of flocculation in suspensions (Durairaj et al., 2009). ICAs samples appear to have very densely packed particles and close contact with continuous interactions between particles. However, all of the samples show hysteresis loops except for S8 which the hysteresis loop is indefinite.

The area within the hysteresis loop represents the energy consumed in structure breakdown. It can be seen that S5 has the largest hysteresis loop. The largest area enclosed by the hysteresis loop in the S5 indicates that this sample underwent a large structural breakdown. Conversely, S9 and S10 show the smallest hysteresis loops. The smaller hysteresis loop area demonstrates that the structure within the inter-particles (a-CNTs) and composite materials in ICAs would recover at a much faster speed as compared to bigger hysteresis

loop area (Durairaj, 2011). The region in between the upward curve and downward curve in hysteresis curve is evidence of the thixotropic behaviour of the paste ((Durairaj, 2011, Lam, 2011). The steady shear rate was then further investigated by three interval thixotropy test (3ITT) in order to study the structure recovery properties.

Figure 5-9 and Figure 5-10 illustrate the steady shear rate of all the samples. All samples experienced the thixotropy behaviour as the viscosity of the samples declines over time upon application of a higher constant shear rate at 10 s^{-1} . The viscosities of all the samples gradually increase after the shear rate is removed to 0.1 s^{-1} . However, for S8, there is a peak at the first interval at 0.1 s^{-1} and exhibits that viscosity increases under an imposed shearing action. This phenomenon is called rheopexy (Altman et al., 2015). Rheopexy is the rare property of some non-Newtonian fluids to display a time-dependent increase in viscosity. The rheopexy fluid can thicken when shaken or agitated. It is worth noting that S8 indicates both thixotropy and rheopexy behaviour. This is due to the higher percentage of MCC solution (10 wt%) has participated in the cross-linking reaction and leading to the polymerisation of DGEBA epoxy resin. Meanwhile, Dulina et al. (2015) explained that the existence of rheopexy is explainable with strong interaction between elementary structural clusters consisting of nanoparticles with polymers tailored into its net. In such way, MCC hinders the movement of the matrix's micro-molecular chain, resulting in high viscosity.

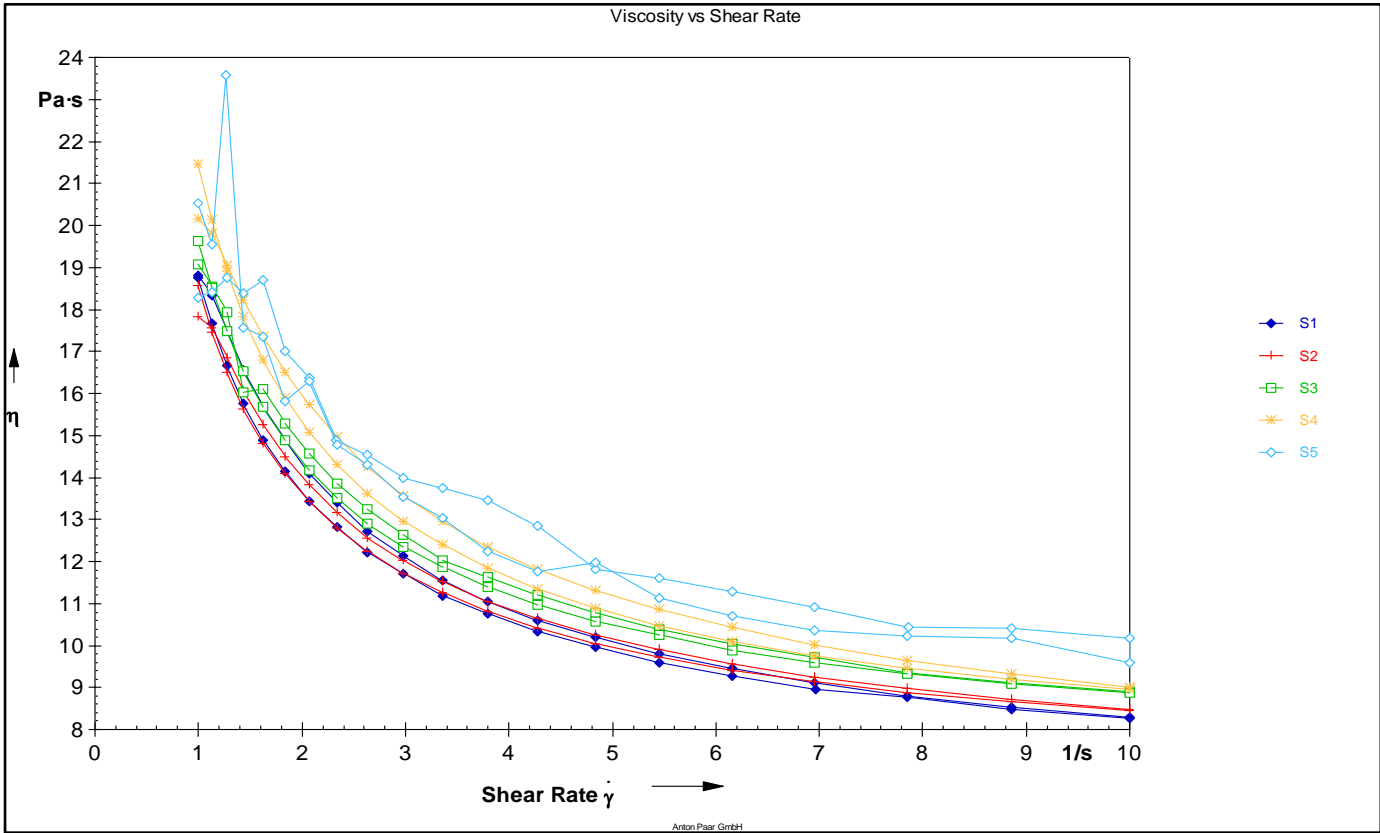


Figure 5-7: Hysteresis test results of S1, S2, S3, S4 and S5

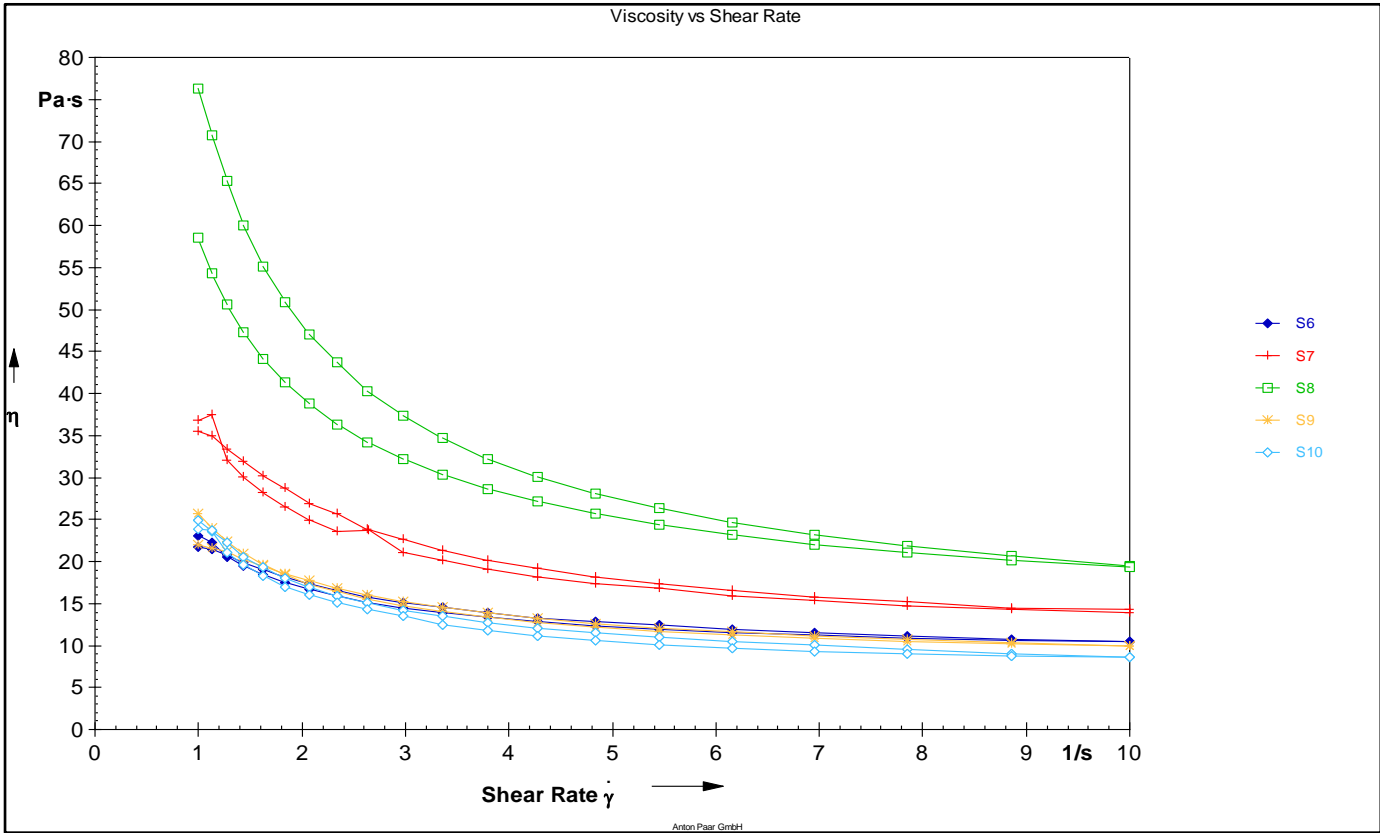


Figure 5-8: Hysteresis test results of S6, S7, S8, S9 and S10

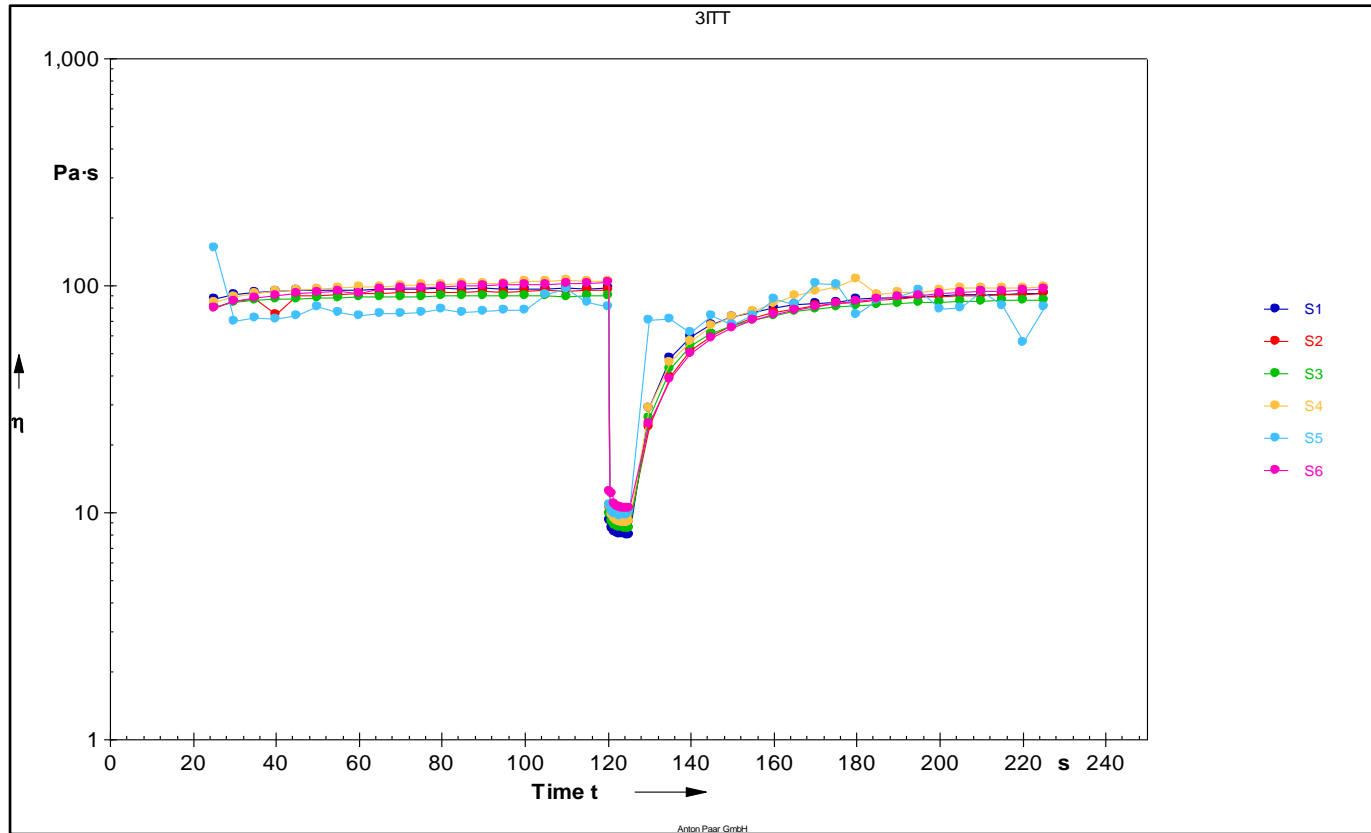


Figure 5-9: Steady shear rate test of S1, S2, S3, S4 and S5

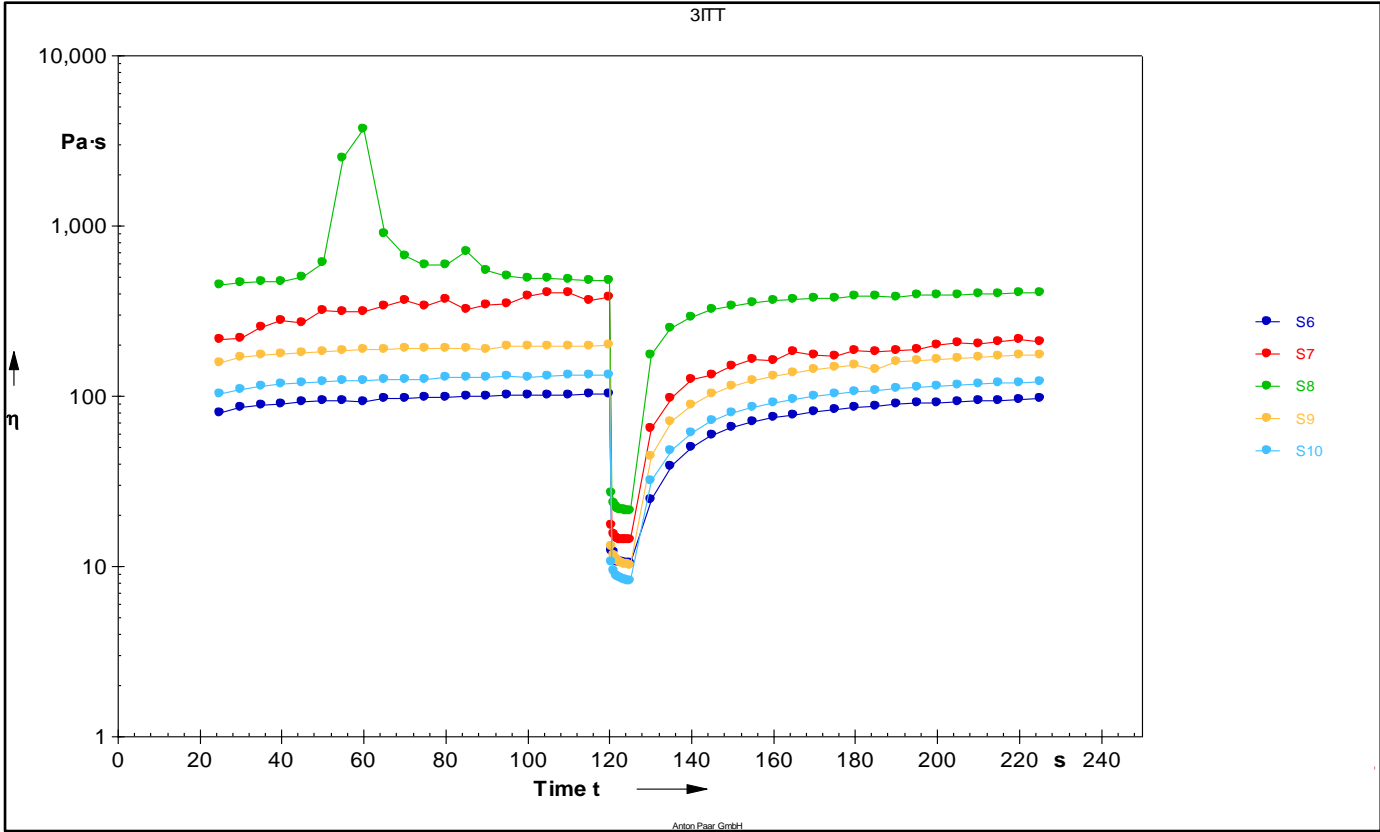


Figure 5-10: Steady shear rate test of S6, S7, S8, S9 and S10

In this 3ITT test, the samples were subjected to low and high shear rates over a period of time, and the recovery index of the sample can be calculated by (3). The percentage of the recovery after the shear rate was removed is tabulated in Table 5-3.

Table 5-3: Viscosity recovery in percentage after shear rate was removed

Sample	Shear interval (breakdown) region (Pa.s)	Recovery interval (build up)region (Pa.s)	Recovery Index (%)
1	96	79	82.3
2	91	77	84.6
3	89	74	83.1
4	99	84	84.8
5	105	87	82.9
6	96	77	80.2
7	253	181	71.5
8	450	358	79.6
9	150	137	91.3
10	134	121	90.3

In Table 5-3, all recovery indexes is more than 70%. It is worth noting that a sample is considered to have a good thixotropic behaviour if its recovery index is at least 70% (Patel and Dewettinck, 2015). Based on the calculated results, the ICAs with a-CNTs experienced the highest recovery index among

all samples. This is attributed to a-CNTs in the ICAs sample that leads to strong interaction between polymer matrix and filler. It is believed that the dispersion of 1D a-CNTs in the polymer matrix enhanced adhesion between fillers and polymer matrix. The nanotubes tend to fill up the spaces in between the resins and filler, which provides the paste highly elastic behaviour.

5.2.5 Creep Recovery

Figure 5-11 and Figure 5-12 show graphs of strain as a function of time in all the formulated samples at 5 Pa constant shear rate for two minutes. The stress was then removed, and the change of strain was monitored until 240 s. It can be seen that the trends of creep recovery of all samples are similar, as the strain increases with time and drops after the stress was removed. The creep recovery index was calculated by using (4) and tabulated in Table 5-4. The measured creep recovery index demonstrates that the ratio between J_3/J_2 is less than 1. This can be suggested that there is some amount of recovery and thus a lower tendency to slump (Nguty et al., 1998). It can be observed that S7, S8, S9, and S10 have a lower ratio of J_3/J_2 as compared to those samples with SNPs filler. However, S8 has the lowest creep recovery index and a greater ability to recover once stress is removed. This is due to the higher weight percentage of MCC solution that lowers the tendency to slump on the sample. Secondly, it can be due to S8 sample experienced both rheopexy and thixotropy behaviour which lower the tendency to collapse. Moreover, the creep recovery results are in the agreement with the hysteresis and 3ITT where

S7 and S9, and S10 (a-CNTs and 5 wt% MCC solution) display the good thixotropy behaviour with lesser tendency to slump than SNPs samples.

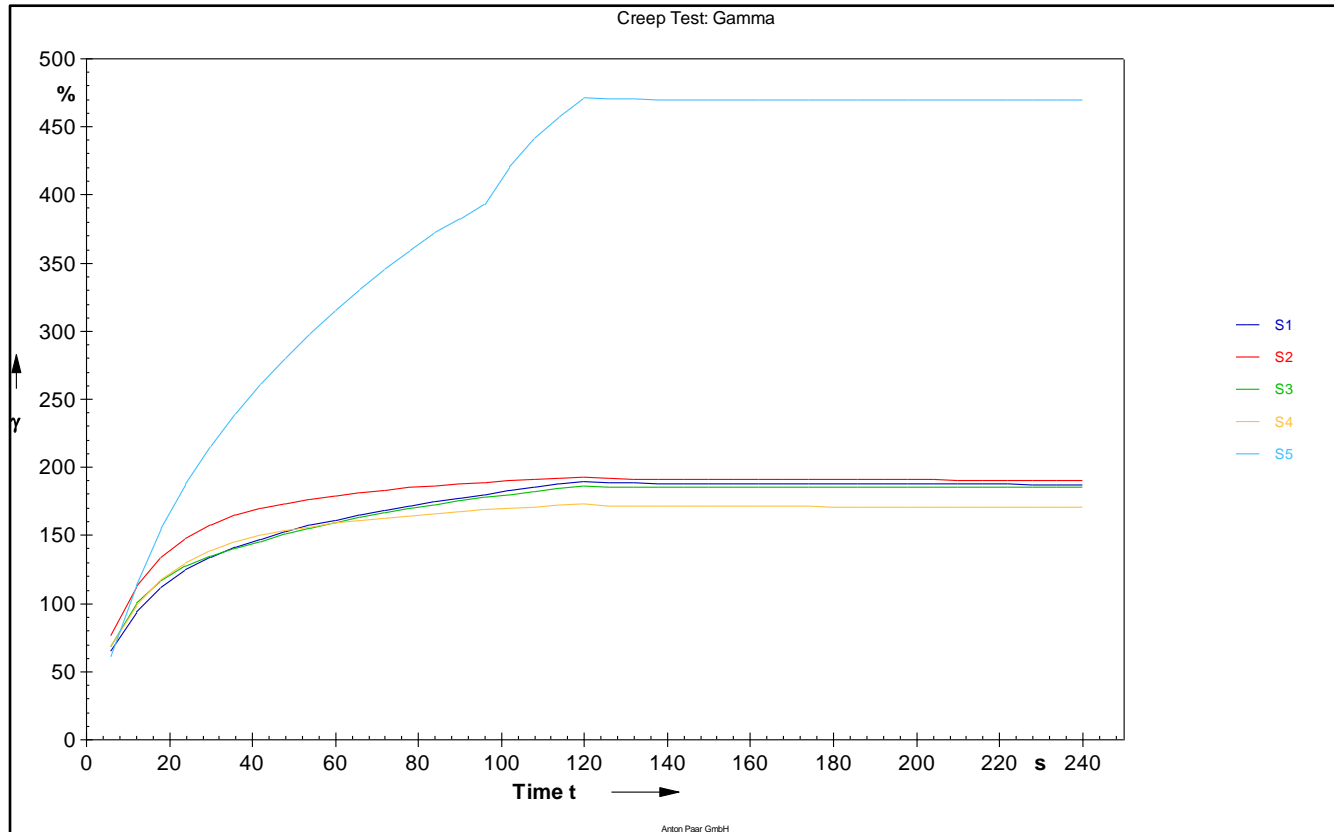


Figure 5-11: Creep recovery test of S1, S2, S3, S4 and S5

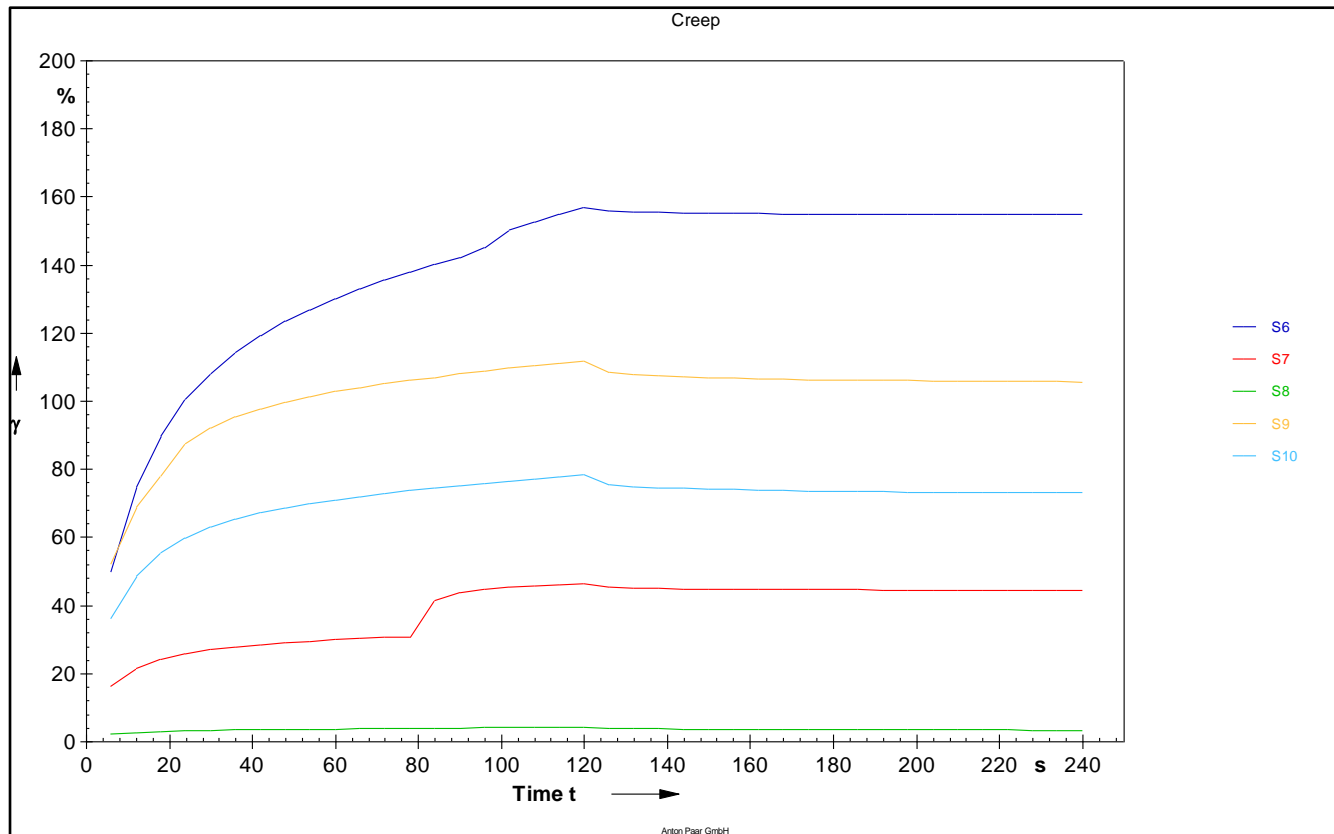


Figure 5-12: Creep recovery test of S6, S7, S8, S9 and S10

Table 5-4: Creep Recovery Index for All ICA Samples

Sample	Initial strain, J1	Recovery strain, J2	End point of strain, J3	Creep recovery index, J3/J2
1	0.654	1.9	1.87	0.984211
2	0.767	1.93	1.91	0.989637
3	0.685	1.87	1.85	0.989305
4	0.684	1.73	1.71	0.988439
5	0.506	1.28	1.26	0.984375
6	0.501	1.57	1.55	0.987261
7	0.165	0.464	0.445	0.959052
8	0.0231	0.0432	0.0339	0.784722
9	0.523	1.12	1.06	0.946429
10	0.362	0.784	0.731	0.932398

CHAPTER 6

STUDY OF THE THERMAL STABILITY AND GELATION POINTS

6.1 Introduction

The thermal stability and gelation temperature of the new formulation ICAs samples were investigated using TGA and DMTA, respectively. These are to study the influence of SNPs, a-CNTs and MCC solution to the gelation points and weight changes of ICAs samples when the heat was imposed. The results obtained from TGA and DMTA are discussed.

6.2 Results and Discussion

6.2.1 Thermal Stability by TGA

Figure 6-1 and Figure 6-2 show the plots of weight change of the ICAs versus the temperature by TGA. The TGA results indicate the same trend of the curve which represents the thermal decomposition at the different temperature up to 550 °C. It can be observed that there are three main stages of decomposition of the formulated ICAs occurred during the heating process up to 550 °C. The first stage of decomposition occurred at 100 ~ 150 °C, followed by the second stage at 250 ~ 300 °C, and the final stage at 340 ~ 550 °C.

The first stage of weight loss which occurs at the temperature range 100 ~ 150 °C, which is due to loss of moisture. This step is attributed to the elimination of water or solvents which content in the chemical. Besides that, the weight loss occurs after 100 °C, and this indicated that removal of water molecules from the ICAs. From 100°C to 150 °C, weight loss is due to the removal of labile oxygen functional groups: CO, CO₂, and possibly remaining water molecules.

Weight loss was observed at the second stage from 250 to 300 °C for all ICAs samples, which is around 20%, this is due to the secondary hydroxyl group of the propyl chain in epoxy resin and the formation of unsaturated C-C bonds.

After that, the weight loss in the range 360-537 °C may be due to the breakdown of the methylene linkage group (Saito et al., 1968). While the highest weight loss occurs within this range which due to the degradation of the chemical bond of DGEBA and loss of bisphenol-A group (Nieu et al., 1996).

From the TGA analysis, it can be suggested that all the formulated ICAs samples are thermally stable when the temperature is more 550 °C expect for S1, S2 and S8. In the TGA results of S1 and S2, weight gain occurred from 600 °C and continued up to 900 °C with a weight gain of 5 %. It is due to oxidation can easily occur on the ICAs samples at low weight percentage of SNPs content. In S8, the presence of hydroxyl groups in the

cellulose should be the reason behind the poor thermal stability after 550 °C. The ICAs still change its weight as more hydroxyl group (higher weight percentage of MCC) that attached to the matrix decompose at the higher temperature.

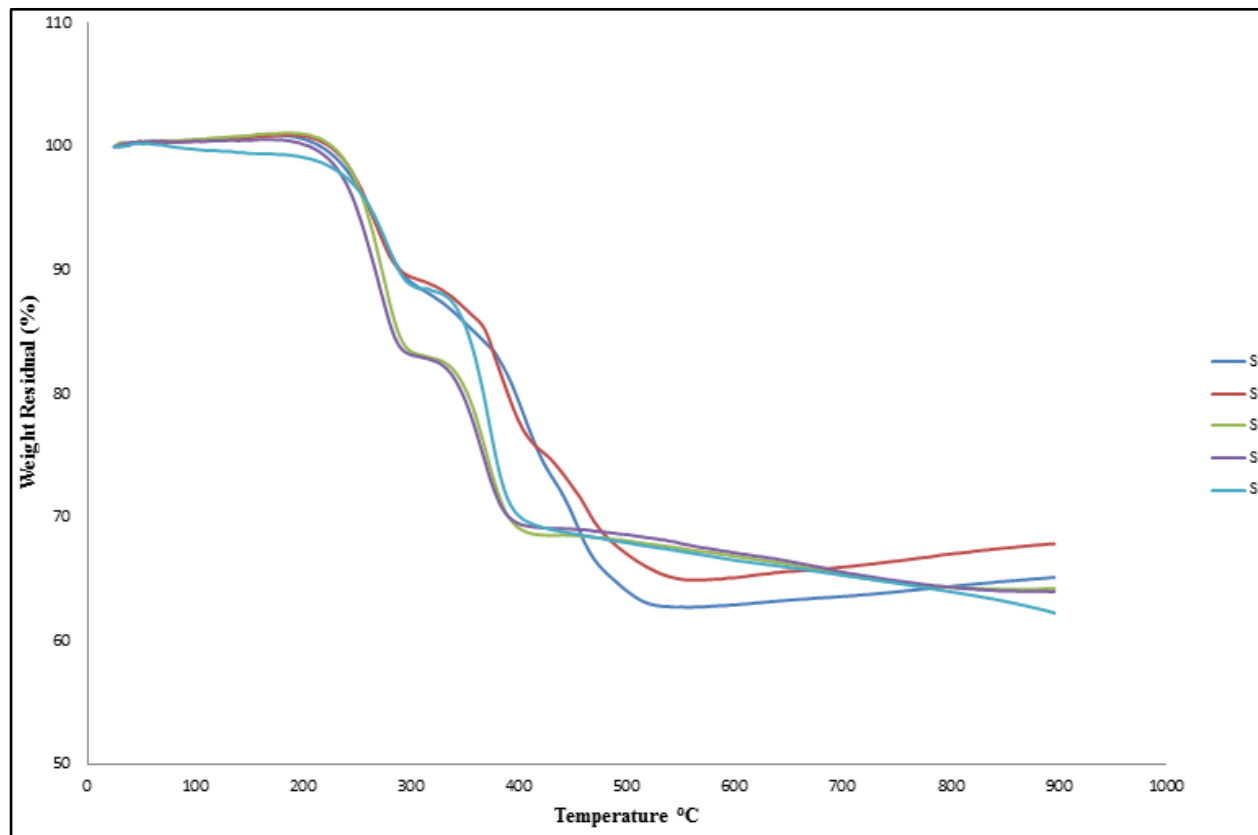


Figure 6-1: Thermogravimetric analysis curve of S1, S2, S3, S4 and S5

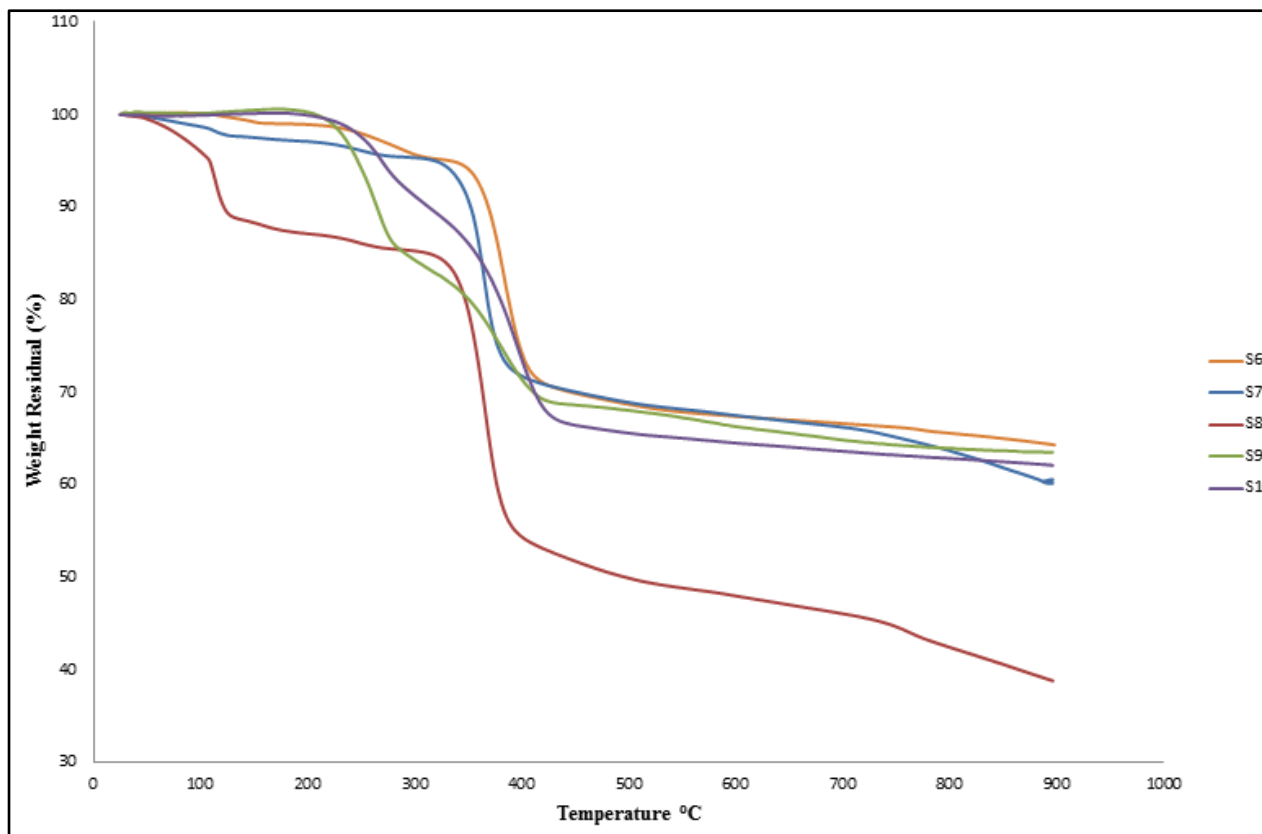


Figure 6-2: Thermogravimetric analysis curve of S6, S7, S8, S9 and S10

6.2.2 Gelation Study by DMTA

Figure 6-3 and Figure 6-4 show the storage modulus (G') and loss modulus (G'') against the temperature of the ten formulated samples. The gelation point was obtained from the crossover values of the G' and G'' from the graphs and tabulated in Table 6-1. It can be noticed that the gelation temperature decreases with increasing of SNPs contents (8 wt% and 10 wt%). This has shown that incorporated with SNPs, the transition from liquid-like behaviour to solid-like behaviour can occur at the lower temperature, which is below 80 °C. Moreover, with the aid of MCC solution and just 2 wt% of a-CNTs, the gelation temperature is also low, which is less than 90 °C. Thus, those samples with lower gelation temperature are suggested to have faster cure rates (Shukla and Rao, 1984, Rao and Pourassamy, 1976). This is supported by the gelation study from previous research by Rao and Pourassamy (1976) and Shukla and Rao (1984), both of which indicated that gelation temperatures decrease when the filler loading increases.

However, from Table 6-1, it can be clearly observed that there are some discrepancies in the results which are not correlated to the research studies by Rao and Pourassamy (1976) and Shukla and Rao (1984). One possible reason for this could be due to the sedimentation that happens after the mixing of the sample. This is in agreement of results shown in rheological studies. The inhomogeneous mixture and poor dispersion of the filler might

have caused the existence of two different phase within the paste as well (Lam, 2011).

Based on the classical model by Flory and Stockmayer (Stauffer et al., 1982), they suggested that concentration of the monomer is one of the important variables throughout the gelation process. In the current case, higher SNPs, which is more than 6 wt% and a-CNTs did play an important role in speeding the crosslinking process, it is due to the nanoparticles and nanotubes occupy the monomers as well as solvent molecules. A bond can be easily formed between neighbour monomers and the small clusters. SNPs and CNTs may permit the coordination of a vast number of ligands due to their extremely high surface area which fills the gaps between non-contacting silver powders (Dey, 2015, Kohinata et al., 2013, Chee and Lee, 2012, Peng et al., 2008). Thus, the gelation temperature becomes lower in higher SNPs loading and low loading of a-CNTs. Moreover, a low gelation temperature is usually desired, as it may produce a lower curing temperature.

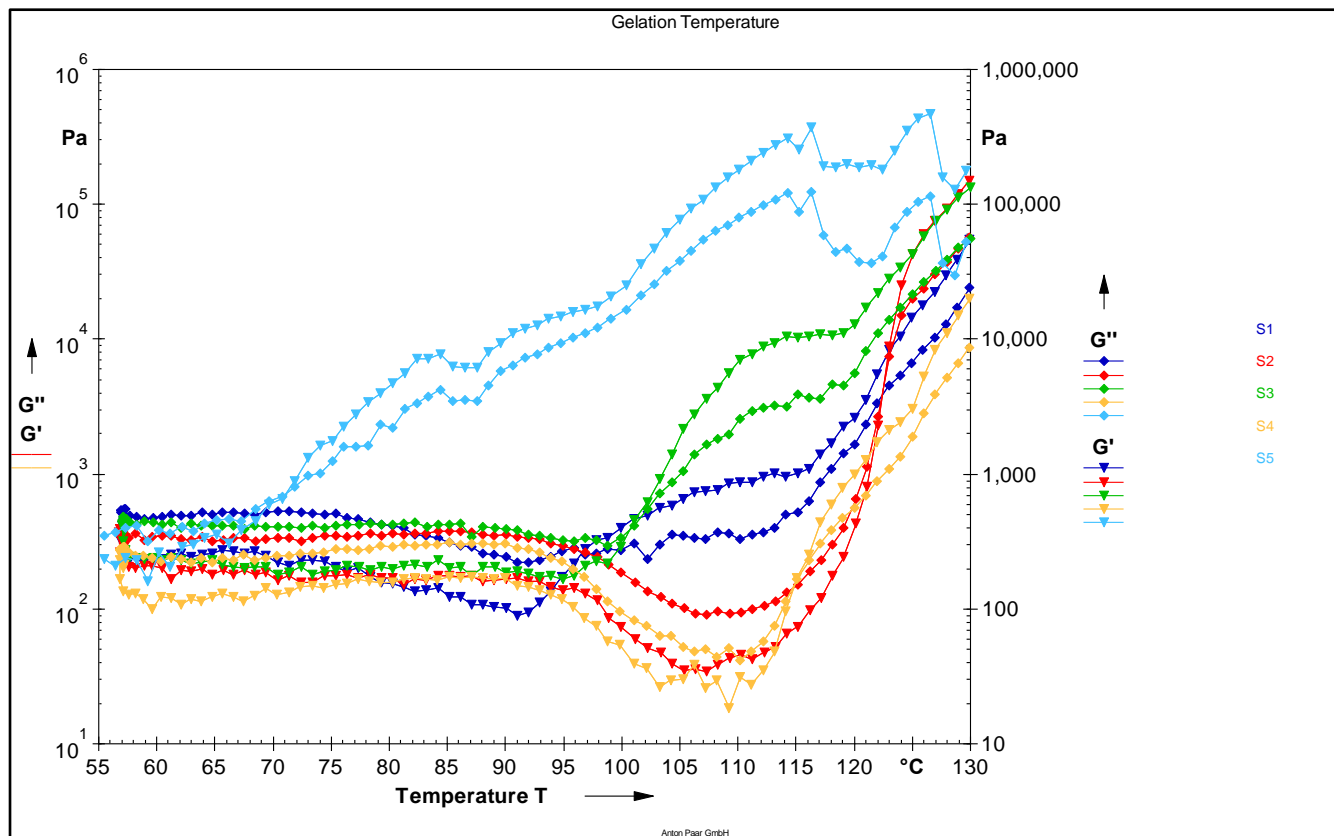


Figure 6-3: Storage modulus (G') and loss modulus (G'') against temperature of S1, S2, S3, S4 and S5

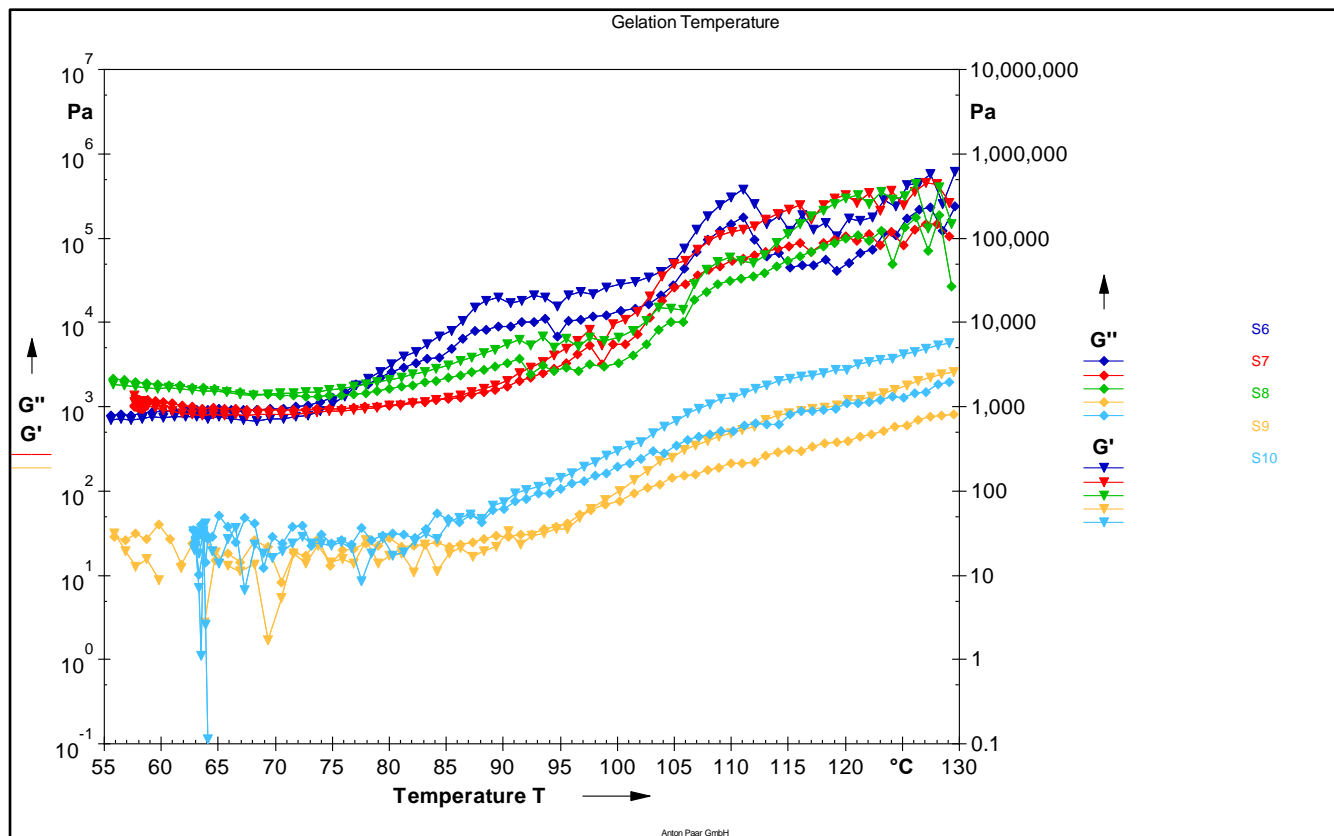


Figure 6-4: Storage modulus (G') and loss modulus (G'') against temperature of S6, S7, S8, S9 and S10

Table 6-1: Gelation points (T_{gel}) of crossover value of the storage modulus (G') and loss modulus (G'')

Sample	Gelation point (°C)
1	96.825
2	121.996
3	101.078
4	115.098
5	70.736
6	77.115
7	82.061
8	69.313
9	97.216
10	86.958

From Table 6-1, it can be seen that S2, S3 and S4 have higher gelation point, which is more than 100 °C, indicating that lower SNPs contents decreases the cross-link between the polymer matrix and silver powder. The contact area between silver powder and polymer matrix is reducing at lower SNPs contents (Mahanta et al., 2015, Jiang et al., 2006). It is suggested that in order to decrease the gelation points, sufficient SNPs should be added to the ICAs system. On the other hand, it is observed that with just 2 wt% of a-CNTs, the gelation temperature is around 87 °C. A lower gelation temperature is usually desired as it will allow cross-linking and formation of the long network across the specimens to occur faster. It is suggested that with

the presence of a-CNTs(forming of 3-D networking), as cross-linking happens faster, the specimen will cure at a faster rate. For an example in multiwall carbon nanotubes (MWCNTs), tend to entangle in the form of curved agglomerates (Song and Youn, 2005). In higher loading of a-CNTs to 2 wt%, it would have more entanglement and leading to more cross-linkage and thus decreases in gelation point.

Meanwhile, the highest percentage of MCC shows the lowest in gelation temperature. This is due to MCC hindering the movement of the matrix's micro-molecular chain and highest concentration of SNPs did play a role in decreasing the gelation temperature. Generally, the gelation point decreases as the MCC loading increases. The possible reason is that the cellulosic fillers in MCC solution. This can result in more intramolecular chains and thus cross-linking reaction could happen more easily. Due to the increase in cross-linking reaction, the gelation becomes lower. Besides, the increase in hydroxyl group in the MCC could contribute to the decrease in gelation point too. A research study by Varma et al. (1984) reported that hydroxyl groups in the cellulose might act as accelerators for the curing process. The gelation temperature of the epoxy curing reaction decreased when the concentrations of the cellulosic fillers increase as the hydroxyl groups increase (Varma et al., 1984). It is worth noting that higher crosslinking will lead to lower resistivity in ICAs (Lu and Wong, 2000).

CHAPTER 7

ELECTRICAL CONDUCTIVITY

7.1 Introduction

Based on the finding from rheological behaviour, thermal stability and gelation points of the formulated ICAs, it can be observed that a-CNTs and 5 wt% MCC solution show optimum results among the samples and better compatibility with epoxy. Thus, the effects of the different composition of a-CNTs and MCC solution on electrical conductivity were measured by four-point probes. The composition of a-CNTs was added from 0 ~ 3 wt%, the MCC was varied from 0 ~ 5 wt% and lastly, the DGEBA was 40 ~ 80 wt%. The remaining material is silver powder. The formulation of 45 samples was generated by Design Expert 6.0 as shown in Appendix A. The bulk resistivity of the ICAs samples were calculated by using equation (5) and plotted in Figure 7-1 to Figure 7-8 using MATLAB™. The equations of each plot were generated by Polynomial Curve Fitting.

7.2 Results and Discussion

Figure 7-1 indicates the three-dimensional relationship of resistivity against MCC and DGEBA at 0 wt% of a-CNTs. This graph represents the overall potential relationship between the three variables. The concept behind 3D plots of the resistivity to MCC and DGEBA is that the three characteristics of

the data can be compared. At higher composition of DGEBA, which is 60 wt% and 80 wt%, higher resistivity can be observed clearly, indicating that the silver powder which added to the ICAs system is sufficiently low to boost its conductivity. Although a higher amount of a-CNTs was added, no significant change of the ICAs resistivity can be found. Moreover, it can be seen that with 40 wt% of DGEBA, the resistivity is lower as compared to 60 wt% and 80 wt% of DGEBA. In order to have a better understanding of the relationship between the DGEBA and MCC composition with different amount of a-CNTs added that effecting the ICAs resistivity value, a Polynomial Curve Fitting by MATLAB™ was used to fit the data with polynomial equations. The polynomial surface function is found in equation (8), where, x is DGEBA wt % and y is MCC wt %. The lowest resistivity can be observed clearly at 40 wt% of DGEBA.

$$f(z) = -20.8304 + 0.6337 x + 0.6483 y - 0.0044 x^2 - 0.0171 x y + 0.0842 y^2 \quad (8)$$

In order to find the lowest electrical resistivity, curve fitting was done at 40 wt% of DGEBA. Figure 7-2 shows the curve fitting of electrical resistivity against MCC solution at 0 wt % a-CNTs and 40 wt% DGEBA. The curve fit equation was found in equation (9), where x is MCC. Where $\frac{\partial y}{\partial x} = 0$ in equation (10), the minimum point can be seen at 1.4 wt% MCC, and the electrical resistivity is $1.763 \times 10^{-3} \Omega \cdot \text{cm}$.

$$y = 0.1976 x^2 - 0.5569 x - 2.3615$$

(9)

$$\frac{\partial y}{\partial x} = 0.3952 x - 0.5569$$

(10)

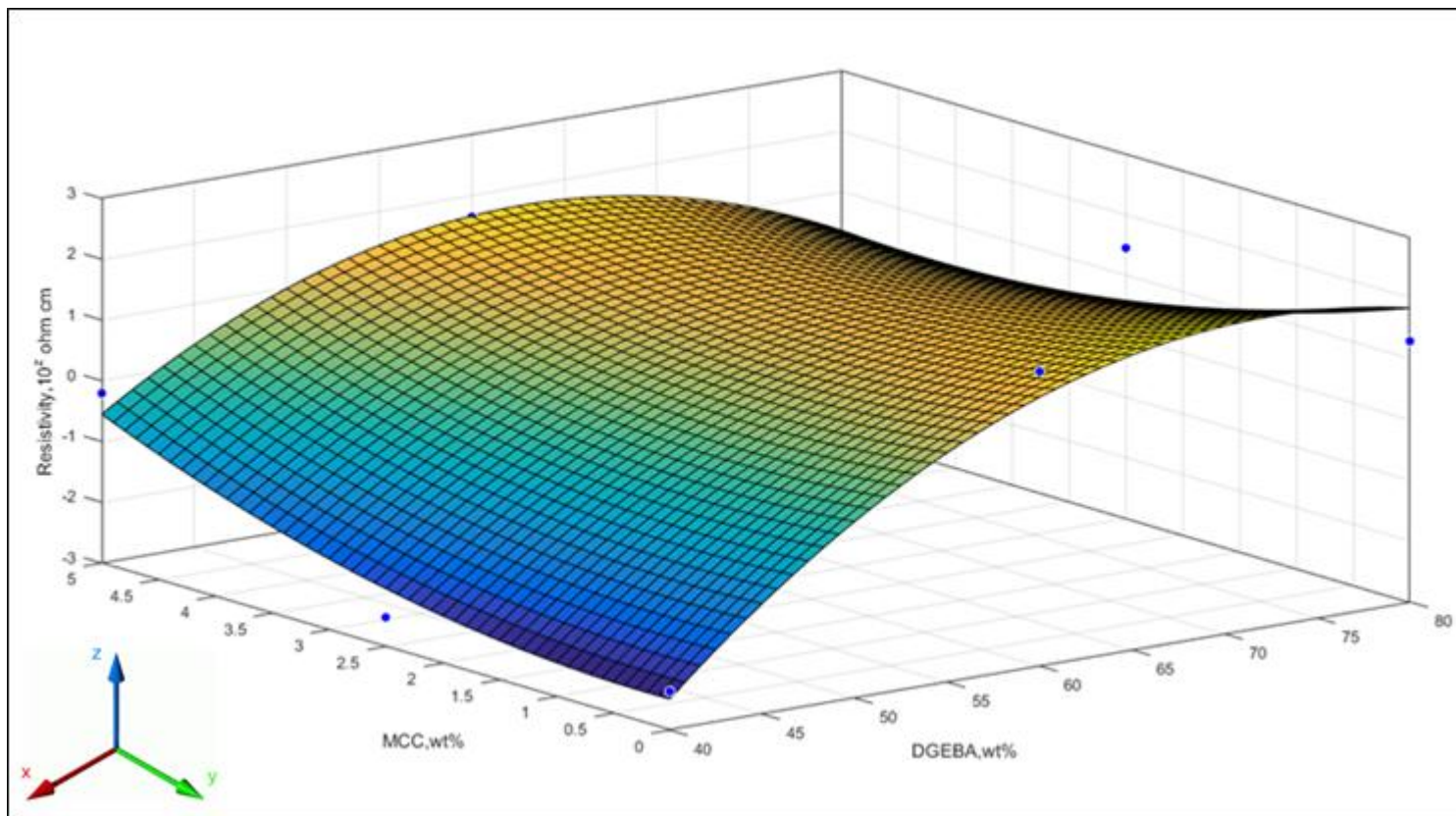


Figure 7-1: Electrical resistivity of ICAs at 0 wt% a-CNTs as function to MCC solution and DGEBA epoxy resin

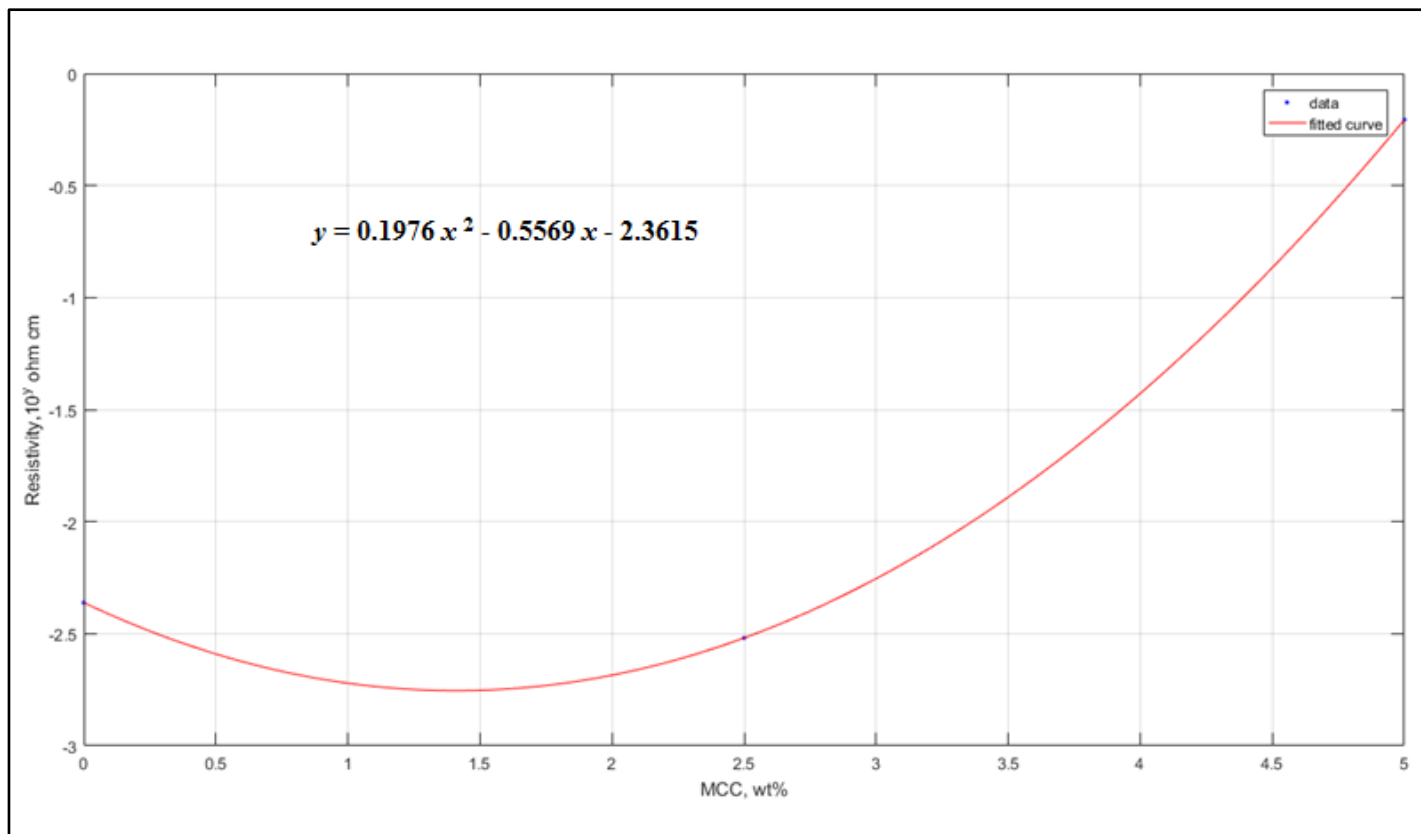


Figure 7-2: Electrical resistivity of curve fitting vsMCC solution at 0 wt% a-CNTs.

Figure 7-3 indicates the three-dimensional relationship of ICAs resistivity against MCC and DGEBA at 1 wt% a-CNTs. The polynomial surface function was found in equation (11), where x is DGEBA wt % and y is MCC wt %. The lowest resistivity can be clearly observed at 40 wt% of DGEBA.

$$f(z) = -21.0526 + 0.6725 x - 0.5139 y - 0.0049 x^2 - 0.0022 x y + 0.0602 y^2 \quad (11)$$

In order to find the lowest electrical resistivity, curve fitting was done at 40 wt% of DGEBA. Figure 7-4 shows the curve fitting of electrical resistivity against MCC solution at 1 wt % a-CNTs and 40 wt% DGEBA. The curve fit was found in equation (12), where x is MCC wt %. Where $\frac{\partial y}{\partial x} = 0$ in equation (13), the minimum point can be observed at 3.1 wt% MCC, where the electrical resistivity is calculated as $7.562 \times 10^{-4} \Omega \cdot \text{cm}$.

$$y = 0.1479x^2 - 0.9107x - 1.7195 \quad (12)$$

$$\frac{\partial y}{\partial x} = 0.2958 x - 0.9107 \quad (13)$$

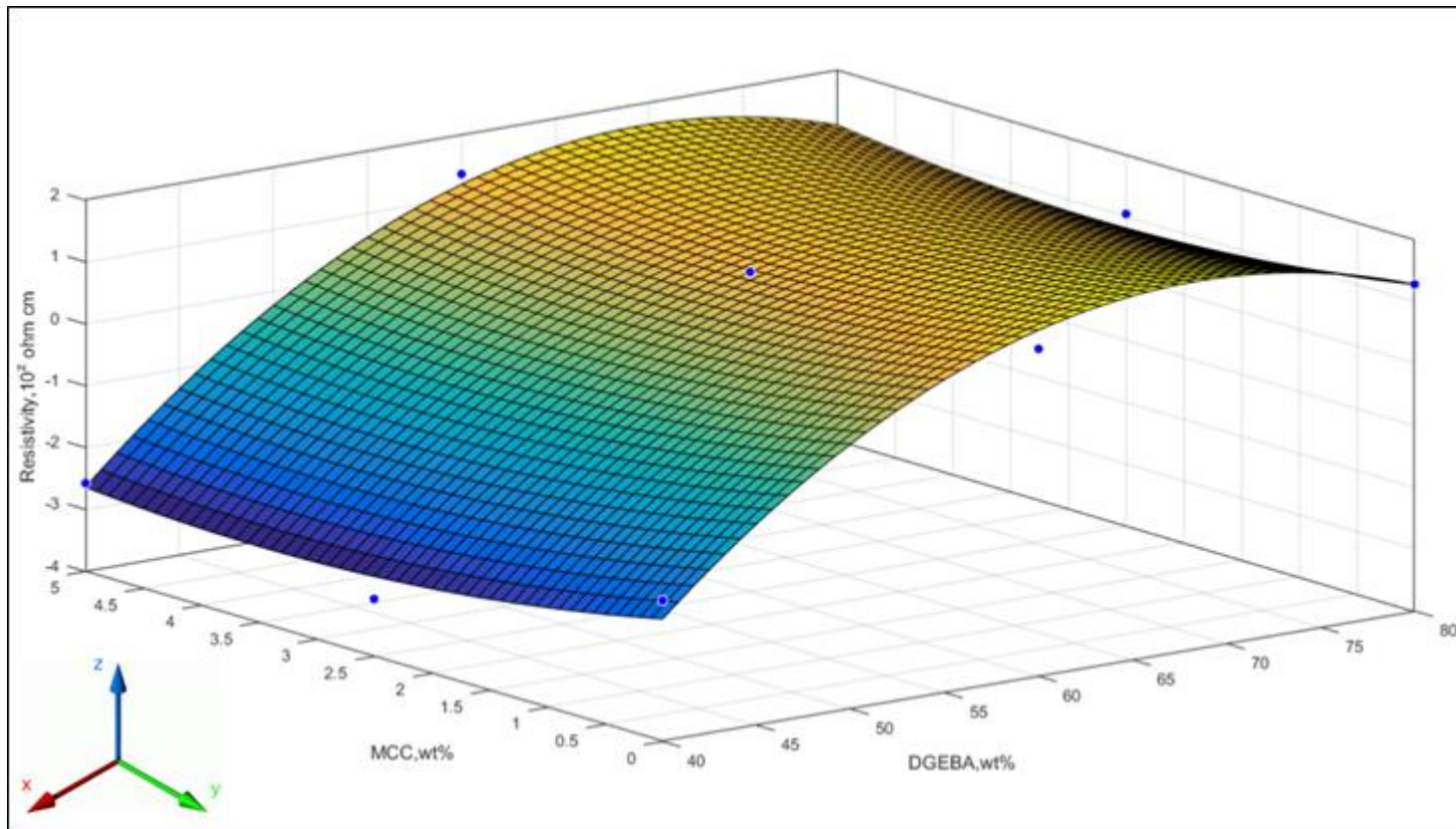


Figure 7-3: Electrical resistivity of ICAs as a function of MCC solution and DGEBA epoxy resinat 1 wt% a-CNTs

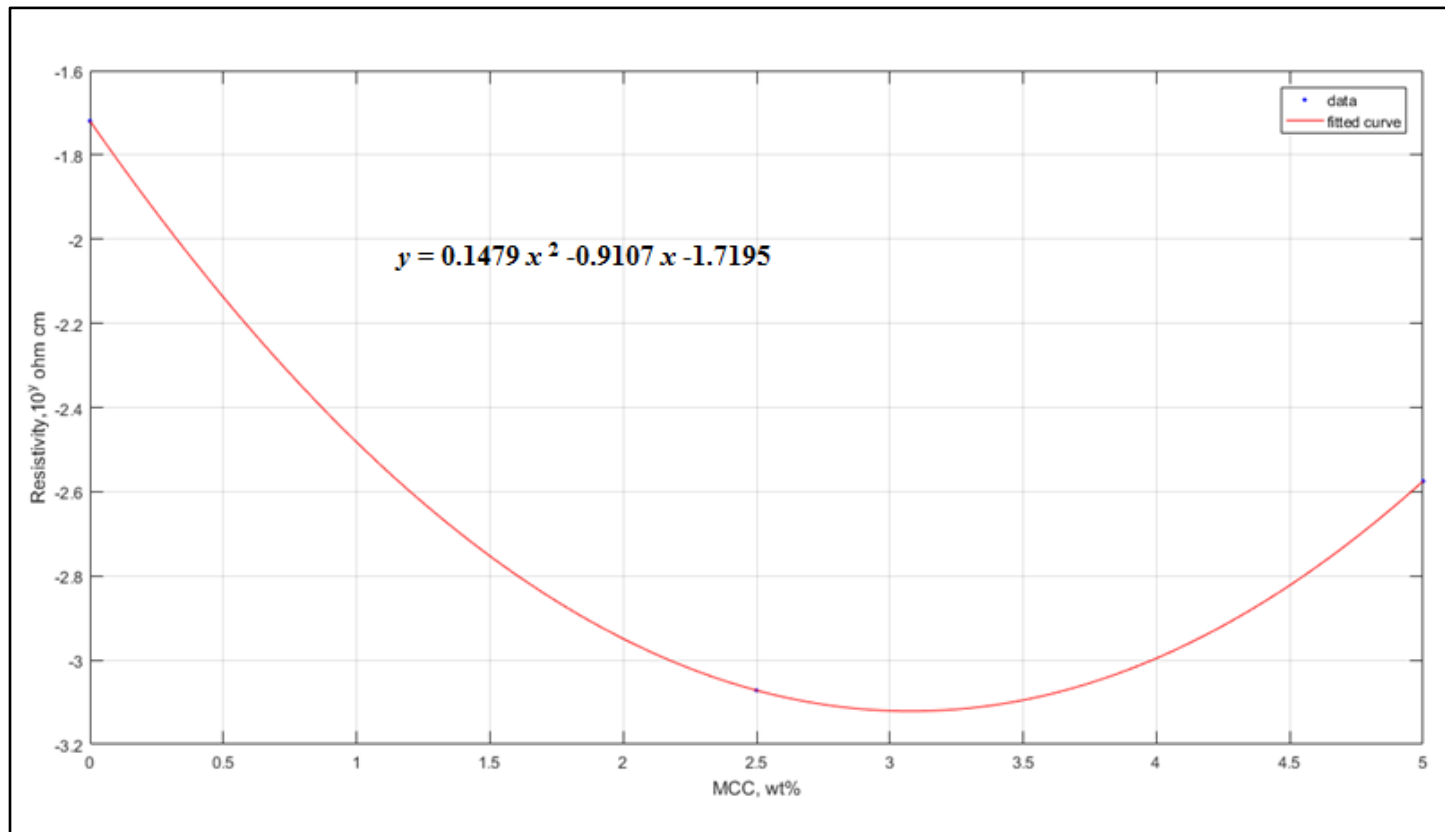


Figure 7-4: Curve fitting of electrical resistivity vs MCC solution at 1 wt% a-CNTs

Figure 7-5 shows the three-dimensional relationship of ICAs resistivity against MCC and DGEBA at 2wt% a-CNTs. The polynomial surface function was found in equation (14), where x is DGEBA wt % and y is MCC wt %. The lowest resistivity can be clearly observed at 40 wt% of DGEBA.

$$f(z) = -23.5758 + 0.7277 x + 0.2510 y - 0.0052 x^2 - 0.0033 x y - 0.0427 y^2 \quad (14)$$

Figure 7-6 displays the curve fitting of electrical resistivity against MCC solution at 2 wt % a-CNTs. The equation was found in equation (15), where x is MCC. The lowest electrical resistivity can be seen at 5 wt% MCC, where the electrical resistivity is $5.523 \times 10^{-4} \Omega \cdot \text{cm}$.

$$y = -0.1066 x^2 + 0.4899 x - 3.0423 \quad (15)$$

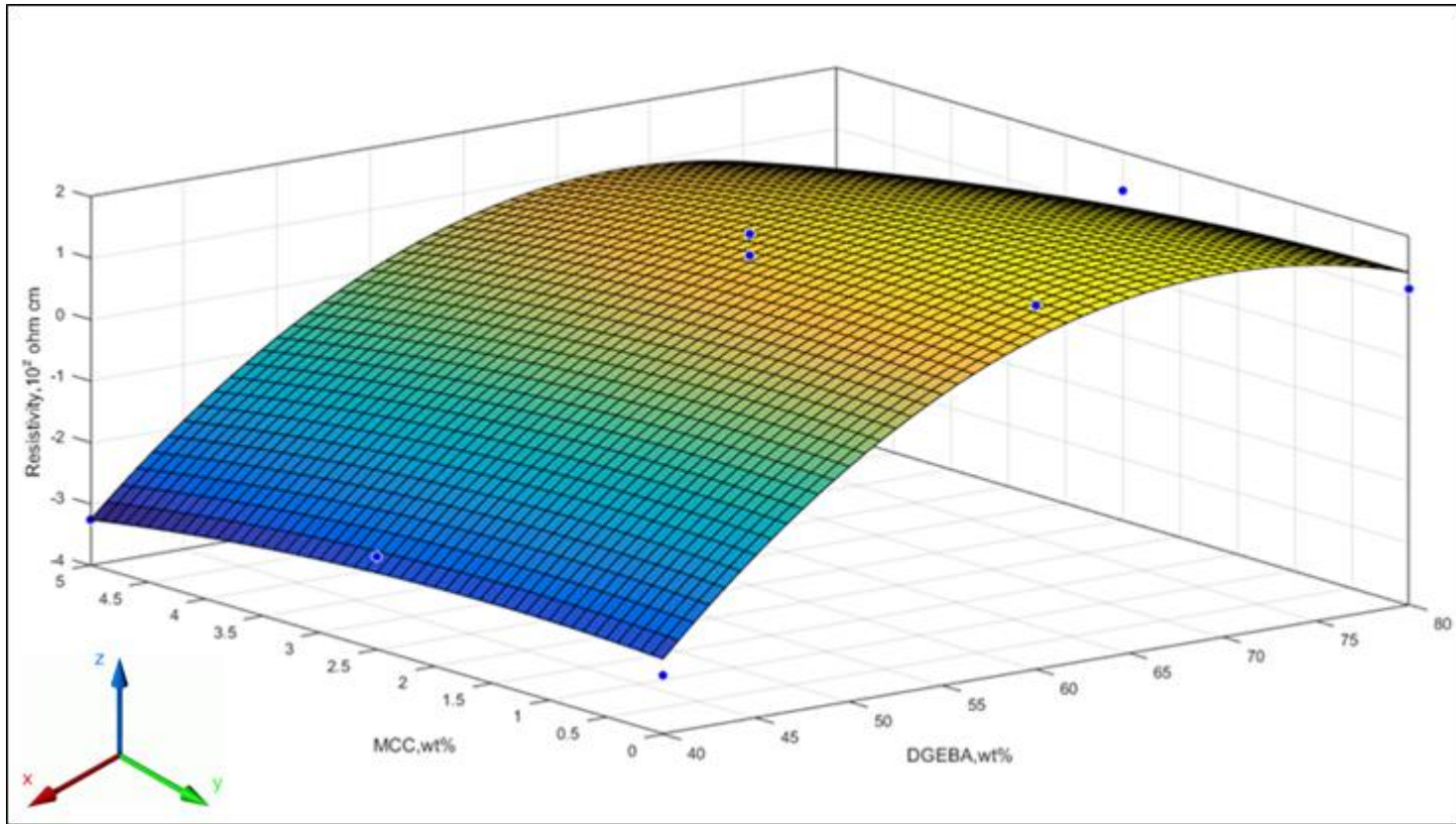


Figure 7-5: Electrical resistivity of ICAs as a function of MCC solution and DGEBA epoxy resin at 2 wt% a-CNTs

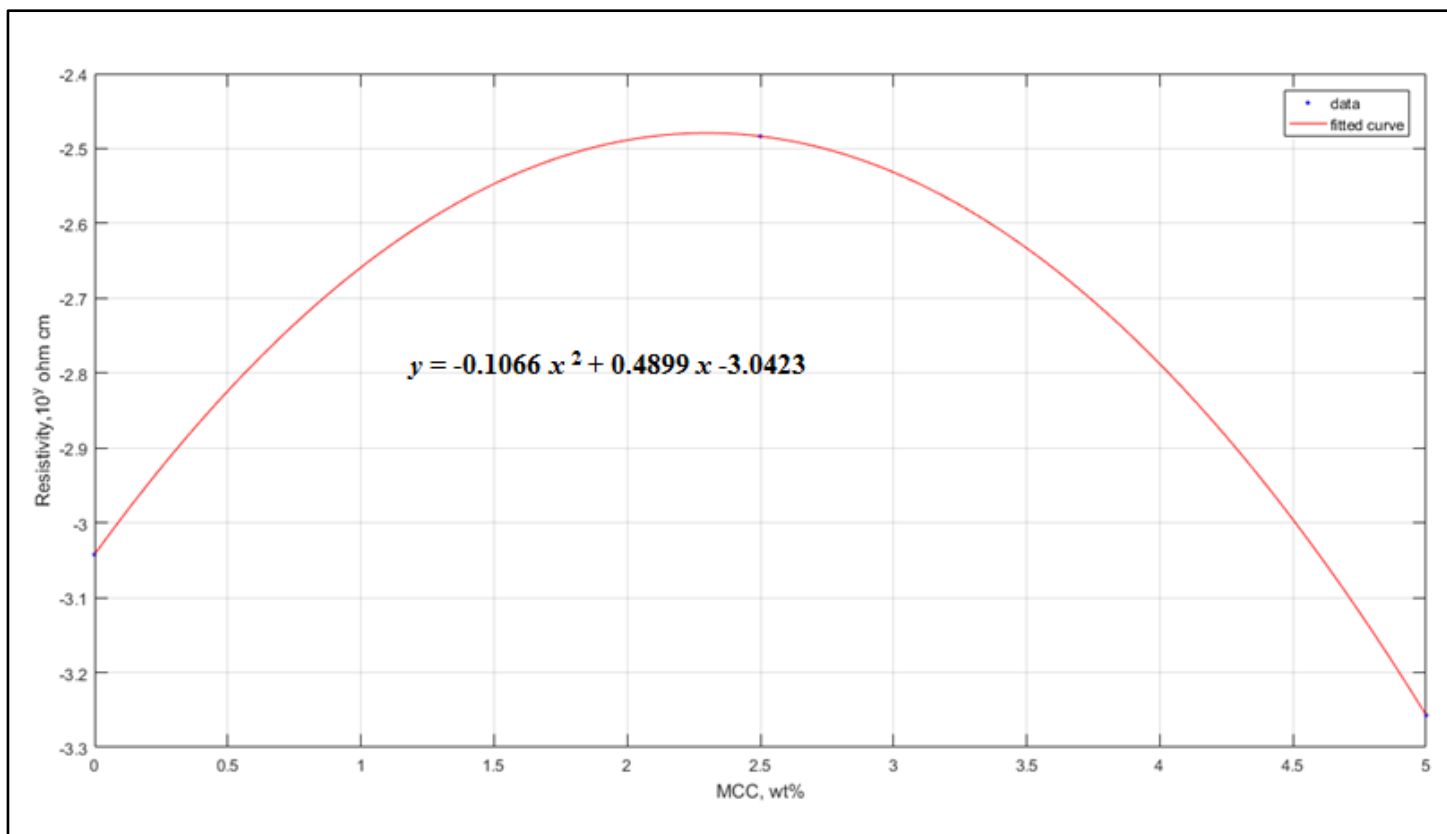


Figure 7-6: Curve fitting of electrical resistivity vs MCC solution at 2 wt% a-CNTs.

Figure 7-7 indicates the three-dimensional relationship of resistivity against MCC and DGEBA at 3 wt% a-CNTs. The polynomial surface function was found in equation (16), where x is DGEBA wt % and y is MCC wt %.

$$f(z) = -17.7161 + 0.5021 x + 1.3525 y - 0.0033 x^2 - 0.0078 x y - 0.1965 y^2 \quad (16)$$

Figure 7-8 shows the curve fitting of electrical resistivity against MCC solution at 3 wt % a-CNTs. The equation was found in equation (17), where x is MCC. The lowest electrical resistivity can be observed at 0 wt% MCC, and the electrical resistivity is $8.588 \times 10^{-4} \Omega \cdot \text{cm}$.

$$y = -0.3346 x^2 + 1.6894 x - 3.0661 \quad (17)$$

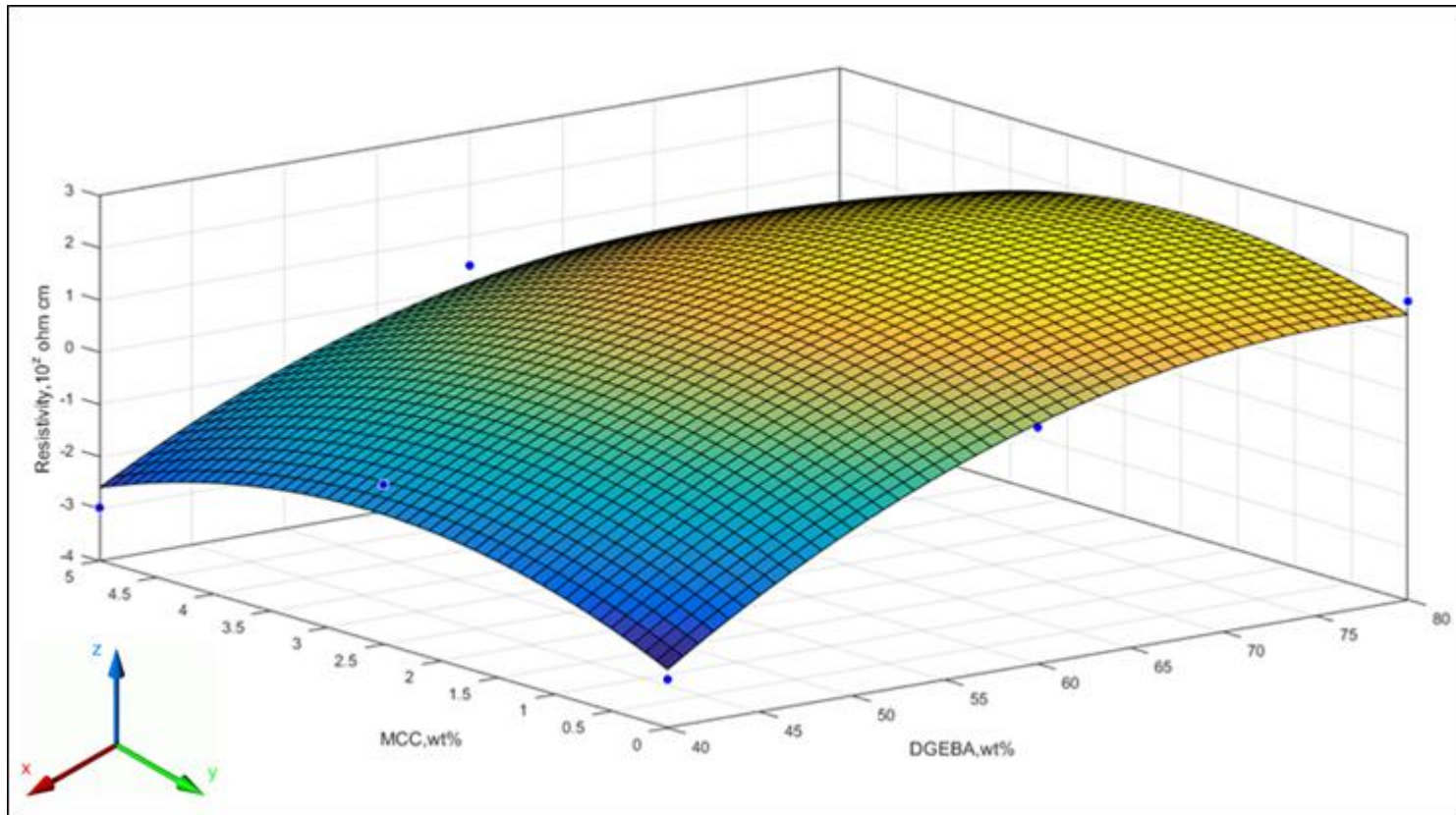


Figure 7-7: Electrical resistivity of ICAs as a function of MCC solution and DGEBA epoxy resin at 3 wt% a-CNTs.

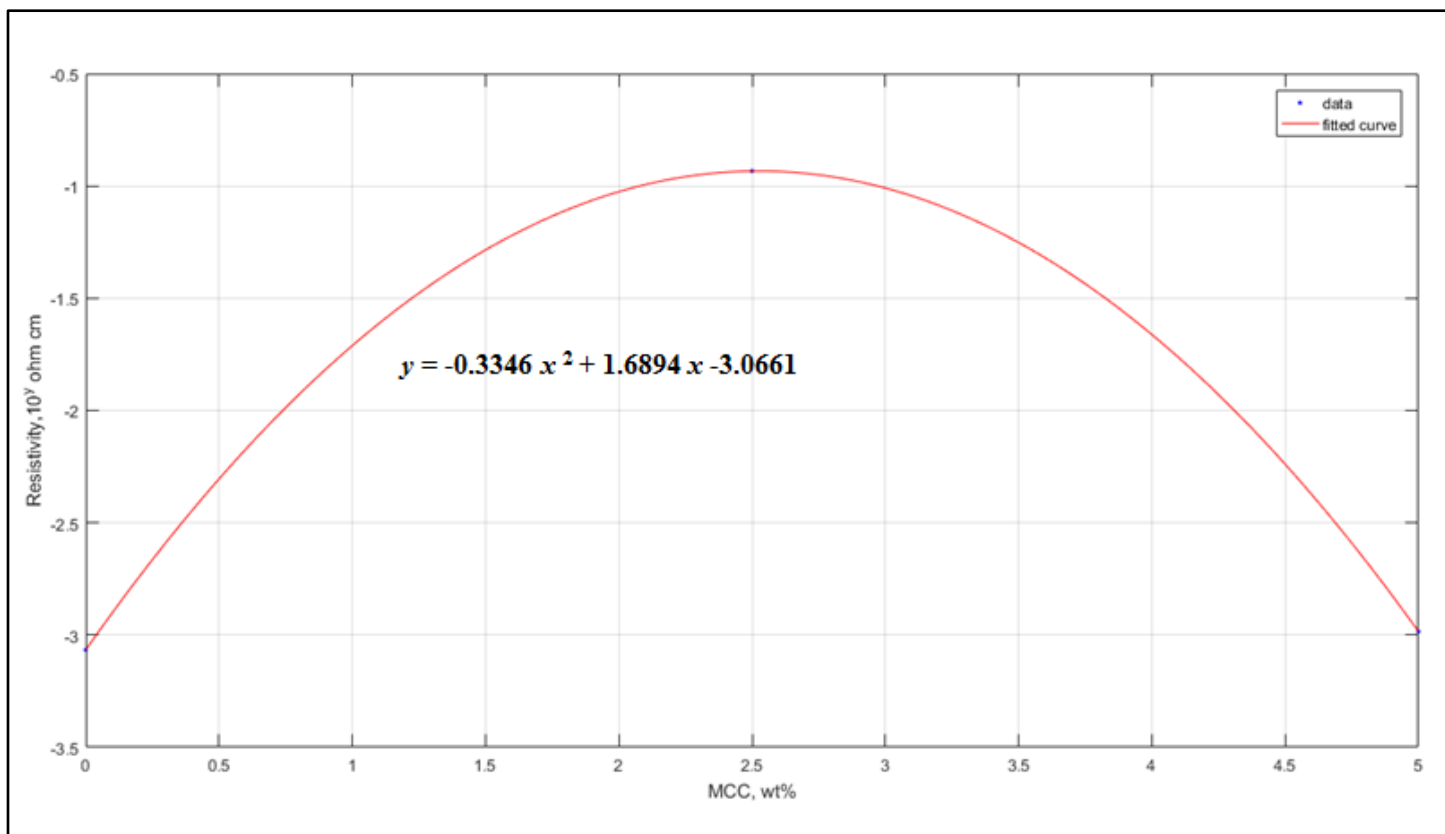


Figure 7-8: Curve fitting of electrical resistivity vs MCC solution at 3 wt% a-CNTs.

From the above results, the overall electrical resistivity varies from 0 to 3 wt % of a-CNTs. The varying levels of a-CNTs, MCC and DGEBA did play a crucial role in electrical resistivity. However, there is no significant trend of the MCC with ICAs resistivity. It can be observed that by increasing the weight percentage of a-CNTs to 3 wt % at 40 wt % DGEBA, which is 57 wt % silver powder, resistivity reached $8.588 \times 10^{-4} \Omega \cdot \text{cm}$. Additional a-CNTs give higher number of contact points and resulting in higher conductivity. This is due to the different tube wall structures of the a-CNTs (composed of discontinuous graphene sheets and carbon clusters) incorporated well in between DGEBA polymer matrix and silver powder and thus enhances its conductivity (Zhao et al., 2014). It can be seen that at 5 wt% MCC solution with the addition of 2 wt% a-CNTs into the ICAs systems, the electrical resistivity is found to be the lowest at $5.523 \times 10^{-4} \Omega \cdot \text{cm}$. This suggested that the cellulosic fillers in MCC solution linked well with a-CNTs and boosted the electrical conductivity of the ICAs. This can result in more intramolecular chains and thus cross-linking reaction could happen more easily.

The best formulated ICAs with very low resistivity $5.523 \times 10^{-4} \Omega \cdot \text{cm}$ could enable the electrical interconnection between temperature-sensitive surface mounted devices and non-solderable.

CHAPTER 8

CONCLUSIONS AND RECOMMENDATIONS

8.1 Introduction

Isotropic conductive adhesives (ICAs) have attracted attention because of their unique properties. One of the main disadvantages of ICAs is the lower conductivity as compared to lead solder. This will limit its performance in many applications. In order to achieve higher conductivity, higher loading of silver has been incorporated into the ICAs system. However, the higher loading of silver fillers indirectly will deteriorate the mechanical strength. To increase the electrical conductivity while lowering the usage of silver powder filler, silver nanoparticles (SNPs) and amorphous carbon nanotubes (a-CNTs) were incorporated into ICAs systems.

The aim of this research is to develop highly conductive formulated ICAs by adding the in-house prepared silver nanoparticles (SNPs) and amorphous carbon nanotubes (a-CNTs) while ensuring satisfactory characteristics based on their rheological properties, gelation behaviour and thermal stability.

In this thesis, SNPs and a-CNTs were synthesized by chemical approaches. To purify the a-CNTs, it was treated by hydrochloric acid. SNPS

and a-CNTs were then reinforced into ICAs to form new formulations. For better dispersion of nanoparticles into the polymer matrix, microcrystalline cellulose (MCC) was added to the ICAs. The rheological behaviour, thermal stability and gelation points of the formulated ICAs has been carried out. Based on the optimum results, new ICAs formulations were generated by surface response and electrical conductivity was measured. It is concluded that:

- (1) SNPs and a-CNTs were successfully synthesized by chemical approaches.
- (2) The ICAs samples are considered to have a good thixotropic behaviour with the recovery more than 70 %.
- (3) All the formulated ICAs samples are thermally stable when the temperature is more 550 °C except sample with 10 wt% MCC solution.
- (4) For 5 wt% MCC solution with the addition of 2 wt% a-CNTs to the ICAs systems, electrical resistivity is $5.523 \times 10^{-4} \Omega \cdot \text{cm}$.

The summary of the findings according to four research objectives are further discussed in subsequent sections. The first is to prepare the SNPs and a-CNTs and before reinforcing into the newly formulated ICAs. A few characterizations are carried out to analyse the synthesized SNPs and a-CNTs. The second objective is to investigate the visco-elastic and thixotropy of the new formulation isotropic conductive adhesives (ICAs). The third is to study the gelation points and weight loss of the new formulation ICAs by dynamic mechanical thermal analysis (DMTA) and thermogravimetric analysis (TGA),

respectively. The last objective is to measure the electrical conductivity of the ICAs by four-point probes.

8.2 Characterization of Chemical Synthesized Silver Nanoparticles (SNPs) and Amorphous Carbon Nanotubes (a-CNTs)

A few characterization methods were used such as ultraviolet–visible spectroscopy (UV-Vis), Fourier transform infrared spectroscopy (FTIR), X-ray diffraction (XRD), Raman Spectroscopy, field emission scanning electron microscope (FESEM), energy dispersive X-ray (EDX) and high-resolution transmission electron microscopy (HRTEM) to determine the size, morphology and structure of SNPs, treated a-CNTs and untreated a-CNTs. Based on the XRD results, the peaks of SNPs synthesized correspond to the pure silver metal with face centred cubic symmetry (JCPDS, no 04-0783). The surface morphology of SNPs is spherical, and the average sizes of particles are found to be 15.13 nm. However, the SNPs tend to agglomerate into larger size, with some reaching more than 100 nm.

For the synthesized a-CNTs, the XRD results show that the synthesized carbon nanotubes are an amorphous structure. Based on the Raman spectra, the untreated a-CNTs have higher I_D/I_G ratio due to more defects created after the chemical synthesizing process. A decrease was found in the I_D/I_G ratio after washing with HCl, indicating a higher quality of

nanotubes. From the result of EDX mapping analysis, the weight percentages of chloride and iron elements in untreated a-CNTs are 54.8 wt% and 12.7 wt%, respectively. After treatment, the weight percentages reduced to (Cl) 1.5 wt% and (Fe) 0.2 wt%. The SAED shows the ring and blue pattern of the nanotubes. It can be suggested that CNTs are not a crystallize structure and but an amorphous CNTs. This result agreed with the XRD result.

It is worth noting that based on the experimental results, the SNPs and a-CNTs were successfully synthesized by chemical approaches. They were then reinforced into new ICAs formulations to study its rheological behaviours.

8.3 Investigation of the visco-elastic and thixotropic properties of the new formulation isotropic conductive adhesives (ICAs)

A series of tests were carried in order to study the flow character of SNPs and a-CNTs filled ICAs, for instance, constant shear rate vs time; amplitude sweep; frequency sweep; hysteresis; three interval thixotropy test (3ITT) and creep recovery. In the viscosity test, all the sample were undergone shear thinning behaviour. The shear thinning behaviour of paste materials is typically suggested that the particles adopting a more flow-oriented arrangement through a viscous fluid. The linear visco-elastic region (LVER) was found within the 0.1 % strain. The sample incorporated with a-CNTs had the longest LVER and indicate a well-dispersed and stable system. In the larger length of LVER, the pastes are more stable and well-dispersed in suspensions.

The ICAs samples are considered to demonstrate good thixotropic behaviour with the recovery more than 70 %. When the thixotropic fluid is subjected to the higher shear rate (for instance, mixture of squeegee pressure, velocity or screen tension), the paste turns significantly thinner and resulting in the more steadily flow. Amorphous-CNTs and 5 wt% MCC solution display the good thixotropy behaviour with less tendency to slump as compared to SNPs samples. It is worth noting that excellent thixotropy is essential for good processability or printability that indicating low viscosity at the higher shear rate.

8.4 Study of the gelation points and weight loss of the new formulation ICAs

The thermal stability and gelation temperature of the new formulation ICAs samples were investigated using TGA and DMTA, respectively. From the results of thermal analysis of the new ICAs formulations, it can be suggested that all the ICAs samples are thermally stable when the temperature is more 550 °C expect for S1, S2 and S8. It can be noticed that the gelation temperature decreases with increasing of SNPs contents (8 wt% and 10 wt%). This has shown that incorporated with SNPs, the transition from liquid-like behaviour to solid-like behaviour can occur at the lower temperature, which is below 80 °C. Moreover, with the aid of MCC solution and just 2 wt% of a-CNTs, the gelation temperature remained low at less than 90 °C. Thus, those

samples with lower gelation temperature are suggested to have faster cure rates. The higher weight percentage of SNPs, a-CNTs and MCC do act in a way in forming a barrier and block the movement of DGEBA. As the result, the crosslinking increases at a faster rate, lowering the gelation temperature of the ICAs.

8.5 Measurement of the electrical conductivity of the ICAs

The effects of the different composition of a-CNTs and MCC solution on electrical conductivity were measured by four-point probes. The varying levels of a-CNTs, MCC and DGEBA did play a crucial role in electrical resistivity. However, there is no significant trend of the MCC with ICAs resistivity. It can be observed that by increasing the weight percentage of a-CNTs to 3 wt % at 40 wt % DGEBA, which is 57 wt % silver powder, resistivity reached $8.588 \times 10^{-4} \Omega \cdot \text{cm}$. It can be seen that for 5 wt% MCC solution with the addition of 2 wt% a-CNTs to the ICAs systems, the electrical resistivity is around $5.523 \times 10^{-4} \Omega \cdot \text{cm}$. This suggests that in-house prepared a-CNTs reduce the electrical resistivity.

8.6 Recommendations

In this thesis, synthesized CNTs were prepared in amorphous form. The electrical resistivity which can be achieved is at $5.523 \times 10^{-4} \Omega \cdot \text{cm}$. It is clear that the a-CNTs leads to significant increase in electrical conductivity.

However, further research need to be conducted. Some potential improvements, recommendations and suggestions are as follows:

1. The a-CNTs can be treated by adding a new functional group to the outer layer of a-CNTs to change its sidewalls. It can be done through an oxidation process for a-CNTs involving ultrasonic treatment in a mixture of concentrated nitric and sulfuric acid to decorate with a high density of oxygen which is mainly carboxyl groups. This is then followed by subsequent esterification or amidization of the carboxyl groups. With this new modification of a-CNTs, it can lead to a reduction of van der Waals interactions between the a-CNTs. It is suggested to separate the nanotubes bundles into individual tubes which will have more defined nanotubes. It is desired to incorporate the modified a-CNTs into the ICAs and further increase electrical conductivity.
2. Based on the findings, there are a few advantages by adding the microcrystalline cellulose (MCC) into ICAs. However, some further works need to be conducted in order to study its mechanical properties. To date, few researchers have investigated the impact performance of MCC into ICAs. Drop tests should be carried out to evaluate its impact strength. The effect of thermal cycling on mechanical behaviour of MCC filled ICAs can be further investigated to generate in-depth knowledge on its reliability for long term performance.

3. Based on the lowest value of electrical resistivity found from this study, the optimum formulations paste can be placed on different PCB surface finishes to study the interfacial reaction between the PCBs interconnections. The growth behaviour of interfacial intermetallic compound (IMC) form would enhance knowledge of ICAs/ PCBs interactions to understand the reliability of ICAs interconnections from a metallurgical viewpoint.

REFERENCES

- Abou el-nour, K. M. M., Eftaiha, A. A., Al-warthan, A. and Ammar, R. A. A. 2010. Synthesis and applications of silver nanoparticles. *Arabian Journal of Chemistry*, 3, pp. 135-140.
- Allaoui, A., Bai, S., Cheng, H. M. and Bai, J. B. 2002. Mechanical and electrical properties of a MWNT/epoxy composite. *Composites Science and Technology*, 62, pp. 1993-1998.
- Altman, D., Minozzo, F. C. and Rassier, D. E. 2015. Thixotropy and Rheology of Muscle Fibers Probed Using Sinusoidal Oscillations. *PLoS ONE*, 10, e0121726.
- Amaral, C. R., Rodríguez, R. J. S., Junior, L. P. B., Skury, A. L. D. and Monteiro, S. N. 2012. Mechanical Properties and Abrasive Behavior of Diamond Incorporated Epoxy Composites. *Materials Science Forum*, 727-728, pp. 1757-1762.
- An, T. and Qin, F. 2014. Effects of the intermetallic compound microstructure on the tensile behavior of Sn3.0Ag0.5Cu/Cu solder joint under various strain rates. *Microelectronics Reliability*, 54, pp. 932-938.
- Anh-tuan, L., Thi Tam, L., Van Quy, N., Huy Hoang, T., Duc Anh, D., Quang Huy, T. and Dinh Lam, V. 2012. Powerful colloidal silver nanoparticles for the prevention of gastrointestinal bacterial infections. *Advances in Natural Sciences: Nanoscience and io02x3vyfwssdse cv*
- Aswathy, B., Avadhani, G. S., Sumithra, I. S., Suji, S. and Sony, G. 2011. Microwave assisted synthesis and UV-Vis spectroscopic studies of silver nanoparticles synthesized using vanillin as a reducing agent. *Journal of Molecular Liquids*, 159, pp.165-169.
- Awasthi, K., Kumar, R., Raghubanshi, H., Awasthi, S., Pandey, R., Singh, D., Yadav, T. P. and Srivastava, O. N. 2011. Synthesis of nano-carbon (nanotubes, nanofibres, graphene) materials. *Bulletin of Materials Science*, 34, pp. 607-614.
- Banerjee, D., Jha, A. and Chattopadhyay, K. K. 2010. FESEM and HRTEM studies of some novel carbon nanostructures. *Formatex*, pp. 1674-1680.
- Bao, X., Lee, N.-C., Raj, R. B., Rangan, K. P. and Maria, A. 1998. Engineering solder paste performance through controlled stress rheology analysis. *Soldering and Surface Mount Technology*, 10, pp. 26-35.

Barnes, H. A. 1997. Thixotropy—a review. *Journal of Non-Newtonian Fluid Mechanics*, 70, pp.1-33.

Barnes, H. A., Hutton, J. F. and Walters, K. 1989. *An Introduction to Rheology*, Elsevier.

Bell, G., Rosell, C. and Joslin, S. 1987. Rheology of Silver- Filled Glass Die Attach Adhesive for High-Speed Automatic Processing. *IEEE Transactions on Components, Hybrids, and Manufacturing Technology*, 10, pp. 507-510.

Bolotoff, P. V., 2010, *Solder alloys: Physical and Mechanical Properties* [Online]. Available at: http://alasil.com/reference/solder_alloys/ [Accessed: 11 December 2017].

Brown, K. R., Walter, D. G. and Natan, M. J. 2000. Seeding of Colloidal Au Nanoparticle Solutions. 2. Improved Control of Particle Size and Shape. *Chemistry of Materials*, 12, pp. 306-313.

Cai, J., Liu, Y. and Zhang, L. 2006. Dilute solution properties of cellulose in LiOH/urea aqueous system. *Journal of Polymer Science Part B: Polymer Physics*, 44, pp. 3093-3101.

Cai, J., Zhang, L., Zhou, J., Qi, H., Chen, H., Kondo, T., Chen, X. and Chu, B. 2007. Multifilament Fibers Based on Dissolution of Cellulose in NaOH/Urea Aqueous Solution: Structure and Properties. *Advanced Materials*, 19, pp. 821-825.

Chee, S.-S. and Lee, J.-H. 2012. Reduction synthesis of silver nanoparticles anchored on silver micro-flakes and electrical resistivity of isotropic conductive adhesives at percolation threshold. *Electronic Materials Letters*, 8, pp. 315-320.

Chen, D., Qiao, X., Qiu, X., Tan, F., Chen, J. and Jiang, R. 2010. Effect of silver nanostructures on the resistivity of electrically conductive adhesives composed of silver flakes. *Journal of Materials Science: Materials in Electronics*, 21, pp. 486-490.

Chen, S., Liu, K., Luo, Y., Jia, D., Gao, H., Hu, G. and Liu, L. 2013. In situ preparation and sintering of silver nanoparticles for low-cost and highly reliable conductive adhesive. *International Journal of Adhesion and Adhesives*, 45, pp. 138-143.

Cheung, W., Patel, M., Ma, Y., Chen, Y., Xie, Q., Lockard, J. V., Gao, Y. and He, H. 2016. [small pi]-Plasmon absorption of carbon nanotubes for the selective and sensitive detection of Fe³⁺ ions. *Chemical Science*, 7, pp. 5192-5199.

Chew, C. S., Durairaj, R., Hwang, J., Tan, J., Liang, M. S., Tan, C. N. and Chen, K. P. The effect of nano fillers in electrical and mechanical properties of

isotropic conductive adhesive. 36th International Electronics Manufacturing Technology Conference, 11-13 Nov 2014. pp 1-6.

Chrapava, S., Touraud, D., Rosenau, T., Potthast, A. and Kunz, W. 2003. The investigation of the influence of water and temperature on the LiCl/DMAc/cellulose system. *Physical Chemistry Chemical Physics*, 5, pp.1842-1847.

Chrissafis, K. and Bikiaris, D. 2011. Can nanoparticles really enhance thermal stability of polymers? Part I: An overview on thermal decomposition of addition polymers. *Thermochimica Acta*, 523, pp. 1-24.

Cho, N. H., Veirs, D. K., Ager, J. W., Rubin, M. D., Hopper, C. B. and Bogy, D. B. 1992. Effects of substrate temperature on chemical structure of amorphous carbon films. *Journal of Applied Physics*, 71, pp. 2243-2248.

Choi, G. B., and Lee, J. H. (2005). Method for the preparation of silver nanoparticles-polymer composite: Google Patents.

Chu, P. K. and Li, L., 2006. Characterization of amorphous and nanocrystalline carbon films. *Materials Chemistry and Physics*, 96(2-3), pp. 253-277.

Chueh, T.-C., Hu, C.-H. and Yen, S.-C. 2015. Electrically Conductive Adhesives with Low Ag Content Prepared by Ag Self-Activated Plating and PEDOT:PSS. *Journal of The Electrochemical Society*, 162, pp. D56-D61.

Ci, L., Wei, B., Xu, C., Liang, J., Wu, D., Xi, S., Zhou, W., Li, Y., Liu, Z. and Tang, D., 2001. Crystallization behavior of the amorphous carbon nanotubes prepared by the CVD method. *Journal of Crystal Growth*, 233, pp. 823-828.

Dey, P. K. B. A. S. 2015. Effects and applications of silver nanoparticles in different fields. *International Journal of Recent Scientific Research*, 6, pp. 5880-5883.

Dulina, I., Umerova, S. and Ragulya, A. 2015. Plasticizer Effect on Rheological Behaviour of Screen Printing Pastes Based on Barium Titanate Nanopowder. *Journal of Physics: Conference Series*, 602, 012035.

Durairaj, R., Mallik, S., Seman, A., Marks, A. and Ekere, N. N. Viscoelastic properties of solder pastes and isotropic conductive adhesives used for flip-chip assembly. Electronic Manufacturing Technology Symposium (IEMT), 2008 33rd IEEE/CPMT International, 4-6 Nov. 2008. pp. 1-8.

Durairaj, R. and Man, L. W. 2011. Effect of epoxy and filler concentrations on curing behaviour of isotropic conductive adhesives. *Journal of Thermal Analysis and Calorimetry*, 105, pp. 151-155.

Durairaj, R., Namasivayam, S., Zhen Xiong, C., Mannan, S. and Ashayer, R. 2015. Evaluation of the Morphological, Electrical, and Mechanical Properties of Silver Nanopastes. pp. 1020-1027.

Durairaj, R., Pheng, L. S. and Ping, L. J. 2016. Investigation on the mechanical and electrical properties of multiwall carbon nanotubes (MWNCTs) based isotropic conductive adhesives. *Pigment and Resin Technology*, 45, pp. 240-245.

Durairaj, R. M., Lam WaI, Ramesh, S. 2011. Rheological Characterisation and Empirical Modelling of Lead-Free Solder Pastes and Isotropic Conductive Adhesive Pastes. *Journal of ASTM International*, 7, pp. 1-13.

Durairaj, R., Ramesh, S., Mallik, S., Seman, A. and Ekere, N. 2009. Rheological characterisation and printing performance of Sn/Ag/Cu solder pastes. *Materials and Design*, 30, pp. 3812-3818.

Durairaj, R., Sean, C. C., Chiun, T. C. and Ping, L. J. Investigation of dynamic and mechanical thermal behavior of isotropic conductive adhesives. Electronics Packaging Technology Conference (EPTC 2013), 2013 IEEE 15th, 11-13 Dec. 2013. pp. 461-465.

Durairaj, R., Seman, A. and Ekere, N. N. Development of Quality Control (QC) Tools for Solder Pastes used for Flip Chip Assembly based on Oscillatory Tests. Electronics Systemintegration Technology Conference, 2006. 1st, 5-7 Sept. 2006. pp. 347-353.

Dusek, M., Zou, L. and Hunt, C. 2002. Rheology testing of solder pastes and conductive adhesives used in stencil printing.

Fan, Q., Cui, H., Li, D., Hu, Z., Yuan, Z., Ye, L. and Liu, J. The effect of functionalized silver on properties of conductive adhesives. Electronic Packaging Technology and High Density Packaging (ICEPT-HDP), 2011 12th International Conference on, 8-11 Aug. 2011. pp. 1-3.

Fink, J. K. 2005. 3 - Epoxy Resins. *Reactive Polymers Fundamentals and Applications*. Norwich, NY: William Andrew Publishing.

Forrest, M. J. 2007. *Coatings and inks for food contact materials*, Rapra Technology.

Foss, D. R. and Brady, J. F. 2000. Brownian Dynamics simulation of hard-sphere colloidal dispersions. *Journal of Rheology*, 44, pp. 629-651.

Garg, P., Singh, B., Kumar, G., Gupta, T., Pandey, I., Seth, R., Tandon, R. and Mathur, R. 2011. Effect of dispersion conditions on the mechanical properties of multi-walled carbon nanotubes based epoxy resin composites. *Journal of Polymer Research*, 18, pp. 1397-1407.

Gilleo, K. 1989. Rheology and Surface Chemistry for Screen Printing. *Screen Printing*, pp. 128-132.

Goodman, S. W. 1999. Handbook of Thermoset Plastics. 2 ed.: William Andrew.

Govindappa, M., Farheen, H., Chandrappa, C. P., Channabasava, Ravishankar, V. R. and Vinay, B. R. 2016. Mycosynthesis of silver nanoparticles using extract of endophytic fungi, *Penicillium* species of *Glycosmis mauritiana*, and its antioxidant, antimicrobial, anti-inflammatory and tyrosinase inhibitory activity. *Advances in Natural Sciences: Nanoscience and Nanotechnology*, 7, 035014.

Gudikandula, K. and Charya Maringanti, S. 2016. Synthesis of silver nanoparticles by chemical and biological methods and their antimicrobial properties. *Journal of Experimental Nanoscience*, 11, pp. 714-721.

Guzmán, M. G., Dille, J. and Godet, S. 2008. Synthesis of Silver Nanoparticles by Chemical Reduction Method and Their Antibacterial Activity. *International Journal of Chemical, Molecular, Nuclear, Materials and Metallurgical Engineering*, 2, pp. 90-98.

He, H., Li, K., Wang, J., Sun, G., Li, Y. and Wang, J. 2011. Study on thermal and mechanical properties of nano-calcium carbonate/epoxy composites. *Materials and Design*, 32, pp. 4521-4527.

Hong, L. K., Harun, N. S., Jamil, M. S. M. and Yusop, R. M. 2013. Phase Behavior and Rheology of Fatty Alcohol Sulphate, Fatty Alcohol Ether Sulphate from Palm based and Mixtures with other Surfactants. *Malaysian Journal of Analytical Sciences*, 17, pp. 101-108.

Hoornstra, J., Weeber, A. W., Moor, H. H. C. D. and Sinke, W. C. The importance of paste rheology in improving fine line, thick film screen printing of front side metallization. 14th European Photovoltaic Solar Energy Conference, 1997 Barcelona, Spain.

Hsu, S. L.-C. and Wu, R.-T. 2011. Preparation of Silver Nanoparticle with Different Particle Sizes for Low-Temperature Sintering. *International Conference on Nanotechnology and Biosensors IPCBEE*, 2, pp. 55-58.

Hvims, H. 1995. Conductive adhesives for SMT and potential applications. *Components, Packaging, and Manufacturing Technology, Part B: Advanced Packaging, IEEE Transactions on*, 18, pp. 284-291.

Irfan, M. and Kumar, D. (2008). Recent advances in isotropic conductive adhesives for electronics packaging applications. *International Journal of Adhesion and Adhesives*, 28, pp. 362-371.

Ishii, D., Tatsumi, D. and Matsumoto, T. 2008. Effect of solvent exchange on the supramolecular structure, the molecular mobility and the dissolution

behavior of cellulose in LiCl/DMAc. *Carbohydrate Research*, 343, pp. 919-928.

Jagt, J. C. 1998. Reliability of electrically conductive adhesive joints for surface mount applications: a summary of the state of the art. *Components, Packaging, and Manufacturing Technology, Part A, IEEE Transactions on*, 21, pp. 215-225.

Jagt, J. C., Beris, P. J. M. and Lijten, G. F. C. M. 1995. Electrically conductive adhesives: a prospective alternative for SMD soldering? *Components, Packaging, and Manufacturing Technology, Part B: Advanced Packaging, IEEE Transactions on*, 18, pp. 292-298.

Jia, N., Li, S.-M., Zhu, J.-F., Ma, M.-G., Xu, F., Wang, B. and Sun, R.-C. 2010. Microwave-assisted synthesis and characterization of cellulose-carbonated hydroxyapatite nanocomposites in NaOH-urea aqueous solution. *Materials Letters*, 64, pp. 2223-2225.

Jiang, H., Moon, K.-s., Li, Y., and Wong, C. P. (2006). Surface Functionalized Silver Nanoparticles for Ultrahigh Conductive Polymer Composites. *Chemistry of Materials*, 18, pp. 2969-2973.

Kaiser, J. W. P. A. A. F.-J. 2009. Determination and Assessment of the Rheological Properties of Pastes for Screen Printing Ceramics *Annual Transactions of The Nordic Rheology Society*, 17.

Keusseyan, R. L., Dilday, J. L. and Speck, B. S. 1994. Electric Contact Phenomena in Conductive Adhesive Interconnections. *The International Journal of Microcircuits and Electronic Packaging*, 17, pp. 236-242.

Kheybari, S., Samadi, N., Hosseini, S. V., Fazeli, A. and Fazeli, M. R. 2010. Synthesis and antimicrobial effects of silver nanoparticles produced by chemical reduction method. *DARU Journal of Pharmaceutical Sciences*, 18, pp. 168-172.

Ko, C.-J., Lee, C.-Y., Ko, F.-H., Chen, H.-L. and Chu, T.-C. 2004. Highly efficient microwave-assisted purification of multiwalled carbon nanotubes. *Microelectronic Engineering*, 73-74, pp. 570-577.

Koe, K. H. 2012. *Rheological Studies of Silver (Ag) based Epoxy System*. Bachelor (Hons.) of Mechanical Engineering, Universiti Tunku Abdul Rahman.

Kohinata, S., Terao, A., Shiraki, Y., Inoue, M. and Uenishi, K. 2013. Relationship between the Conductivity of Isotropic Conductive Adhesives (ICAs) and the Lubricant Coated on Silver Filler Particles. *Transactions of The Japan Institute of Electronics Packaging*, 6, pp. 104-108.

Kotthaus, S., Gunther, B. H., Hang, R. and Schafer, H. 1997. Study of isotropically conductive bondings filled with aggregates of nano-sized Ag-

particles. *Components, Packaging, and Manufacturing Technology, Part A, IEEE Transactions on*, 20, pp. 15-20.

Kulpinski, P. 2005. Cellulose nanofibers prepared by the N-methylmorpholine-N-oxide method. *Journal of Applied Polymer Science*, 98, pp. 1855-1859.

Lam, W. M. 2011. *Development of environmental friendly electrical conductive adhesives (ecas) as a replacement to lead based solder materials in electronic manufacturing industry*. Master dissertation / Thesis, Universiti Tunku Abdul Rahman.

Lei, Z. and Fan, Y. 2006. Preparation of silver nanocomposites stabilized by an amphiphilic block copolymer under ultrasonic irradiation. *Materials Letters*, 60, pp. 2256-2260.

Leong, K. C. 2016. *RHEOLOGICAL CHARACTERISATION OF SILVER (Ag) BASED ISOTROPIC CONDUCTIVE ADHESIVES*. Master of Engineering Science, Master dissertation / Thesis, Lee Kong Chian Faculty of Engineering and Science Universiti Tunku Abdul Rahman.

Li, Y., and Wong, C. P. 2006. Recent advances of conductive adhesives as a lead-free alternative in electronic packaging: Materials, processing, reliability and applications. *Materials Science and Engineering: R: Reports*, 51, pp. 1-35.

Li, Y.-f., Gan, W.-p., Zhou, J., Lu, Z.-q., Yang, C., and Ge, T.-t. 2015. Hydrothermal synthesis of silver nanoparticles in Arabic gum aqueous solutions. *Transactions of Nonferrous Metals Society of China*, 25, pp 2081-2086.

Li, Y., Lu, D. and Wong, C. P. 2010. *Isotropically Conductive Adhesives (ICAs). Electrical Conductive Adhesives with Nanotechnologies*. Boston, MA: Springer US.

Liao, H., Wu, Y., Wu, M., Zhan, X. and Liu, H. 2012. Aligned electrospun cellulose fibers reinforced epoxy resin composite films with high visible light transmittance. *Cellulose*, 19, pp. 111.

Lim Fui, Y., Khoo Ly, H., Tiu Kong, B. and Yow Kai, Y. High thermal performance ICP die attach process design and development for LQFP-EP. *Electronics Packaging Technology Conference (EPTC)*, 2011 IEEE 13th, 7-9 Dec. 2011. pp. 190-194.

Lin, X. and Lin, F. The improvement on the properties of silver-containing conductive adhesives by the addition of carbon nanotube. High Density Microsystem Design and Packaging and Component Failure Analysis, 2004. HDP '04. *Proceeding of the Sixth IEEE CPMT Conference on*, 30 June-3 July 2004. pp. 382-384.

Liu, J. 1999. *Conductive Adhesives for Electronics Packaging*, Isle of Man, British Isles, Electrochemical Publications Ltd.

Liu, J., Gustafsson, K., Lai, Z. and Li, C. 1997. Surface Characteristics, Reliability, and Failure Mechanisms of Tin/Lead, Copper, and Gold Metallizations. *IEEE Transactions on Components, Packaging, and Manufacturing Technology-Part A*, 20, pp. 21-30.

Liu, J., Lai, Z., Kristiansen, H. and Khoo, C. Overview of conductive adhesive joining technology in electronics packaging applications. Adhesive Joining and Coating Technology in Electronics Manufacturing, 1998. *Proceedings of 3rd international Conference on*, 28-30 Sep 1998. pp. 1-18.

Liz-marzán, L. M. and Lado-touriño, I. 1996. Reduction and Stabilization of Silver Nanoparticles in Ethanol by Nonionic Surfactants. *Langmuir*, 12, pp. 3585-3589.

Lu, D., Tong, Q. K. and Wong, C. P. 1999. A study of lubricants on silver flakes for microelectronics conductive adhesives. *Components and Packaging Technologies, IEEE Transactions on*, 22, pp. 365-371.

Lu, D. and Wong, C. P. 2000. Effects of shrinkage on conductivity of isotropic conductive adhesives. *International Journal of Adhesion and Adhesives*, 20, pp. 189-193.

Lu, D. and Wong, C. P. 1999. High performance conductive adhesives. *Electronics Packaging Manufacturing, IEEE Transactions on*, 22, pp. 324-330.

Lu, D. and Wong, C. P. Development of conductive adhesives filled with low-melting-point alloy fillers. *Advanced Packaging Materials: Processes, Properties and Interfaces, 2000. Proceedings. International Symposium on*, 2000. pp. 7-13.

Ma, M.-G., Zhu, J.-F., Li, S.-M., Jia, N. and Sun, R.-C. 2012. Nanocomposites of cellulose/iron oxide: influence of synthesis conditions on their morphological behavior and thermal stability. *Materials Science and Engineering: C*, 32, pp. 1511-1517.

Majeed Khan, M. A., Kumar, S., Ahamed, M., Alrokayan, S. and Alsalhi, M. 2011. Structural and thermal studies of silver nanoparticles and electrical transport study of their thin films. *Nanoscale Research Letters*, 6, pp. 434.

Mallik, S., Schmidt, M., Bauer, R. and Ekere, N. N. Influence of solder paste components on rheological behaviour. *Electronics System-Integration Technology Conference*, 2008. ESTC 2008. 2nd, 1-4 Sept. 2008. pp. 1135-1140.

Malkin, A. Y. and Kulichikhin, S. G. 2008. *Rheokinetics*, Wiley.

Malkin, A. Y., Kulichikhin, S. G., Emel'yanov, D. N., Smetanina, I. E. and Ryabokon, N. V. 1984. Rheokinetics of free-radical polymerization. *Polymer*, 25, pp. 778-784.

Manivasagan, P., Venkatesan, J., Senthilkumar, K., Sivakumar, K. and Kim, S.-K. 2013. Biosynthesis, Antimicrobial and Cytotoxic Effect of Silver Nanoparticles Using a Novel *Nocardiosis* sp. MBRC-1. *BioMed Research International*, 2013, pp. 9.

Mahanta, N. K., Loos, M. R., Manas Zloczower, I. and Abramson, A. R. 2015 "Graphite-graphene hybrid filler system for high thermal conductivity of epoxy composites," *Journal of Materials Research*. Cambridge University Press, 30(7), pp. 959-966.

Manson, J. A. 2012. Polyether resins. McGraw-Hill Education.

Marcq, F., Demont, P., Monfraix, P., Peigney, A., Laurent, C., Falat, T., Courtade, F. and Jamin, T. 2011. Carbon nanotubes and silver flakes filled epoxy resin for new hybrid conductive adhesives. *Microelectronics Reliability*, 51, pp. 1230-1234.

Mewis, J. and Wagner, N. J. 2009. Current trends in suspension rheology. *Journal of Non-Newtonian Fluid Mechanics*, 157, pp. 147-150.

Mir, I. and Kumar, D. 2008. Recent advances in isotropic conductive adhesives for electronics packaging applications. *International Journal of Adhesion and Adhesives*, 28, pp. 362-371.

Moakes, R. J. A., Sullo, A. and Norton, I. T. 2015. Preparation and rheological properties of whey protein emulsion fluid gels. *RSC Advances*, 5, pp. 60786-60795.

Mohanty, A. and Srivastava, V. K. 2012. Compressive failure analysis of alumina nano-particles dispersed short glass carbon fiber reinforced epoxy hybrid composites. *International Journal of Scientific and Engineering Research*, 3, pp. 1-7.

Mombeshora, E. T., Simoyi, R., Nyamori, V. O. and Ndungu, P. G. 2015. Multiwalled carbon nanotube-titania nanocomposites: Understanding nano-structural parameters and functionality in dye-sensitized solar cells. *South African Journal of Chemistry*, 68, pp. 153-164.

Montazeri, A., Javadpour, J., Khavandi, A., Tcharkhtchi, A. and Mohajeri, A. 2010. Mechanical properties of multi-walled carbon nanotube/epoxy composites. *Materials and Design*, 31, pp. 4202-4208.

Morissette, S. L., Lewis, J. A., Clem, P. G., Cesarano, J. and Dimos, D. B. 2001. Direct-Write Fabrication of $\text{Pb}(\text{Nb,Zr,Ti})\text{O}_3$ Devices: Influence of Paste Rheology on Print Morphology and Component Properties. *Journal of the American Ceramic Society*, 84, pp. 2462-2468.

Nana, X., Zhiling, L., Hui, X., Yuzhen, Z., Yuehui, W., and Jingze, L. 2016. Influence of Curing Procedures on the Electrical Properties of Epoxy-Based Isotropic Conductive Adhesives. *Rare Metal Materials and Engineering*, 45, pp. 2524-2528.

Nguty, T. A., Ekere, N. N. and Adebayo, A. Correlating solder paste composition with stencil printing performance. Electronics Manufacturing Technology Symposium, 1999. Twenty-Fourth IEEE/CPMT, 1999. pp. 304-312.

Nguty, T. A., Riedlin, M. H. A. and Ekere, N. N. Evaluation of process parameters for flip chip stencil printing. Electronics Manufacturing Technology Symposium, 1998. Twenty-Third IEEE/CPMT, 19-21 Oct 1998. pp. 206-216.

Nieu, N. H., Tan, T. T. M. and Huong, N. L. 1996. Epoxy—phenol—cardanol—formaldehyde systems: Thermogravimetry analysis and their carbon fiber composites. *Journal of Applied Polymer Science*, 61, pp. 2259-2264.

Núñez, L., Fraga, F., Castro, A., Núñez, M. R. and Villanueva, M. 2001. TTT cure diagram for an epoxy system diglycidyl ether of bisphenol A/1,2 diamine cyclohexane/calcium carbonate filler. *Polymer*, 42, pp. 3581-3587.

Ohde, H., Hunt, F. and Wai, C. M. 2001. Synthesis of Silver and Copper Nanoparticles in a Water-in-Supercritical-Carbon Dioxide Microemulsion. *Chemistry of Materials*, 13, pp. 4130-4135.

Pal, R. 2005. Modeling viscoelastic behavior of particulate composites with high volume fraction of filler. *Materials Science and Engineering: A*, 412, pp. 71-77.

Patel, A. R. and Dewettinck, K. 2015. Comparative evaluation of structured oil systems: Shellac oleogel, HPMC oleogel, and HIPE gel. *European Journal of Lipid Science and Technology*, 117, pp. 1772-1781.

Pearce, E. M., Khanna, Y. P. and Raucher, D. 1981. CHAPTER 8 - Thermal Analysis in Polymer Flammability A2 - TURI, EDITH A. *Thermal Characterization of Polymeric Materials*. Academic Press.

Peng, C., Zhang, S., Jewell, D. and Chen, G. Z. 2008. Carbon nanotube and conducting polymer composites for supercapacitors. *Progress in Natural Science*, 18, pp. 777-788.

Périchaud, M. G., Delétage, J. Y., Frémont, H., Danto, Y. and Faure, C. 2000. Reliability evaluation of adhesive bonded SMT components in industrial applications. *Microelectronics Reliability*, 40, pp. 1227-1234.

Pettersen, S. R., Kristiansen, H., Redford, K., Helland, S., Kalland, E., Zhang, Z. and He, J. Controlling the Conduction Mechanisms in Isotropic Conductive Adhesives with Silver-Coated Polymer Spheres. *2016 IEEE 66th Electronic Components and Technology Conference (ECTC)*, May 31 2016-June 3 2016. pp. 2494-2500.

Phair, J. W. and Kaiser, A. F.-J. 2009. Determination and Assessment of the Rheological Properties of Pastes for Screen Printing Ceramics. *ANNUAL TRANSACTIONS OF THE NORDIC RHEOLOGY SOCIETY*, 17.

Pittroff, R. R. 2007. *Relationship between the Physical Properties and Curing System of an Epoxy Matrix Material*. Magister Technologiae: Engineering: Mechanical, Tshwane University of Technology.

Prime, R. B. 1981. CHAPTER 5 - Thermosets. In: EDITH, T. (ed.) *Thermal Characterization of Polymeric Materials*. Academic Press.

Puisto, A., Mohtaschemi, M., Alava, M. J. and Illa, X. 2015. Dynamic hysteresis in the rheology of complex fluids. *Physical Review E*, 91, 042314.

Quang HUY, T., Van Quy, N. and Anh-Tuan, L. 2013. Silver nanoparticles: synthesis, properties, toxicology, applications and perspectives. *Advances in Natural Sciences: Nanoscience and Nanotechnology*, 4, 033001.

Rao, R. M. V. G. K. and Pourassamy, A. 1976. Studies on the curing of a loaded unsaturated polyester binder. *Polymer*, 17, pp. 611-612.

Reddy, S. M. M., Shanmugam, G., Duraipandy, N., Kiran, M. S. and Mandal, A. B. 2015. An additional fluorenylmethoxycarbonyl (Fmoc) moiety in di-Fmoc-functionalized l-lysine induces pH-controlled ambidextrous gelation with significant advantages. *Soft Matter*, 11, pp. 8126-8140.

Roy, C., Budtova, T. and Navard, P. 2003. Rheological properties and gelation of aqueous cellulose-NaOH solutions. *Biomacromolecules*, 4, pp. 259-264.

Roy, R., Jha, A., Banerjee, D., Sankar das, N. and Chattopadhyay, K. K. 2013. Edge effect enhanced electron field emission in top assembled reduced graphene oxide assisted by amorphous CNT-coated carbon cloth substrate. *AIP Advances*, 3, 012115.

Saito, S., Sasabe, H., Nakajima, T. and Yada, K. 1968. Dielectric relaxation and electrical conduction of polymers as a function of pressure and temperature. *Journal of Polymer Science Part A-2: Polymer Physics*, 6, pp. 1297-1315.

Saleh, A. B. B., Ishak, Z. A. M., Hashim, A. S. and Kamil, W. A. 2009. Compatibility, Mechanical, Thermal, and Morphological Properties of Epoxy Resin Modified with Carbonyl-Terminated Butadiene Acrylonitrile Copolymer Liquid Rubber. *Journal of Physical Sciences*, 20, pp.1-12.

- Samanta, B. C. and Maity, T. 2012. Effectiveness of amine functional aniline furfuraldehyde condensate as toughening agent for epoxy resin. *Pigment and Resin Technology*, 41, pp. 344 - 350.
- Sankal, S. and Kaynak, C. 2013. Using various techniques to characterize oxidative functionalized and aminosilanized carbon nanotubes for polyamide matrix. *Journal of Reinforced Plastics and Composites*, 32, pp. 75-86.
- Sangsuk, S. 2010. Preparation of high surface area silver powder via Tollens process under sonication. *Materials Letters*, 64, pp. 775-777.
- Sarkar, S., Banerjee, D., Das, N. S. and Chattopadhyay, K. K. 2015. A simple chemical synthesis of amorphous carbon nanotubes–MnO₂ flake hybrids for cold cathode application. *Applied Surface Science*, 347, pp. 824-831.
- Shapee, R. A. A. S. M. 2012. Rheological Behaviors and Their Correlation with Printing Performance of Silver Paste for LTCC Tape. In: VICENTE, D. J. D. (ed.) *Rheology*.
- Shivananda, C. S., Asha, S., Madhukumar, R., Satish, S., Narayana, B., Byrappa, K., Youjiang, W. and Sangappa, Y. 2016. Biosynthesis of colloidal silver nanoparticles: their characterization and antibacterial activity. *Biomedical Physics and Engineering Express*, 2, 035004.
- Shukla, A. and Rao, R. M. V. G. K. 1984. Curing studies on modified epoxy and unsaturated polyester resins. *Journal of Applied Polymer Science*, 29, pp. 1553-1558.
- Singh, V. K., Shukla, A., Patra, M. K., Saini, L., Jani, R. K., Vadera, S. R. and Kumar, N. 2012. Microwave absorbing properties of a thermally reduced graphene oxide/nitrile butadiene rubber composite. *Carbon*, 50, pp. 2202-2208.
- Stauffer, D., Coniglio, A. and Adam, M. 1982. Gelation and critical phenomena. In: DUŠEK, K. (ed.) *Polymer Networks*. Berlin, Heidelberg: Springer Berlin Heidelberg.
- Sondi, I., Goia, D. V. and Matijević, E. 2003. *Preparation of highly concentrated stable dispersions of uniform silver nanoparticles*.
- Song, Y. S. and Youn, J. R. 2005. Influence of dispersion states of carbon nanotubes on physical properties of epoxy nanocomposites. *Carbon*, 43, pp. 1378-1385.
- Tan, K. H., Ahmad, R., Leo, B. F., Yew, M. C., Ang, B. C. and Johan, M. R. 2012. Physico-chemical studies of amorphous carbon nanotubes synthesized at low temperature. *Materials Research Bulletin*, 47, pp. 1849-1854.
- Tao, L., Guohua, M. and Tongjiang, P. 2015. Mechanism of Preparing Spherical Nano-sized Silver Particles via o-Phenylenediamine Reduction

Process in Water-NMPD Mixed Solution System. *Rare Metal Materials and Engineering*, 44, pp. 1071-1074.

Tao, Y., Xia, Y., WanG, H., Gong, F., WU, H. and Tao, G. 2009. Novel Isotropic Conductive Adhesives for Electronic Packaging Application. *IEEE Transactions on Advanced Packaging*, 32, pp. 589-592.

Tsai, T.-N. 2008. Modeling and optimization of stencil printing operations: A comparison study. *Computers and Industrial Engineering*, 54, pp. 374-389.

Varma, A. J., Jamdade, Y. K. and Nadkarni, V. M. 1984. Curing characteristics of epoxy resins filled with cellulose and oxidized cellulose. *Die Angewandte Makromolekulare Chemie*, 122, pp. 211-218.

Vertelov, G. K., YU, A. K., Efremenkova, O. V., Olenin, A. Y. and Lisichkin, G. V. 2008. A versatile synthesis of highly bactericidal Myramistin® stabilized silver nanoparticles. *Nanotechnology*, 19, 355707.

Vijayaraghavan, K. and Nalini, S. P. K. 2010. Biotemplates in the green synthesis of silver nanoparticles. *Biotechnology Journal*, 5, pp. 1098-1110.

Wang, Y. 2008. *Cellulose Fiber Dissolution in Sodium Hydroxide Solution at Low Temperature: Dissolution Kinetics and Solubility Improvement*. Doctor of Philosophy in the Department of Chemical and Biomolecular Engineering, Georgia Institute of Technology.

Wani, I. A., Ganguly, A., Ahmed, J. and Ahmad, T. 2011. Silver nanoparticles: Ultrasonic wave assisted synthesis, optical characterization and surface area studies. *Materials Letters*, 65, pp. 520-522.

Weisstein E., 2017, *Least Squares Fitting*[Online]. Available at: <http://mathworld.wolfram.com/LeastSquaresFitting.html> [Accessed: 17 December 2017].

Weng, L., Zhang, L., Ruan, D., Shi, L. and Xu, J. 2004. Thermal Gelation of Cellulose in a NaOH/Thiourea Aqueous Solution. *Langmuir*, 20, pp. 2086-2093.

Wong, C. P. and Daoqiang, L. Recent advances in electrically conductive adhesives for electronics applications. *Adhesive Joining and Coating Technology in Electronics Manufacturing, 2000. Proceedings. 4th International Conference on, 2000*.pp. 121-128.

Wu, J., Zhang, J., Zhang, H., He, J., Ren, Q. and Guo, M. 2004. Homogeneous Acetylation of Cellulose in a New Ionic Liquid. *Biomacromolecules*, 5, pp. 266-268.

Wu, H. P., Liu, J. F., Wu, X. J., Ge, M. Y., Wang, Y. W., Zhang, G. Q., and Jiang, J. Z. 2006. High conductivity of isotropic conductive adhesives filled

with silver nanowires. *International Journal of Adhesion and Adhesives*, 26, 617-621.

Xiong, Y., Xie, Y., Li, X. and Li, Z. 2004. Production of novel amorphous carbon nanostructures from ferrocene in low-temperature solution. *Carbon*, 42, pp. 1447-1453.

Xianxue, L., Bingyun, Z., Limei, X., Dandan, W., Zonglin, L. and Huichai, Z. 2012. Study on Properties of Conductive Adhesive Prepared with Silver Nanoparticles Modified by Silane Coupling Agent. *Rare Metal Materials and Engineering*, 41, pp. 24-27.

Yang, S., Shao, D., Wang, X., Hou, G., Nagatsu, M., Tan, X., Ren, X. and Yu, J. 2015. Design of Chitosan-Grafted Carbon Nanotubes: Evaluation of How the -OH Functional Group Affects Cs⁺ Adsorption. *Marine Drugs*, 13, pp. 3116.

Yim, B.-S. and Kim, J.-M. 2016. Thermo-mechanical reliability of a multi-walled carbon nanotube-incorporated solderable isotropic conductive adhesive. *Microelectronics Reliability*, 57, pp. 93-100.

Yim, B.-S., Kim, K., Kim, J. and Kim, J.-M. 2016. Influence of functionalized graphene on the electrical, mechanical, and thermal properties of solderable isotropic conductive adhesives. *Journal of Materials Science: Materials in Electronics*, pp. 1-10.

Yim, B.-S., Lee, B. H., Kim, J. and Kim, J.-M. 2014. Effect of dispersion condition of multi-walled carbon nanotube (MWNT) on bonding properties of solderable isotropic conductive adhesives (ICAs). *Journal of Materials Science: Materials in Electronics*, 25, pp. 5208-5217.

Youngseok, O., Daewoo, S., Youngjin, K., Eungsuek, L., Jee Soo, M., Jaeboong, C. and Seunghyun, B. 2008. Silver-plated carbon nanotubes for silver/conducting polymer composites. *Nanotechnology*, 19, 495602.

Yu, Y.-H., Ma, C.-C. M., Teng, C.-C., Huang, Y.-L., Tien, H.-W., Lee, S.-H. and Wang, I. 2013. Enhanced thermal and mechanical properties of epoxy composites filled with silver nanowires and nanoparticles. *Journal of the Taiwan Institute of Chemical Engineers*, 44, pp. 654-659.

Yudianti, R., Onggo, H., Sudirman, Saito, Y., Iwata, T. and Azuma, J.-I., 2011. Analysis of Functional Group Sited on Multi-Wall Carbon Nanotube Surface. *The Open Materials Science Journal*, 5(1), pp. 242-247.

Zhang, Q. K., Long, W. M. and Zhang, Z. F. 2015. Growth behavior of intermetallic compounds at Sn-Ag/Cu joint interfaces revealed by 3D imaging. *Journal of Alloys and Compounds*, 646, pp. 405-411.

Zhang, R. May 2011. *Novel conductive adhesives for electronic packaging applications: a way towards economical, highly conductive, low temperature*

and flexible interconnects. Doctor of Philosophy, Georgia Institute of Technology

Zhang, R., Moon, K.-s., Lin, W., and Wong, C. P. 2010. Preparation of highly conductive polymer nanocomposites by low temperature sintering of silver nanoparticles. *Journal of Materials Chemistry*, 20, pp. 2018-2023.

Zhang, S., Tang, Y. and Vlahovic, B. 2016. A Review on Preparation and Applications of Silver-Containing Nanofibers. *Nanoscale Research Letters*, 11, pp. 1-8.

Zhao, T., Hou, C., Zhang, H., Zhu, R., She, S., Wang, J., LI, T., Liu, Z. and Wei, B. 2014. Electromagnetic Wave Absorbing Properties of Amorphous Carbon Nanotubes. *Scientific Reports*, 4, pp. 5619.

Zhao, T. K., Li, G. M., Liu, L. H., Liu, Y. N., and Li, T. H. 2011. Physical model for the growth of amorphous carbon nanotubes. *Applied Physics Letters*, 98(16), 163111. doi: <http://dx.doi.org/10.1063/1.3583445>

Zhou, J., Zhang, L. and Cai, J. 2004. Behavior of cellulose in NaOH/Urea aqueous solution characterized by light scattering and viscometry. *Journal of Polymer Science Part B: Polymer Physics*, 42, pp. 347-353.

Zhu, S., Wu, Y., Chen, Q., Yu, Z., Wang, C., Jin, S., Ding, Y. and Wu, G. 2006. Dissolution of cellulose with ionic liquids and its application: a mini-review. *Green Chemistry*, 8, pp. 325-327.

Zulfli, M., H., N., A., A. B. and S., C. W. 2012. Mechanical and Thermal Behaviours of Glass Fiber Reinforced Epoxy Hybrid Composites containing Organo-Montmorillonite Clay. *Malaysian Polymer Journal*, 7, pp. 8-15.

Zwolinski, M., Hickman, J., Rubin, H., Zaks, Y., Mccarthy, S., Hanlon, T., Arrowsmith, P., Chaudhuri, A., Hermansen, R., Lan, S. and Napp, D. 1996. Electrically conductive adhesives for surface mount solder replacement. *IEEE Transactions on Components, Packaging, and Manufacturing Technology: Part C*, 19, pp. 241-250.

APPENDICES

APPENDIX A: Forty five ICAs samples composition generated by surface response. The remaining material is silver powder.

Sample	Matrix (wt%)		Filler (wt%)
	DGEBA	MCC	a-CNTs
S11	40	5	3
S12	60	2.5	2
S13	60	2.5	2
S14	80	5	2
S15	80	2.5	1
S16	40	0	2
S17	60	2.5	1
S18	40	2.5	1
S19	80	0	3
S20	60	2.5	3
S21	80	0	2
S22	40	0	3
S23	60	5	2
S24	80	5	3
S25	60	5	3
S26	60	0	3
S27	40	5	2

S28	60	0	2
S29	80	0	1
S30	80	2.5	3
S31	60	2.5	2
S32	40	0	1
S33	40	2.5	2
S34	60	2.5	2
S35	80	5	1
S36	60	0	1
S37	80	2.5	2
S38	40	2.5	3
S39	40	5	1
S40	60	2.5	2
S41	60	2.5	2
S42	60	5	1
S43	80	5	0
S44	80	0	0
S45	60	2.5	0
S46	80	2.5	0
S47	60	2.5	0
S48	60	2.5	0
S49	60	0	0

S50	60	2.5	0
S51	60	5	0
S52	40	0	0
S53	40	2.5	0
S54	40	5	0
S55	60	2.5	0

APPENDIX B: Preparation of the amount of ethylenediamine (EDA).

In this study, it is desired to cross link a bisphenol A diglycidyl ether (DGEBA), $C_{21}H_{24}O_4$ epoxy resin using ethylenediamine (EDA), $C_2H_8N_2$. The EDA formula has 2 nitrogen atoms. In the epoxy molecule, there are two epoxy groups, the epoxy equivalent weight is therefore: $= 340.42/2 = 170.21 \text{ g}\cdot\text{mol}^{-1}$.

The molar mass of DGEBA is $340.42 \text{ g}\cdot\text{mol}^{-1}$

The molar mass of EDA is $60.10 \text{ g}\cdot\text{mol}^{-1}$

There are 4 available hydrogens in the EDA molecule. The value of molecular weight of amine over the number of available hydrogens per molecule is: $60.10 \text{ g}\cdot\text{mol}^{-1}/4 = 15.025 \text{ g}\cdot\text{mol}^{-1}$

Parts by weight of amine to be used with 100 parts by weight of epoxy resin are: $\% = 15.025/170.21 \times 100 = 8.827\%$.

For 100g of epoxy, the amount of EDA curing agent to be used is: 8.8 g